Models for spatial information encoding in neuronal populations

Maria Luísa Morais e Sousa Castro Guedes

Tese de doutoramento apresentada à Faculdade de Ciências da Universidade do Porto para obtenção do Grau de Doutora em Matemática Aplicada.

Julho de 2013

Orientador: Professor Paulo de Castro Aguiar,
Centro de Matemática da Universidade do Porto

Co-orientador: Professor Vasco Galhardo,
Departamento de Biologia Experimental da Faculdade de Medicina da Universidade do Porto

FACULDADE DE CIÊNCIAS DA UNIVERSIDADE DO PORTO

DEPARTAMENTO DE MATEMÁTICA

Abstract

The work described here has the goal of providing mathematical models for important spatial information processing mechanisms in the brain. Two original models were developed targeting two core mechanisms: one dedicated to the phase precession effect and the other to the formation of hexagonal firing patterns of grid cells. Both mechanisms are embedded on the general problem of spatial information coding in the animal brain and, possibly in the human brain. The models were constructed in close relation with the known biophysical details of the brain areas being modeled.

Phase precession is one of the most well-known examples within the temporal coding hypothesis. Here we present a biophysical spiking model for phase precession in hippocampal CA1 which focuses on the interaction between place cells and local inhibitory interneurons. The model's functional block is composed by a place cell (PC) connected with a local inhibitory cell (IC) which is modulated by the population theta rhythm. Both cells receive excitatory inputs from the entorhinal cortex (EC). These inputs are both theta modulated and space modulated. The dynamics of the two neuron types are described by integrate-and-fire models with conductance synapses. The EC inputs are described using non homogeneous Poisson processes. Phase precession in our model is caused by increased drive to specific PC/IC pairs when the animal is in their place field. The excitation increases the IC's firing rate, and this modulates the PC's firing rate such that both cells precess relative to theta. Our model implies that phase coding in place cells may not be independent from rate coding. The absence of restrictive connectivity constraints in this model predicts the generation of phase precession in any network with similar architecture and subject to a clocking rhythm, independently of the involvement in spatial tasks.

The second model addresses grid field formation. Grid cells (GCs) in the medial entorhinal cortex (mEC) share the property of having their firing activity spatially tuned to a regular triangular lattice. Several theoretical models for grid fields formation have been proposed but most of them fail to account for important biological constraints such as the lack of high recurrence levels and absence of topographic organization in mEC. As such, models for grid fields' formation are still under active improvement. In this thesis we present an original model for the formation of grid like firing patterns supported on

two key hypothesis: i) spatial information in GCs is directly linked to place cells (PCs) rate activity and ii) grid hexagonal fields result from a combined synaptic plasticity rule involving inhibitory and excitatory units mediating the connections between PCs and GCs. Depending to the location of its receptive field, each PC can affect the activity of the GC with excitatory inputs or inhibitory inputs. Besides its nature, the magnitude attributed to the PC input is a function of the distance to the place field center, which is inferred from rate decoding. A biologically plausible learning rule drives the evolution of the connections strengths from PCs to a GC. In this model, place cells compete for grid cell activation and the plasticity rule favors efficient packing of the space representation. This leads to grid like firing patterns, while not requiring a topographic organization. In a new environment grid cells continuously recruit new place cells to cover the entire space. The model described here can represent the feed-forward connections from hippocampus CA1 towards deeper mEC layers.

Resumo

O trabalho desenvolvido para esta tese consiste na proposta e implementação de modelos matemáticos e biofísicos capazes de reproduzir importantes mecanismos de processamento de informação espacial atribuídos ao hipocampo e ao córtex cerebral. Dois modelos originais foram criados: um dedicado à reprodução do mecanismo de *phase precession* e outro à formação dos campos recetivos hexagonalmente distribuídos, característicos das células *grid*. Os dois processos referidos fazem parte de um problema geral, o da aprendizagem e formação da memória espacial em mamíferos.

A *phase precession* é um dos exemplos mais conhecidos dentro da hipótese de codificação temporal. Nesta tese apresenta-se um modelo biofísico do tipo *spiking* para a precessão de fase na região CA1 do hipocampo baseado na interação existente entre *place cells* e os interneurónios inibitórios. O bloco funcional deste modelo é composto por uma *place cell* (PC) ligada a uma célula inibitória local (IC) que é modulada pelo ritmo *theta* (característico da população de células inibitórias). Ambas as células recebem *inputs* excitatórios do córtex entorrinal (EC) modelados espacialmente e pelo ritmo *theta*. A dinâmica dos dois neurónios é descrita por modelos do tipo *integrate-and-fire* com sinapses condutoras. Os *inputs* provenientes do EC são gerados usando processos de Poisson não homogéneos. No nosso modelo, o efeito de precessão de fase é conseguido através de um aumento do *input* que chega a pares específicos de PC/IC quando o animal atravessa os seus campos recetivos. A excitação aumenta a taxa de disparo do IC afetando por sua vez a taxa de disparo do PC. Consequentemente ambas a células mostram um avanço no disparo relativamente à fase do ciclo *theta*. A implicação mais importante que se obtém deste modelo é que a codificação em fase nas *place cells* pode não ser independente da codificação em taxa. Adicionalmente, a ausência de condições restritivas relativamente à conectividade entre as células envolvidas, torna este modelo capaz de gerar precessão de fase em qualquer rede com uma arquitetura similar e sujeita a um ritmo, independentemente do seu envolvimento em tarefas espaciais.

As *grid cells* (GCs) do córtex entorrinal médio (mEC) possuem tipicamente uma atividade de disparo espacialmente distribuída sob os vértices de uma malha triangular regular. Vários modelos teóricos/computacionais para a formação deste tipo de padrões de disparo já foram propostos. No entanto, na sua maioria, não entram em consideração com importantes condicionantes do mEC tais como a falta de elevados níveis de

recorrência e a ausência de uma organização topográfica das suas células espaciais. Desta forma, a criação de modelos robustos para a formação dos campos recetivos das *grid cells* está ainda sob estudo. Nesta tese apresenta-se um modelo original para a génese de padrões de disparo do tipo *grid* que assenta em duas hipóteses chave: i) a informação espacial das GCs está diretamente relacionada com a atividade das PCs e ii) os campos recetivos *grid* resultam de um mecanismo de plasticidade sináptica combinado que envolve neurónios inibitórios e excitatórios intermediando as ligações entre PCs e GCs. Dependendo da sua localização espacial, cada PC contribui com *inputs* excitatórios ou inibitórios para a atividade da GC. A natureza e a força do *input* de cada PC é função da distância ao centro do seu campo recetivo que é inferido por descodificação da sua taxa de disparo. Uma regra de aprendizagem fundamentada em pressupostos biológicos gere a evolução da força das ligações de várias PCs para uma GC. Neste modelo, as *place cells* competem pela ativação da GC e a regra de plasticidade favorece um empacotamento eficiente da representação do espaço. Como consequência, padrões de disparo do tipo *grid* são formados sem necessidade de impor uma organização topográfica às células. Quando expostas a um novo recinto, as *grid cells* continuam a recrutar novas *place cells* de forma a cobrirem por completo o espaço disponível. O modelo descrito pode ser considerado como representativo das ligações *feed-forward* da região CA1 do hipocampo às camadas mais profundas do mEC.

Preface

If the human brain were so simple that we could understand it, we would be so simple that we couldn't.

Emerson M. Pugh (Quoted by George E. Pugh in The Biological Origin of Human Values, p. 154, 1977)

The work developed and described in this thesis fits in an interdisciplinary field combining neuroscience, computer science, physics and mathematics - computational neuroscience. In this field of study, qualitative elements and quantitative data extracted from the animal (or human) nervous system are ingredients for computational models aimed at representing behavior features. Researchers in this relatively new area address problems that can go from synaptic, neural, networks to systems of networks, through one or a combination of several gates. Psychology, physiology, physics, mathematics, engineering sciences and neurobiology are examples of entries into the broad field of computational neuroscience. Interdisciplinary groups employ quantitative and modeling methodologies to enlarge the current knowledge of the nervous system function, for example by developing synthetic models to replicate animal and human behavior.

The term neural networks has been used to describe networks of biological neurons from the nervous system of animals. Nowadays, this term refers to a parallel computation field receiving inspiration from brain units. Generally, in neural networks, modeling is pursued disregarding most of the biological constraints of neurons. In contrast, computational neuroscience keeps a close contact with biological systems throughout all the steps, contributing in great extent to the development of brain theory.

Computational neuroscience involves several subfields, from which memory encoding and spatial navigation are two topics of relevance since (at least the second one) the first cells with spatial specificity were reported, in 1971. Thanks to the improvement of recording techniques allied with predictions extracted from theoretical models, the discovery of more spatial neural units has proceed and, nowadays, several are reported in the literature. Personally, the idea that a spatial map of our house, city or place of work could be engraved in networks of neurons in our brain (or in their connections, to be more precise) was enough motivation to proceed studies in this area.

Mostly relevant for the appropriate approach in any branch of theoretical neuroscience, is the acquaintance with the underlying neurobiology. Accordingly, a previous background study was necessary to assure a close relation of the models developed with the related biophysical features.

The first chapter of this thesis provides a general introduction, where the basis of the developed work are described. Though not extensive, this chapter intends to elucidate the readers less acquainted with the field, covering the main experimental findings on the spatial brain context, together with the mathematical tools used in the computational models developed. In chapter 2 a review of proposed models for the phase precession effect and grid cell formation (more extensively) is presented. Chapter 3 is dedicated solely to the phase precession mechanism with our contribution to the area consisting on an original model. In chapter 4, focusing on the characteristic grid cell firing pattern, an original model for this pattern formation is described. The last two chapters correspond to a summary of main conclusions regarding each of the models created together with suggestions for further work which naturally flow from the thesis accomplishments.

Acknowledgments

I am grateful for Paulo Aguiar's short course in Computational Neuroscience, in March 2008, where I got in touch for the first time with this passionate field of study. Together with the FCT grant, this course triggered the change in direction in my professional path.

This thesis would not have been possible without Paulo Aguiar. I profited immensely from having Paulo as my supervisor. I am grateful for his guidance, motivation, patience and critical comments on this thesis. I am also grateful for the important advises given by Vasco Galhardo, co-supervisor of this thesis.

My sincere gratitude goes to my husband who provided valuable suggestions and patiently heard my thoughts. I am also grateful for my parents and brother encouragement and support since the beginning of this work.

My research had financial support from *Fundação para a Ciência e para a Tecnologia* (FCT), Portugal, through the programs QREN - POPH, with European Union Funding (FSE) and national funding, from the grant SFRH/BD/46329/2008.

To my six closest connections:

Tim,

Finza,

Mané,

Manel,

missed Avó Fina

and Inês, who gracefully arrived during this pleasant journey.

Contents

List of figures and tables

Some physical parameters

Symbol	Description	Units and magnitude
V_m	Membrane potential	mV (mili Volts)
I_m	Membrane current	nA (nano Ampers)
R_m	Membrane resistance	MΩ (mega ohms) (V/A)
C_m	Membrane capacitance	nF (nano Farads) (sA/V)
τ_m	Membrane time constant	ms
Q	Membrane charge	pC (pico coulombs) (FV or sA)
g	Channel conductance	μS (micro Siemens) (Ω^{-1})
E_{ion}	Equilibrium potential of an ion	mV
g_L	Leak conductance	μS
E_L	Leak reversal potential	mV
r	Firing rate	Hz (events/s)
τ_r	Rise time constant	ms
τ_d	Decay time constant	ms

Tera (T)	Giga (G)	Mega (M)	Kilo (k)	unit	milli (m)	micro (μ)	nano (n)	pico (p)
10^{12}	10^{9}	10^{6}	10^{3}	1	10^{-3}	10^{-6}	10^{-9}	10^{-12}

1. Background

The modeling developed in this thesis was done in close relation with neurobiological mechanisms, therefore, a detailed introduction to the neurobiology involved becomes essential.

It is known, since Darwin studies, that most animals possess extraordinary abilities in learning suboptimal trajectories and keeping track of their location relative to a reference point. Rats, in particular, are capable of latent learning, i.e., learning during exploration in the absence of motivation or goals (such as food, predators …). For example, female rodents are able to reach pups that have been removed from their nests. Some species have shown to be able to follow a direct line into the original location of their "home", even in cases where the nest has been displaced (McNaughton et al. 2006).

Unravelling the mechanisms behind space representation in the rat's brain is a major step towards the understanding of how these processes occur in the human brain. Moreover, finding efficient solutions to navigation as those used by neural systems, adds new tools to navigation challenges, faced for example in autonomous robots development. Hence, in this thesis, the focus is given to space information encoding in neural populations of rodents.

Space representation in the rat's brain is a short expression for a complex procedure, played at distinct neural locations at different time scales. In this introductory chapter, this concept will be addressed in some detail, starting with the anatomic framework about where, in the rat's brain, this representation takes place.

1.1 Anatomical and cellular framework

Hippocampus has received growing attention from diverse neuroscience researchers involved in human amnesia, Alzheimer's disease and, of most importance in this study, in learning processes and in memory formation in mammals (Burgess and O'Keefe 1998). The volume of humans (monkeys) hippocampus is about 100 (10) times larger than the rat's hippocampus. In humans the organization of the different areas is more complex and some of them are more developed than in animals' brain. Nevertheless, the basic structure

of hippocampus, its regions and connectivity, is common to all three species (see Figure 1.1 for the rat and human examples) (Amaral and Lavenex 2006).

The hippocampal formation in rats comprehends several regions which differ in the anatomical and physiological properties of their cells and their connectivity: dentate gyrus (DG), cornus ammonis 1 (CA1), cornus ammonis 2 (CA2), cornus ammonis 3 (CA3), subiculum, presubiculum, parasubiculum and entorhinal cortex (EC). Within hippocampus formation, connections are essentially made in a feed-forward fashion along the transversal axis, where DG is the most proximal region and EC is the most distal one (see Figure 1.1) (Amaral and Lavenex 2006; Freund and Kali 2008).

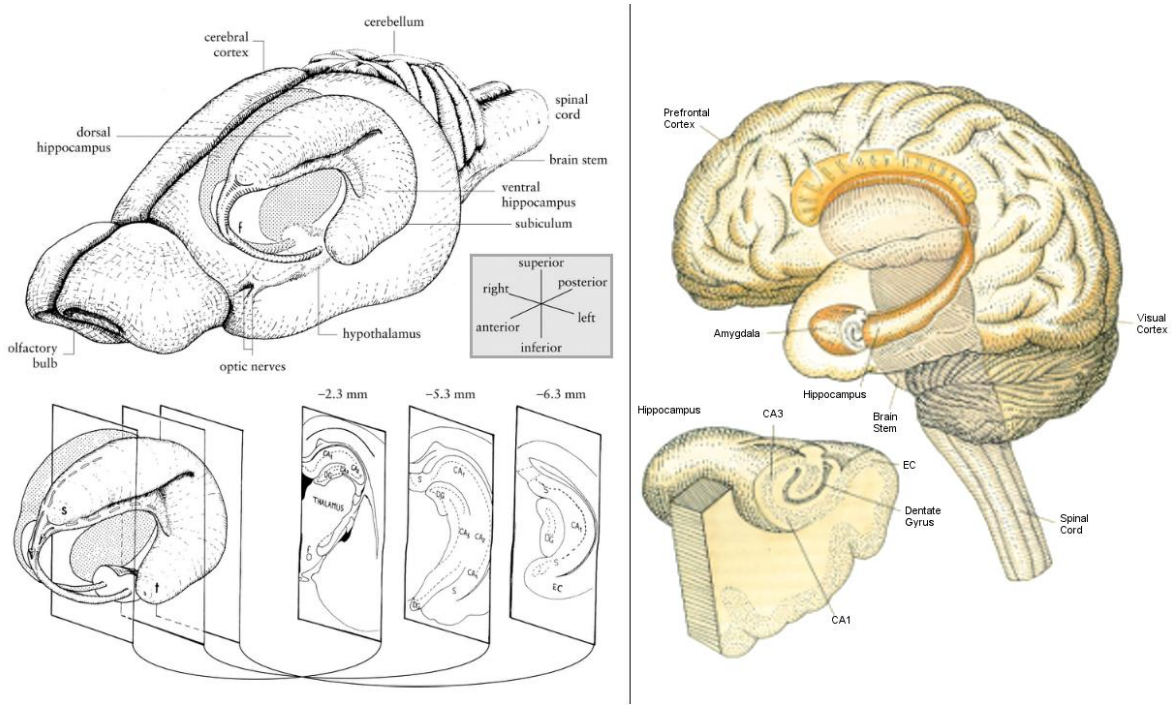

Figure 1.1 Diagram of the hippocampus and related structures in the rat (left panel) and in humans (right panel). In the top of the head is the dorsal = septal = superior region; more close to the neck is the ventral = temporal = inferior region; in the frontal side of the head is the rostral = anterior region; in the back of the head is the caudal region, where dorsal and ventral hippocampal regions merge originating the posterior region. Rat drawing adapted from (Cheung and Cardinal 2005) and human illustration adapted from (Kandel and Squire 2002).

Typically organized by morphology clusters, distinct types of neuron cells fill up the hippocampal formation areas, such as granule cells (the rat's DG has approximately 1.2×10^6 granule cells), pyramidal cells (CA1 and CA3 contain roughly 0.5×10^6 pyramidal cells), mossy cells (responsible for the recurrence in some fields like DG) and inhibitory interneurons of various types (basket cells, axo-axonic or chandelier cells, bistratified cells and many others).

Neurons have different names according to their morphology (stellate or granular), the

nature of their activity profile (neuron cells either excite or inhibit the cells they project to) and their baseline firing rate. Nevertheless, they all participate in the nervous transmission roughly by the same biophysical mechanisms. According to Ramon & Cajal's doctrine, the neuron is the signaling unit of the brain. It was in the beginning of the 20th century that he and other neuroanatomists found that nervous cells have four distinct components: a cell body or soma, a certain number of dendrites, an axon (together with its collaterals) and a set of axons terminals, called synapses (or presynaptic terminals) (see Figure 1.2). Through the dendrites the neurons receive signals from other cells (presynaptic), signals follow into the soma and affect the membrane potential of the soma component. When firing threshold is reached, the soma fires an action potential (spike) which follows through the axon and is "delivered" to other cells (postsynaptic cells) through synapses.

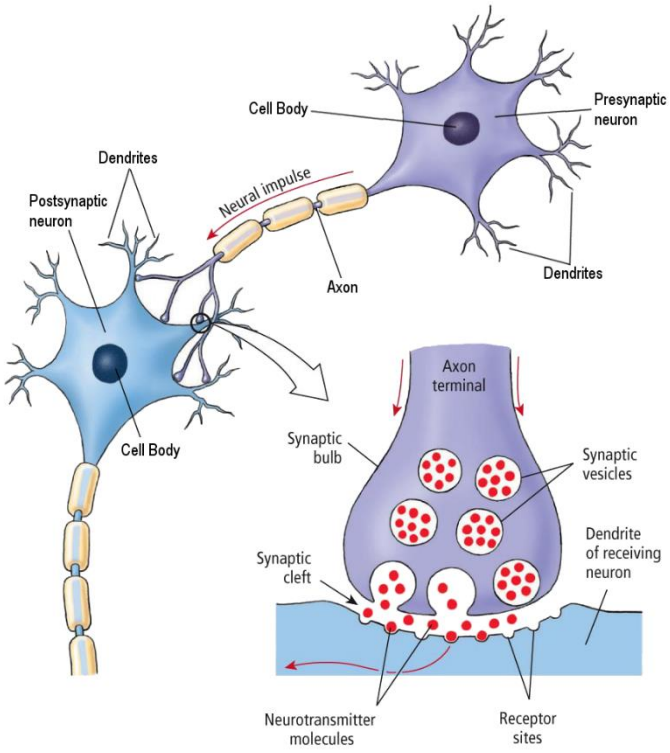

Figure 1.2 Anatomy of the typical neuron and zoom of its synaptic connection onto a postsynaptic neuron. Through the dendrites the neurons receive signals from other cells (presynaptic) which follow into the soma or cell body affecting its membrane potential. When firing threshold is reached, the soma produces an action potential (spike) which follows through the axon and is delivered to other cells (postsynaptic cells) through synapses. Scheme of the neurotransmitter release from the presynaptic cell onto the synaptic cleft, and binding to the postsynaptic neuron receptor sites (adapted from (Wade and Tavris 2000)).

Granule cells are the only principal cell in the DG, meaning that only granule cells in DG innervate to other hippocampal regions. In general, principal cells are neurons that have axons connecting to other cells populations further than where their cell bodies and

dendrites are located. Principal cells are mainly excitatory in nature. Interneurons are commonly inhibitory and their local axons are responsible for maintaining the population in controlled levels of excitability. These are distinguishable from principal cells for having high rates of spontaneous activity, moreover they also show a particular modulation which will be addressed later. Principal cells are often complex spike cells, being characterized by a much lower baseline activity than interneurons, by occasional short bursts (complex spike patterns) of action potentials with successive decreasing amplitudes and experiencing long periods of no activity at all. In hippocampus proper (CA1, CA2 and CA3), principal cells are pyramidal; interneurons, as in DG, populate this region throughout its extent. Cells in CA2, CA3 and DG are also innervated by collaterals of their own axons, meaning that recurrence is a prevailing feature of this regions (Amaral and Lavenex 2006). The hippocampal formation is located in an advantage brain position, receiving sensory information through entorhinal cortex (EC) which in turn retrieves the processed data to neocortex (see Figure 1.3).

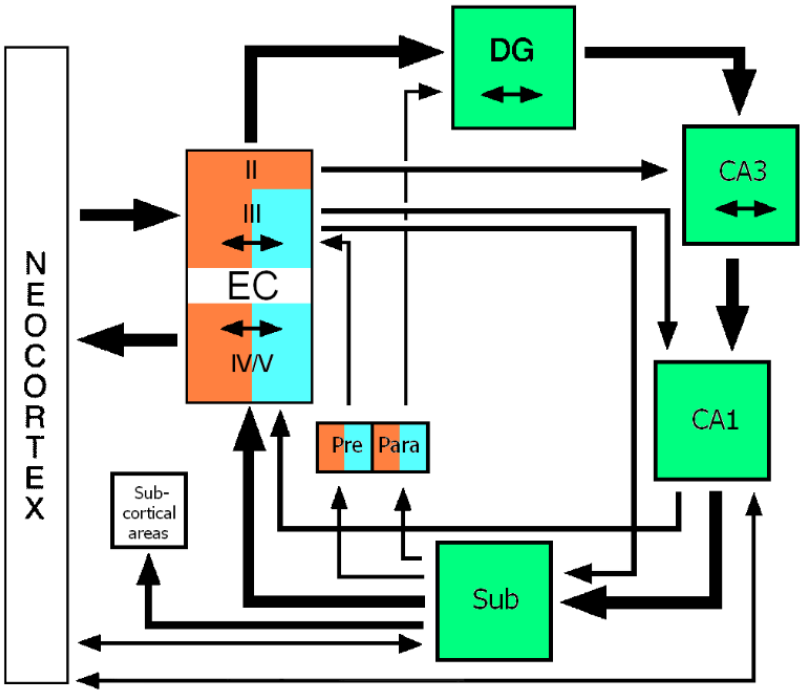

Figure 1.3 The entorhinal cortex and the hippocampal formation. Neurons in layer III from EC project to CA1 field by the perforant path to temporal CA1 and alvear path to septal CA1. Neurons in layer II from EC project to the dentate gyrus (DG) and to the CA3 fields via the perforant pathways. Cells in the DG project to the CA3 field via mossy fibers. Double sided arrows represent recurrent connections within the respective regions. Colors indicate presence of place cells (green), grid cells (orange) and head-direction cells (blue) (adapted from (Amaral and Lavenex 2006)).

EC is divided in two regions, the lateral entorhinal cortex, lEC, at a rostro-lateral position and the medial entorhinal cortex, mEC, at a caudal-medial position. They both project to the same cells in DG and CA3, while connecting to different groups of cells in CA1 and

subiculum (Witter 2011). Most important to this study is the subdivision of EC (both medial and lateral regions) into 6 layers, each constituted essentially by one cell type. Information regarding EC typical neurons and enervating projections is summarized in Table 1.1.

Table 1.1 Characterization of entorhinal cortex layers regarding the existent cells and projections within layers, between layers and with the remaining hippocampal areas.

EC Layers	**Contents**	**Projections**
I	Fibers and few cells.	The few cells project to layer II.
II	Stellate cells (big and medium size cells) and pyramidal cells (small and clustered in groups, especially in lEC).	Both project to CA3 and DG.
III	Essentially pyramidal cells.	Pyramidal cells project to CA1 and subiculum; intralaminar connections exist between principal neurons.
IV	*Lamina dissecans* (Scattered fusiform or pyramidal cells, although generally referred as having no cells).	Project to the white matter and their dendrites extend up to layer I.
V	Pyramidal cells, small spherical cells and fusiform neurons.	Axons collaterals reach layers V (intralaminar) and VI and occasionally layer II; their dendrites extend up to layer I and II.
VI	Cells with different shapes and sizes.	Project essentially to V and VI layers; collateralized axons also influence layers I, II, III, DG and hippocampus proper.

As to interneurons, essentially inhibitory, they are found throughout all EC being more abundant in superficial layers. Moreover, non local inhibitory cells have been found in layers II and III that project to DG (Amaral and Lavenex 2006). A remark for Table 1.1,

is that intralaminar excitatory connections within layers III and V of EC have been reported to be around 10% and inexistent for layer II, where the existing connections are thought to be between principal neurons and interneurons (Dhillon and Jones 2000).

Adding to the unidirectional flow of information in the hippocampus formation is the topographic organization of the connections. This means that septal (temporal) parts of the hippocampus receive projections from the lateral (medial) EC (see Figure 1.1) whereas the same scheme is maintained in the main projections from subiculum and CA1 back to EC (Amaral and Lavenex 2006). This organized connectivity regime allows for an information flow, that follows along the loop, being updated whenever extra input is provided by cortical areas or as signals are processed by inner ones.

Although information is already spatially modulated at the entrance, the capacity of generating a structure able to support spatial memory and navigation is commonly attributed to the hippocampus. Each one of these processes incorporates complex mechanisms of information integration and processing (Fyhn et al. 2004), two of which are the focus of the work developed for this thesis described in chapters 3 and 4.

1.2 Spatial cells

Some of the most remarkable results obtained by measuring cells activity in rat's hippocampus and entorhinal cortex regions during foraging are that some cells play distinct and complementary tasks in the spatial orientation process. The most important spatial cells reported in the literature are described in this section: place cells, grid cells, head-direction cells and border cells. Particular emphasis is given to the first two as they are crucial elements in the models created for this thesis. No grid cells or other spatial related activity neurons were found in the lateral lobe of EC, so it is commonly assumed that from the entorhinal cortex, only mEC is involved in navigation (Moser and Moser 2008).

1.2.1 Place cells

More than 40 years ago O' Keefe and Dostrovsky reported the existence of a cell type with consistent (across trials) activity confined to a certain place of the environment – the place cell (O'Keefe and Dostrovsky 1971). This particular firing pattern can be found in

DG granule cells, in pyramidal cells from layers CA1 and CA3 of the hippocampus and also in subiculum (see green fields in Figure 1.3). Experimentally, for the purpose of recording cells' activity, micro-electrodes are implanted in the rats' brain in an adequate position (during a surgery). With this micro-electrodes experimentalists are able to record single-neuron activity in the awake animal.

As the rat runs in a one way maze or in a two dimensional maze, the place cell's firing map obtained is characterized by one limited region of high activity (red) – the place field – on a silent background (see Figure 1.4 a). The maximum firing rate achieved by a place cell is variable throughout different regions, reaching 20 Hz in hippocampus versus 15 Hz in subiculum.

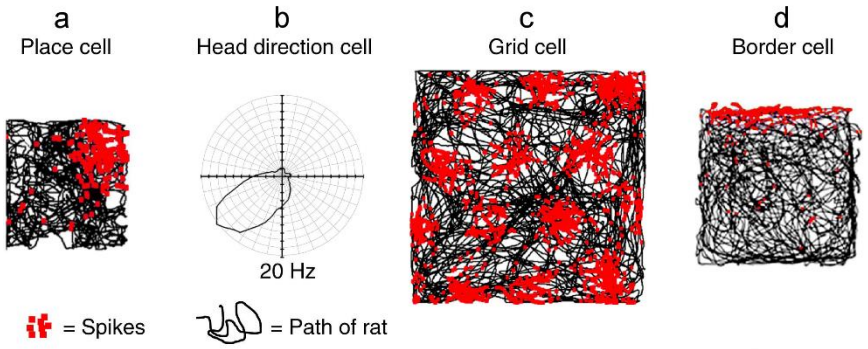

Figure 1.4 Representative firing profiles of the canonical spatial cells. a – Place cell's spikes position (red squares) superimposed on the rat trajectory (black path) in a square maze with 60×60 cm. The firing activity of this cell is tuned to the northeast region of the maze. b – Polar plot indicating a head-direction cell's strong directional tuning for the southwest of the maze (the rate correspondent to the longer radius length is indicated below). c – Grid cell's spikes position (red squares) superimposed on the rat trajectory (black path) in a square maze with 120×120 cm. d – Border cell's spikes position (red squares) superimposed on the rat trajectory (black path) in a square maze with 100×100 cm. The firing activity of the cell is tuned to the north wall of the maze (adapted from (Marozzi and Jeffery 2012)).

Cells' firing maps are obtained by recording simultaneously the rat trajectory (monitoring a light placed in the rat's head or abdominal region) and the times at which the cell spiked. To compute the firing rate, the maze is subdivided into small adjacent bins (e.g. 2 × 2 cm^2) and in each bin the number of spikes is divided by the time the rat spent in that same bin. Frequently this data is space averaged and smoothed. As a result, a place cell firing rate map commonly resembles a two dimensional Gaussian profile (O'Keefe 2006).

At each hippocampal location, all portions of the environment are represented by local place cells, with ventral cells exhibiting broader fields than dorsal ones throughout the hippocampal layers (Kjelstrup et al. 2008). However, place cells coding for nearby positions in an environment are not found in neural neighboring locations, providing no evidence of a topographic mapping of hippocampus neural tissue onto physical space. On the other hand, distinct environments are coded by different assemblies of place cells,

thus a place cell may be silent in one environment as it could be active in two distinct environments. Normally, the animal runs searching for food spread throughout the available maze and this could induce the idea that place cell firing is correlated to food location. However experiences have provided evidence that place cell firing is uncorrelated to goal location (Quirk et al. 1992).

In the search for factors that affect place cell shape, several experiences have been made where the rat is placed to forage in diverse shaped mazes. One of the first reported experiments regarded the behavior in linear versus open field apparatus. In one dimensional mazes, place fields seem to be directional i.e., the place field of a cell is not at the same maze position as the path is crossed in the two possible directions. In contrast, when placed in a maze where the animal can chose its running direction, the cell's receptive field reveals no direction correlation (O'Keefe 2006). Some authors attribute this directionality in linear mazes to the ability of some cells to code for future/past positions of the rat, which is known as prospective coding and retrospective coding, respectively. Besides the knowledge of current position, the capacity to program the next move or to recall the last ones is prone to be critical in solving spatial tasks (Frank et al. 2000).

The act of squeezing or enlarging mazes also has an effect on place fields shape, but in general it is not consistent between reports. In circular mazes, when the diameter doubles, less than half of the place fields suffer size increase while in general, receptive fields remap to unpredictable positions and shapes. When square mazes are enlarged into rectangles by sliding one of the walls, place fields in the square maze remain intact while in the new areas, new fields are created from cells that were silent in the square region (O'Keefe 2006). However other reports conclude that fields expand or split during experiences where the sides of rectangular boxes are extended (Moser et al. 2008). Recent trials with rat pups reveal that early cells' place fields also change after environment shape modifications (Langston et al. 2010).

Another relevant experience was made with a square maze that was progressively modified into a circular one, across an octagonal series of intermediate shapes, with the rat placed inside the maze. Almost all of the place cells, recorded simultaneously, switched abruptly in one of the intermediary mazes (roughly the same for all cells). Some cells lost/gain a field in the maze while others had their locations changed (Wills et al. 2005).

Place cells have also been recorded as the rat forages in the hairpin maze, which is a one dimensional maze with enforced changes in direction. Each arm of the maze is coded as a distinct one dimensional maze, thus suggesting that some internal mechanism resets the special code at each turn of the hairpin (Derdikman et al. 2009).

Rotation of the box or rotation of a cue card on the box wall, usually originates rotation of the field (relative to the box) in the same angle. If the lights are switched off when the animal is in the box, place fields are likely to remain intact. However, if the rat is moved and then placed back on the apparatus in the dark, then about half of the fields are changed (O'Keefe 2006). In contrast, experiences where the cue card is completely removed, produce no effect on shape, size, intensity and radial position on the majority of place fields. The maintenance of place fields' position after removal of cues provides support that something more complex than simple sensory information is responsible for the receptive fields of these cells (Quirk et al. 1992). Nevertheless, a common result throughout place fields' recordings is that they are more sensitive to changes in distal sensory clues than in proximal ones (Moser et al. 2008).

Independent studies have conveyed the notion that place cells are able to represent simultaneously information about not only place but also content of a trial. Concerning this finding, a relevant observation of firing patterns of place cells during experiences is that the receptive fields of a unit can change in rate and/or preferred space position when something in the environmental configuration or in the experience context is modified. This concept, known as remapping, is often divided in two separable items. Rate remapping corresponds to a change, relatively to a previous configuration, in the rate distribution along the receptive field. Global remapping corresponds to a more radical effect, such as the disappearance/appearance of the place field or its change in position and rate. The softer remapping is verified after slight modifications of the cues arrangement in a single location while global remapping occurs in situations where the animal moves between different scenarios or sometimes when environmental cues are markedly changed (McNaughton et al. 2006).

Subiculum has not been subject to the same scrutiny as other hippocampal regions. Interestingly, a recent report has found multi-peaked cells in this hippocampal region but more studies on subiculum neurons are needed to establish a reasonable description of their cellular properties (Kim et al. 2012). Place cells found in subiculum region have particular features, not shared with regular place cells from CA1, CA3 and DG. In the

subiculum, fields of spatial cells are broader (some occupy an entire maze with 74 cm in diameter) and their responses to environmental changes resemble those of grid cells more closely (Sharp 2006).

In conclusion, a widely accepted strategy for the neurons to code rat's position is through their Gaussian shaped receptive field which is consistently locked to certain regions of the environment – rate coding. Place cells and possibly grid cells, are considered as the neurons in charge for providing this spatial information to the rest of the brain.

1.2.2 Grid cells

Medial entorhinal cortex grid cells were reported by the first time in 2005, although some experimentalists had already suggested the presence of multi place fields in mEC cells (see (Fyhn et al. 2004) for a previous work which did not explored the cells hexagonal pattern). Grid cells are named after the firing pattern some mEC cells exhibit when the rodent forages for food in a maze. These particular cells are characterized by multi-peaked firing rate maps whose nodes are the vertices of a geometrically regular, triangular virtual lattice which tiles the entire recording maze (see Figure 1.4 c). Each grid map is characterized by three parameters (see Figure 1.5): phase or position of the grid vertices in the plane; spacing between the centers of activity and orientation defined by the lines that intersect the grid nodes (Hafting et al. 2005).

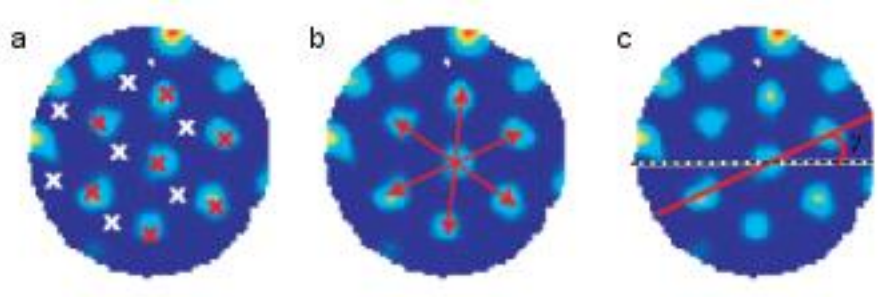

Figure 1.5 Grid cell parameters extracted from a typical firing map. a – Spatial phase: Cartesian coordinates of the grid vertices. In red (real data) and white (imaginary) are examples of the sets of phases from two grid cells. b – Spacing: average of the distances from any vertex to the six alternative adjacent ones. c – Orientation: smallest positive angle between the horizontal line crossing one vertex (dashed line) and the 3 lines passing through that vertex and the each one of other vertices (γ) (adapted from (Moser and Moser 2008)).

Grid cells in rodents have been found essentially in mEC, throughout all principal cell layers (II, III, V, VI) intermingled with other navigation related activity cells (Sargolini et al. 2006). More recently the same hexagonal firing patterns have been found in cells recorded from pre and parasubiculum (Boccara et al. 2010) (see orange regions in Figure

1.3).

Experiments show that for a complete activity coverage of the available environment it is enough to record, simultaneously and in the same neural tissue position, a small number of grid cells. In fact, the distribution of the vertex sites or grid phases has been reported to be close to uniform assuring the coverage of the maze. There is no evidence of topographic relation between the relative position of cells in the cortex and their receptive fields' relative position. Nevertheless, neural neighboring cells show fields with common orientation and spacing while their vertices location differs (Hafting et al. 2005). Another important feature, reminding us about the heterogeneity of the tessellation, is that the various nodes of one grid map can display disparate firing rates, ranging from above 30 Hz in some vertices to a few spikes in others. Concerning the orientation of grid fields, there is no pattern, to our knowledge, about the orientation distribution throughout the dorsoventral axis of mEC (Hafting et al. 2005).

In grid cells' firing maps, the spacing and size of the receptive fields increase from dorsalmost to ventralmost recording locations (Hafting et al. 2005; Sargolini et al. 2006). It is common belief that these multi-peaked spatial cells have been recorded before but failed to reveal their hexagonal tessellating pattern due to the unfortunate combination of small mazes with cells in ventral portions of mEC (Quirk et al. 1992).

Some experimental studies have been carried out in order to access the effect of environment changes on the receptive fields of grid cells. One example, made simultaneously with place cells in CA3 and grid cells in mEC's layer II, has showed that when rate remapping occurs in place cells, grid vertices remain stable in mEC cells. Moreover, when global remapping occurs, e.g., a different set of place cells is active, grid fields realign shifting their vertices location, but without losing their intrinsic spatial phase structure (Fyhn et al. 2007; Savelli et al. 2008). Similarly to cells in CA1, prospective and retrospective coding has also been reported for EC neurons (Frank et al. 2000).

According to one of the first reports on grid cells, the hexagonal like structure in their receptive fields is present when the rat enters in a maze for the first time (Hafting et al. 2005). However experiences with baby rats show that grid firing is not innate but takes a short period (4-5 weeks) of the early animals' life to acquire adult properties (Langston et al. 2010; Wills et al. 2010).

Reports of grid like firing cells are emerging in mammals besides rodents. Experiments with walking bats have revealed that grid cells are also present in the cortex of these animals (Yartsev et al. 2011). Moreover, grid cells have been observed in the visual cortex of primates, when those were subject to visual tasks with their head fixed (Killian et al. 2012).

Several models have been proposed for the emergence of these characteristic cells. The second chapter of this thesis is dedicated to a complete review of existent models for grid cell formation. Part of the work in this thesis consisted in producing this hexagonally distributed firing map in a simulated cell. In the fourth chapter, a computational model originally created for this purpose is described.

Gridness Score

Along with the first reports of grid cells throughout mEC, experimentalists needed to define a measure to classify cells in order to distinguish grid cells in an objective and universal fashion. This measure, named gridness score, was reported in its original form in Sargolini's supporting material of the 2006's paper (Sargolini et al. 2006). Some have published alternative methods, which have not been used as broadly as the original. With proved value for experimental reports, this measure is also useful for computational models for grid cell formation. In fact, it provides a tool for defining how simulated grid fields are in line with the cellular ones.

To evaluate how well the firing bumps of a cell form a grid structure, the spatial autocorrelation of the cell's rate map is computed. Let $f(x, y)$ denote the average firing rate of the cell at location (x, y) of the firing rate map. Each pixel of the autocorrelogram corresponds to the Pearson's correlation coefficient between each bin of the rate map and the correspondent bin in the same rate map shifted by τ_x on the x axis and τ_y on the y axis. The Pearson's correlation coefficient applied to lags (obviously discrete), τ_x and τ_y, is given by:

$$r(\tau_x, \tau_y) = \frac{n\sum f(x,y) f(x-\tau_x, y-\tau_y) - \sum f(x,y) \sum f(x-\tau_x, y-\tau_y)}{\sqrt{n\sum f^2(x,y) - \left[\sum f(x,y)\right]^2} \sqrt{n\sum f^2(x-\tau_x, y-\tau_y) - \left[\sum f(x-\tau_x, y-\tau_y)\right]^2}}$$

, where the summations are over all n pixels in $f(x, y)$ for which rate was estimated for both positions: (x, y) and $(x - \tau_x, y - \tau_y)$ (only accounted for lag pairs such that $n \geq 20$). In

other words, the goal of this tool applied to firing rate maps is to measure the amount of correlation between the firing rates in any two positions of the maze, separated by lags τ_x and τ_y, attributing that correlation value to position (τ_x, τ_y) of the autocorrelogram.

In the normalized autocorrelogram map of a cell, only the central ring region is considered: excluding the central peak of the autocorrelogram[1] and including the closest surrounding peaks (ideally six). Then, other maps are generated by performing rotations of the ring map with center on the map central point by angles from 0º to 180º (because of the mirror symmetry of the autocorrelation), by steps of 6º (or less). For each one of the rotated maps or matrixes, a correlation value is computed between them and the original non rotated map.

Finally, the measure evaluating how grid a cell is, is expressed as the difference between the minimum correlation at 60º and 120º (where a peak correlation would be expected due to the triangular nature of the grid) and the maximum correlation at 30º, 90º, and 150º (where the minimum correlation would be expected). In Sargolini's report, cells were classified as grid cells whenever their gridness score was greater than 0, however other reports have provided higher thresholds for this categorization such as 0.30 (Langston et al. 2010). Denoting by $rrot_\alpha$ the correlation of the original and the rotated ring map by α degrees, the formula for computing the gridness score of a map is given by:

$$Gridness\ Score = \min\left(rrot_{60^\circ}, rrot_{120^\circ}\right) - \max\left(rrot_{30^\circ}, rrot_{90^\circ}, rrot_{150^\circ}\right).$$

1.2.3 Other spatial cells

Head-direction cells discovery dates from 1990, when Taube and colleagues reported the existence of cells whose firing was highly correlated with the direction of the animal's head, with tuning curves stable across different trials (see Figure 1.4 b) (Taube et al. 1990). The first recordings were made in the postsubiculum region which corresponds to the dorsal presubiculum. However, recent reports provide evidence of head-direction cells also in parasubiculum and in EC layers III to VI (see blue regions in Figure 1.3).

These cells activity can go from low rates (0.5 Hz) up to a maximum value in the range 5 to 40Hz. Experiments show that in the same recording location the distribution of their

[1] Notice that by construction, the normalized autocorrelogram of a firing rate map has value 1 on its center – corresponding to zero lag for each coordinate – and doubled sides length, when compared to the rate map.

preferred directions is close to uniform. In EC, head-direction cells are found together with grid cells. Conjunctive cells have also been found in mEC, gathering properties of place (grid like) and head direction coding (Sargolini et al. 2006).

Interestingly, head-direction cells recorded in distinct environments have tuning curves displaced by the same degree amount. More precisely, the preferred directions on one setting are rotations in the same angle of the preferred directions on another environment (Wills et al. 2010).

Regardless of combinations of the three already mentioned, the fourth most important space cell has a pattern of firing related to the borders of the maze where the animal is located (see Figure 1.4 d). Border cells first extensive description is from 2008 although their existence had been previously predicted by navigation related models. These cells are present in all mEC layers and parasubiculum. The tuning of this cells firing can be set to a wall in one direction, two sides of the maze, a straight line parallel to a wall (not contiguous to it) or to the set of all the maze borders, for example in a circular arena. Just like head-direction cells, border cells also rotate their preferred region of firing when the maze is subject to a cue card rotation (Solstad et al. 2008).

1.2.4 Ontogeny of spatial cells

Soon after the discovery of the various spatial cells probably engaged in some part of the navigation process, the need for an ontogeny characterization of those cells emerged and studies with newborn rodents gained relevance.

Place cells are shown to reach adult levels performance by the first 4-5 weeks after birth, however at younger ages some animals exhibit already consistent receptive fields between trials. After that time, information content or coherence of place fields do not increase throughout the place cells subpopulation (Langston et al. 2010; Ainge and Langston 2012).

Grid cells reach adult levels after place cells, while head-direction cells are completely active and tuned even before the pup is taken from the nest for the first time. (Langston et al. 2010; Wills et al. 2010; Ainge and Langston 2012). There are no reports (to our knowledge) on the development of border cells' specialization throughout rats' life.

1.3 Neuronal dynamics

When modeling a single neuron or a group of connected neurons, suitable types of mathematical dynamical models should be adopted, in accordance with the cellular and temporal detail required for the a specific situation.

As previously showed, a typical neuron is divided into four specific sections: the soma, the dendrites, the axon and a set of synapses (recall Figure 1.2). Some mechanisms require the biophysics activity to be computed separately for each compartment, other do not demand such division. In the work developed for this thesis the compact approach has been used, which intends to model a neuron as a single compartment unit.

Models with spiking neurons require detailed analyses and are biologically compliant; they range from complex dynamical systems of differential equations (Hodgkin-Huxley model) to simpler and more user friendly versions. Users may favor spiking models if the time of each spike or the oscillatory activity of the neurons membrane is of relevance for the study. Otherwise, firing rate models are preferred, with less variables to tune and simpler in their analyses (Dayan and Abbott 2001).

Nevertheless, before going through the established mathematical formalism for cells activity, a biophysical detailed description of the mechanisms behind an action potential urges.

The action potential

A neuron cell state of activation is measured by the electrical potential difference between the intracellular and the extracellular medium, which is called the membrane potential of the neuron. This charge is due to the presence of ions in both sides of the membrane such as sodium (Na^+, mostly extracellular), potassium (K^+, essentially intracellular), calcium (Ca^{2+}) and chloride (Cl^-). A lipid bilayer forms the membrane of the cell (3 to 4 nm thick) which, by its molecular structure, does not allow ions to cross over it, being thus responsible for the maintenance of the ionic gradient.

The distribution of the ions, at resting state, is responsible for a negative difference of potential between intracellular and extracellular mediums (around -70 mV). By convention, the medium submersing the cells has zero potential and thus the interior of the cell is charged at -70 mV. At rest, the cell is said to be polarized because an excess of

negative ions exist inside the cell close to the membrane and positive ions lie in the outer side of the membrane.

Specialized proteins exist located in the lipid bilayer membrane of the cell. Such proteins are crossed by pores which allows for ions to flow in and out of the cell – ion channels. These gates open and close in response to voltage changes, they are voltage gated chemical synapses. Normally these channels are ion selective, controlling and regulating ion gradients. Others synapses exist, called electrical synapses, which form gap junctions and intermediate the passage of ions and small molecules from one cell to another, with no direction defined. When positive ions flow inside the membrane (or negative ions flow outside) the cell is said to be depolarized as its membrane potential gets less negative. If the membrane potential gets more negative (by the outflow of positive ions or inflow of negative ones) the cell is hyperpolarized.

The action potential (spike) is a rise and fall pattern in a neuron's membrane potential, of about 100 mV, which indicates the transmission of an electrical signal to the neuron(s) connected at axons terminals. In a more biophysical approach, the process is triggered by a depolarization of the neuron above a certain threshold that sets the opening of sodium channels. Being more concentrated outside the cell, Na^+ ions flow inside the cell depolarizing the neuron even more. At higher membrane potential voltages, the sodium channels close and the potassium channels open allowing the outflow of K^+ ions. This loss of positive ions turns the neurons charge more negative again and the ions gradient gets back to resting values while the potassium channels end up closing too. This fluctuation lasts about 1 millisecond: initiates at the soma and follows through the axon until it reaches postsynaptic neurons by synapses and sends its message. If in addition to the Na^+ flow, a transient Ca^{2+} current is present, then a slow and temporary depolarization of the membrane potential occurs. In this case, instead of a single spike, the neuron fires a burst of action potentials, which resemble a sequence of faster spikes on top of an elevated membrane potential period. For tens of milliseconds after a spike, or a burst of spikes, the neuron crosses the refractory period during which it is not able to fire another spike (Dayan and Abbott 2001).

The cells depolarization that triggers the action potential may be obtained artificially by the direct introduction of an excitatory current, using an electrode, or due to the arrival of presynaptic electric signals. In a synaptic derived action potential, a presynaptic spike depolarizes the postsynaptic cell in the synapse terminal, leading to an inward flux of

calcium through synaptic calcium channels. When Ca^{2+} goes into the presynaptic cell it causes the release of vesicles which are full of neurotransmitters in the space – synaptic cleft – between the two neurons. Neurotransmitters are chemicals which are responsible for transporting signals from one neuron to the other such as glutamate – excitatory signals – and dopamine or GABA – inhibitory signals. The neurotransmitter approaches the postsynaptic neuron causing the opening of its channels. Different neurotransmitters activate different receptors which bind, by their turn, to different channels opening them (see Figure 1.2). This allows for the ion flux to cross the cells' membrane. For excitatory synapses, the most common receptors are AMPA and NMDA which are activated by glutamate; some inhibitory synaptic transmission is activated by GABA (γ-aminobutyric acid) neurotransmitters which activate $GABA_A$ and $GABA_B$ receptors[2] (Roth and van Rossum 2009).

In the following section we briefly present the canonical models for spiking neurons' activity, which are constructed taking into account the biochemical aspects just referred.

1.3.1 Spiking models

When using a spiking model, the user obtains (normally through numerical methods) not only the spike times, but also the oscillations of the membrane potential of the neuron, as a function of time. In the following lines one possible derivation of the best known spiking neural model is given, the integrate-and-fire model together with a brief reference on the complex Hodgkin-Huxley model.

Integrate-and-fire model

Neuron cell compartments are endowed with certain properties which influence the way electric membrane potential is affected by injected current. The passive properties of the membrane are associated with the fact that small injected currents produce membrane potential oscillations that evolve linearly (in relation to the amount of current injected) onto an asymptotic value. Some properties are those present in any circumstance, and can be derived based on the parallelism established between the membrane of a cell and a resistor-capacitor electrical circuit.

[2] AMPA, NMDA and $GABA_A$ receptors are ionotropic, that is, they directly induce the opening of channels which are permeable to specific ions.

The lipid bilayer, given its ability to maintain a sheet of positive charge on its outside and a sheet of negative charge on its inside, is commonly compared to a (parallel plate) capacitor. From physics, when a potential difference is applied to a parallel plate capacitor, it causes a certain amount of charge to flow in the plates. In the cell's case, the capacity of the membrane (C_m) tells how much charge (Q) the membrane can hold for a given membrane potential difference:

$$Q = C_m V_m .$$

This means that the membrane can store charge and release it in the form of current. The current that crosses a capacitor, I_C, is given by the derivative of its charge in relation to time:

$$I_C = \frac{dQ}{dt} .$$

The derivative of the equation $Q = C_m V_m$, together with the last relation, results in:

$$I_C = C_m \frac{dV_m}{dt} .$$

The membrane channels, turning the membrane permeable to ions are compared to the resistor in the electrical circuit with a certain resistance, also referred as the membrane resistance (R). In other words, the membrane resistance sets the opposition offered by the membrane to the flow of electric current.

Finally, the battery of the electric circuit, is compared to the ionic bumps present in the cell's membrane. When no current is injected in the cell, the battery is responsible for maintaining the membrane potential at -70 mV (-70 mV in the inside and 0 mV in the outside – the reference point). For example, potassium ions are more concentrated inside the cell than outside, thus they are prone to diffuse in the direction that sets their concentrations even. Potassium is able to cross the membrane by diffusion through potassium selective channels (not voltage dependent). Once K^+ leaves the cell, the cell's charge gets imbalanced and consequently the potential outside the cell becomes greater than in the inside. The current is not equal for all the ions because it depends on their electric charge, on the membrane potential and on the ionic concentration difference between inside and outside the cell. The membrane potential at which an ion's flow is zero, is called the equilibrium potential of that ion, E_{ion} (for example: $E_K \approx$ -80 mV, $E_{Na} \approx$ 50 mV, $E_{Ca} \approx$ 150 mV, $E_{Cl} \approx$ -65 mV).

The equilibrium potential of a membrane at rest (passive, without stimuli) is represented by E_L (L from leak) and its value is usually set at E_L=-70 mV.

According to Ohm's law, the current across a resistor is given by the difference in potential divided by the resistance of the resistor. The resistor potential drop is given by V_m - E_L and then, the current that crosses the membrane by the ion channels, I_R, can be obtained from:

$$I_R = \frac{V_m - E_L}{R}.$$

When there is current coming into the circuit (injected current, I_e) then by Kirchhoff's charge conservation law, the currents going through these two components of the cell (capacitor I_C, and resistor I_R) must totalize the total injected current, which results in:

$$I_e = I_C + I_R \Leftrightarrow C_m \frac{dV_m}{dt} = -\frac{V_m - E_L}{R} + I_e.$$

Multiplying both members in this last equation by the resistance, we obtain the leak integrate-and-fire differential equation for the membrane potential of a neuron:

$$RC_m \frac{dV_m}{dt} = -V_m + E_L + RI_e.$$

From this formulation, with a constant small current, we can deduce that the membrane potential will evolve exponentially towards an equilibrium, at $E_L + RI_e$, with time constant given by $\tau_m = RC_m$. With no injected current, the membrane potential will settle at E_L, also called the membrane resting value or membrane equilibrium value.

Active properties of the membrane are associated with the fact that high injected currents produce membrane potential oscillations that do not evolve linearly, in relation to the amount of current injected. Instead, the already referred action potentials are produced, reflecting a nonlinear behavior which is not well described by the above electrical circuit. In the leak integrate-and-fire model the mechanism of the action potential is inserted artificially by a rule. Accordingly, each time the membrane potential reaches some threshold value (V_{th}, commonly set at -50 mV), a rule for resetting the membrane potential to a resting value (V_{rest} or E_L) is added to the above equation.

$$\begin{cases} \tau_m \frac{dV_m}{dt} = -V_m + E_L + RI_e \\ V_m(t) > V_{th} \rightarrow V_m = V_{rest} \end{cases}.$$

This formulation assumes an instantaneous action potential event which represents a simplification of the biophysical phenomenon such is the one modeled by the Hodgkin-Huxley equations (described shortly). Nevertheless it is a plausible model for mechanisms that do not depend on a detailed mathematical description of the action potential.

The injected current I_e is often used for experimental procedures and theoretical studies to study the effect of a controlled current in the neurons activity. When modeling neurons activity, users may need in addition/alternative to introduce currents that better represent inputs provided by other neurons – synaptic currents. Synaptic currents can be included in the above model formulation, but with a time varying conductance that takes presynaptic spike times into account – synaptic conductance. These currents are often distinguished by the nature of their input to the neuron, defined by the synaptic reversal potential. For simplification purposes, excitatory synapses are commonly modeled with a reversal potential equal to 0 mV and for inhibitory synapses an accepted value is -80 mV.

The formulation of such scenario is as follows (Dayan and Abbott 2001; Ermentrout and Terman 2010):

$$\begin{cases} \tau_m \dfrac{dV_m}{dt} = -V_m + E_L + R\left(I_e - I_{syn}\right) \\ V_m\left(t\right) > V_{th} \rightarrow V_m = V_{rest} \end{cases}.$$

Note the different signs of the current terms in the dynamical equation. By convention, electrode driven currents are defined as coming inside the cell – positive sign – while synaptic and membrane currents are defined as going outside – negative sign.

Synaptic transmission

Here we describe the most common forms of synaptic transmission which can be coupled with the integrate-and-fire spiking model to account for variable synaptic conductances. The generation of an action potential by synaptic inputs is the result of synaptic conductance and, depending on modelling purposes, the mathematical implementation of such mechanism may use different approaches. A simple way to express the conductance for a synapse (or a group of synapses) is to assume that each time a presynaptic spike occurs, there is an instantaneous rise of the conductance of amount Δg (μS). In the absence of presynaptic spikes, the conductance, g, decays exponentially with time constant τ_{syn}. The dynamical equation and additional condition that represents this behavior, known as single exponential model, is the following:

$$\begin{cases} \tau_{syn} \dfrac{dg}{dt} = -g \\ t = t_{sp} \rightarrow g(t) = g(t) + \Delta g \end{cases},$$

where t_{sp} represents the time of the presynaptic spike.

Instantaneous conductance rising times are plausible for modeling inhibitory synapses and AMPA mediated excitatory synapses. But some postsynaptic currents, as those mediated by NMDA receptors, have slower rising time and are thus better represented by dual exponential synaptic conductance functions. In those cases, the time constants of the rise, τ_s, and decay, τ_d, periods are distinct and a normalizing factor, f, to account for an amplitude of Δg is included. The dynamics of the conductance can be described by a differential equations system:

$$g(t) = \Delta g \cdot f \cdot h(t) \text{ with: } \begin{cases} \dfrac{dh}{dt} = -\dfrac{h}{\tau_d} + h_r \\ \dfrac{dh_r}{dt} = -\dfrac{h_r}{\tau_r} + h_0 \cdot \sum_{t_{sp}} \delta(t - t_{sp}) \end{cases},$$

where h_0 is a scaling factor and δ is the Dirac's Delta function.

Synaptic transmission is not instantaneous. In fact, the electric charge flow through the axon, synapse and dendrite is subject to delays which may sum to several milliseconds. Delays can be incorporated in spiking models, affecting the synchronization and oscillation of its units' activity (Roth and van Rossum 2009).

Hodgkin-Huxley model

Inspired on the squid giant (because it is visible at naked eyes) axon, Hodgkin and Huxley derived a detailed model for the dynamics of the membrane potential of a neuron including its active responses (action potentials). In this model, three resistors and three batteries are considered, corresponding to the three types of ionic channels. One of the channels corresponds to the leak component, and represents mainly potassium channels present in the membrane which are not voltage dependent. This term has similar meaning of the leak term in the integrate-and-fire model. The other two are the sodium and the potassium active channels which have variable resistances, not obeying Ohm's law. The current derived by each one of these channels takes into account the conductance of the channel, specific for each ion (g_{ion}, which is the inverse of the channel resistance), and is

defined by:

$$I_{ion} = g_{ion}\left(V_m - E_{ion}\right).$$

The difference $V_m - E_{ion}$ is called the driving force by which the ions will diffuse through the neurons membrane. The differential equation for the Hodgkin-Huxley model then becomes:

$$C_m \frac{dV_m}{dt} = -g_L\left(V_m - E_L\right) - g_K\left(V_m - E_K\right) - g_{Na}\left(V_m - E_{Na}\right) + I_e .$$

However, to account for voltage dependent conductances, this differential equation is coupled with dynamical equations for the gating variables of potassium and sodium channels:

$$\frac{dm}{dt} = \alpha_m\left(1-m\right) - \beta_m m,$$

$$\frac{dn}{dt} = \alpha_n\left(1-n\right) - \beta_n n \text{ and}$$

$$\frac{dh}{dt} = \alpha_h\left(1-h\right) - \beta_h h,$$

In these equations, α and β are functions of the membrane potential, tuned to experimental data, defining the properties of the action potential.

These variables are used to obtained the values for the conductances in the following manner: $g_K = \Delta g_K n^4$ and $g_{Na} = \Delta g_{Na} m^3 h$, where Δg_K and Δg_{Na} are constants.

Additionally other channels can be added to this model in order to account for the generation of complex spiking patterns as bursts (Dayan and Abbott 2001; Ermentrout and Terman 2010).

1.3.2 Firing rate models

Models that neglect the effect of spike timing in their outcome or inputs, taking only rate of firing into account are called firing rate models. This approach is usually chosen when no short time scales are required. It assumes that information is coded in the rate of firing instead on the precise times of spikes. Firing rate models have simpler formulation than spiking models being in result easier and faster to compute.

In firing rate models the neuron(s) being modeled receives inputs in the form of rate (u) of the presynaptic units. The effect presynaptic activity has in a spiking neuron is coded in conductances together with respective driving forces. In firing rate models, this process has two steps. First, the synaptic input is obtained from presynaptic rates according to the correspondent connection strengths (w, dimensionless). In the second processing step a transfer function (f) is chosen for the conversion of total synaptic input (or current) into firing rate change. Transfer functions come in many flavors, but their rational is to map slow current (or negative) into small or zero (or negative, representing inhibition) change in rate and strong synaptic input into a bounded rate step to prevent excessively high output firing rates. Some possible choices for this activation function are sigmoid functions (such as the logistic function), the Heaviside function and the threshold linear function. Representing the output firing rate of the neuron as v, the firing rate equation becomes:

$$\tau_r \frac{dv}{dt} = -v + f(\sum_i w_i u_i),$$

where the sum is over all the i presynaptic neurons, connected to the output neuron. τ_r is a time constant which represents how fast the output firing rate incorporates changes of the input (Dayan and Abbott 2001).

For this version of the firing rate function, the room for variability lies in the argument of the activation function. Here, excitatory synapses and inhibitory synapses (determined by the signal of the weight parameter) can be incorporated, as well as time dependent weights and time dependent input rates.

The spatial models developed for this thesis and described in chapters 3 and 4 are: a spiking model to mimic the mechanism of phase precession and firing rate models which intend to provide a possible method for the formation of the hexagonally distributed firing nodes of a grid cell.

1.3.3 Synaptic plasticity

A neuron transmits electrical signals to other neurons and the choice of neurons to connect is in some cases defined by gene expression during the development of the animal. Frequently, the strength of those connections is not constant but plastic, and influenced by neural activity. Activity is known to be responsible for the establishment of new points

of connection (spines) or the deletion of others, between connecting neurons (van Rossum et al. 2000). By their turn, recent studies suggest that spines play a critical role in controlling the maximum weight of a synapse (O'Donnell et al. 2011). Memory coding is made precisely on the connection strength between neurons where synaptic plasticity, experienced during learning, is thought to provide the basic mechanisms for the storage of information.

The simplest form of a plasticity rule was suggested by Hebb in 1949 and is still commonly employed. His idea is that if two neurons are repetitively active simultaneously then the connection between them is strengthened. Later the rule was generalized and applied also in the decreased of connection strength between neurons which activity is not consistently coordinated.

When postsynaptic receptors are constantly desensitized, less transmission of ions is made and the response of that synapse decreases – this is called synapse depression, and basically means that the synapse strength has been reduced. On the other hand, if vesicles are successively releasing neurotransmitters in the synaptic cleft, then channels are constantly being activated. This allows for an increase of the synapse efficacy called synapse facilitation, for short term effects, or potentiation for long term effects.

Detailed short term synaptic plasticity (facilitation and depression) effects are usually modeled by the dynamics of available synapse resources. Short term effects are commonly associated to short term memory which is not directly related to the type of learning addressed in this thesis.

When pre and postsynaptic neurons are simultaneously subject to a period of high/low activity, their synapse can experience a long period of augmented/decreased synapse strength. These longer time effects are called long term potentiation, LTP, and long term depression, LTD. Their computational implementation is usually done using conductance as a function of presynaptic spike times for spiking units, or connection strengths dynamics in firing rate models.

Modeling synaptic plasticity

In this subsection, a brief approach to the mathematical formulation of the plasticity rules mentioned above is given. For simplification only one synapse weight is represented throughout the equations, which can be straightforwardly extended to account for arrays

of synapses. In plasticity models for firing units, firing rate is usually a normalized variable in order for the equation to be dimensionally coherent.

One of the simplest rules is the Hebb's LTP mechanism where the weight (w) changes as a function of pre and postsynaptic rates (u and v respectively):

$$\tau_w \frac{dw}{dt} = \alpha v u \,,$$

where τ_w is the time constant of the weight change and α is an optional scaling constant. In this formulation, the amount by which the synapse weight is incremented is set by a correlation measure between pre (input) and postsynaptic (output) signals, replicating the well-known statement: "neurons that fire together wire together".

In a simpler LTP form, the synapse weight can be set to increase as a function of the presynaptic rate alone:

$$\tau_w \frac{dw}{dt} = \alpha u \,.$$

For a combination of both LTP and LTD effects, the covariance rule is often used allocating the weight change to the difference of the pre and postsynaptic rate from some threshold values:

$$\tau_w \frac{dw}{dt} = \left(u - \theta_u\right) \cdot \left(v - \theta_v\right) .$$

Here θ_u is the rate threshold for the input and θ_v is the rate threshold for the output. The inadequate effect of potentiation obtained by this rule when both neurons are silent is overcome if one of the threshold values is set to zero[3]. If only the input (output) threshold is set to zero, then the shift between potentiation and depression effects is triggered only by the postsynaptic rate (pre) and the presynaptic rate (post) acts as a scaling factor. If both thresholds are set to zero, the original Hebbian rule is obtained.

Just like all the rules mentioned so far, this formulation of LTP and LTD is not stable and requires some conditions to assure that the activity and thus the weights do not grow unbounded. An alternative is to use sliding values for θ_u and θ_v, adjusted to pre and

[3] The covariance designation comes from the fact that if the thresholds are chosen to match the respective firing rate average values and the output is written as the product of input and weight, the two rules produce the same average rule. This average rule, for a vector of inputs, states that change in weights is the input covariance matrix multiplied by the weight vector.

postsynaptic activity, such as in the case of the Bienenstock-Cooper-Munro (BCM) rule. Interestingly, this weight modification rule models with great accuracy real situations although the rule has no direct equivalence with biological mechanisms.

Another common rule for long term synaptic plasticity, modeled only with spiking models, is the spike time dependent plasticity (STDP). Although not employed in the models described in this work, this formulation is worth to be referred for its unquestionable importance when writing about synaptic plasticity. STDP states that the strength of a synapse is a monotonically decreasing function of the time between two consecutive spikes, one of the presynaptic neuron and the other of the postsynaptic neuron (t_{pre} and t_{post}, respectively). In particular, for $t_{pre} - t_{post} < 0$ ($t_{pre} - t_{post} > 0$), the synapse is potentiated (depressed) as a decreasing function of this difference. As the majority of enunciated rules for firing rate models, STDP must also be implemented together with limiting constraints or reducing the potentiation amount as the weights increase, for preventing weights to grow indefinitely (Dayan and Abbott 2001; Roth and van Rossum 2009).

1.4 Phase coding

Another coding mechanism is thought to exist related to population level rhythmic signals which are observed in the electroencephalogram (EEG) signal. Exploratory activities during rat's motion in an environment (like walking, running, swimming) are accompanied by an oscillatory activity pattern in the hippocampus' EEG with a frequency range from 6 to 12 Hz – the theta rhythm (Buzsaki 2002). The generation of theta waves is in part attributed to the medial septal nucleus which projects to hippocampal regions (Amaral and Lavenex 2006). Experimentally, if a set of electrodes is placed in the rat's hippocampus recording spike trains[4] of the neural population, the total smoothed activity representation should exhibit a sinusoidal pattern with frequency between 6 and 12 Hz. As mentioned in section 1.1, some cells, especially inhibitory neurons, show a rhythmic electrical activity, at the frequency of the theta rhythm and are thus called theta cells (O'Keefe 2006). The alternative coding mechanism emerged in the 90's, after several reports provided evidence that place cells firing times showed selectivity regarding the

[4] An array of consecutive spike times of a cell is commonly termed a spike train.

phases of the theta rhythm. Specifically, as the rat runs across place cells' receptive fields, spiking occurs at progressively earlier cycle phases of the theta rhythm (see Figure 1.6).

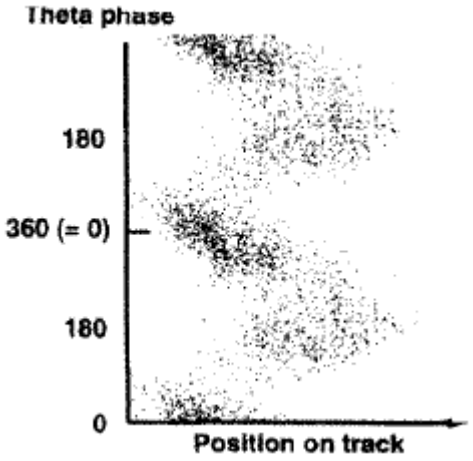

Figure 1.6 Spike times theta phase for a CA1 pyramidal cell as a function of rat's position in the linear track (triangular maze "linearized"). The position axis extends from 0 to 60 cm and the motion of the rat was from left to right. To better illustrate the phase advance of the spikes as the rat crosses the CA1 cell place field, the data for one cycle is repeated filling 2 cycles of the theta rhythm. Accordingly, phase values range from 0 to 2 completed theta cycles (720º) (adapted from (Skaggs et al. 1996)).

The detection of this complex pattern, named phase precession, generated a new form of spatial coding – phase coding. Their supporters claim that phase coding might be a strategy to refine the location primarily derived by rate coding, the more traditional approach (O'Keefe and Recce 1993; Skaggs et al. 1996). This is because, in a straight line, a Gaussian curve has two positions with the same rate intensity, but the advance in phase will be higher at the exiting compared to the entering of the receptive field, allowing then to distinguish between the two (which would not be possible with the rate profile alone). In the third chapter an original plausible model for the emergence of the phase precession effect developed for this thesis is presented in detail.

2. State of the art

Several models for the phase precession effect or the formation of grid cells' firing patterns have been proposed. Interestingly, some of the base ideas present in literature models for grid cell formation appeared before grid cells were actually found.

One of these ideas started with a model for path integration mechanism and place cell formation which used cells recurrently arranged in a continuous attractor network (Samsonovich and McNaughton 1997). This model also exhibits a phase precession effect due to a time advance in updating neural activity positions relative to the real spatial position of the animal. Moreover, the toroidal topology of place units' recurrent connections had an unexpected effect in longer mazes: a multi-peak firing pattern grid cell.

The other idea is that the interference of two oscillations with similar frequencies produces a firing pattern which can both explain place cell formation and phase precession effect ((O'Keefe and Burgess 2005), one dimension). However, in sufficiently long trajectories, several firing nodes appear instead of just one, which also turned this approach into a plausible one for the generation of grid cells' firing pattern formation.

These two classic models have generated two distinct lines for spatial models, either for phase precession effect or for grid cell firing patterns: continuous attractor networks (CANs) and oscillations' interference (OIs). In the following section, a brief introduction on the emergence of each of these class of models is provided, starting with a contextualization of path integration and the associated cognitive map. In the subsequent two sections a short review on existent models for phase precession is provided followed by a more complete description on existent models for grid cell formation.

2.1 The emergence of two model classes

In 1978, probably with an additional inspiration from the newly place unit cells recorded throughout the hippocampus proper, a possible way for a cognitive map of the environment to be located in the hippocampus was suggested. In the cognitive map model, DG, CA1 and CA3 are engaged in collecting input environmental data, converting it to

place units. Place units are, by their turn, connected with each other in an organized pattern defined by information about the direction and distance between their receptive fields. At that time, they were already assuming the existence of neurons providing directional information in the hippocampus, head-direction cells, which were found more than 10 years later. Theta rhythm role in the navigation system was also already relevant. In DG, theta frequency is thought to provide a timing pulse in the output signals to CA3. In a later stage, theta rhythm plays a part in the switching of excitation from one position in the map to another. CA1 field is also the locus of the misplace system, which basically accounts for exploring new environments, signaling the presence of something new in some place or the absence of something that was usually there.

According to the authors, this cognitive map can be used in several ways to control motor outputs. As the animal feels sleepy, for example, memories previously created about home are emphasized, exciting place cells coding for the nest position over the others. Cells coding for current position are excited by the rat's position. As a result, the motor program which activates simultaneously these two units is called and activated, guiding the animal from the actual position to the nest location (O'Keefe and Nadel 1978).

Path integration basically states that as the animal moves from a base point, inputs coding for direction and speed of self-motion are computed to derive the trajectory followed since the initial base. As previously mentioned, there is evidence that animals are in fact able to estimate their current position relative to a starting point based only on internal indicators, such as vestibular and proprioceptive[5] signals, sensed during the journey. Experiments show that even after all the position cues have been removed or the lights have been turned off these animals are still capable of returning to their homes, which provides an extra support for the path integration mechanism (Burgess and O'Keefe 1998).

Although not directly linked to the work developed for this thesis, path integration ability is commonly assumed by alternative models for phase precession and grid formation (described shortly).

[5] Relative to the sense of position, location, orientation and movement of the body and its parts.

2.1.1 Continuous attractor networks

In a general network attractor model, a grid map corresponds to a stable firing state (attractor state) which is maintained by recurrence. Each attractor state corresponds to a configuration of cells' activity state that is stable if no input (motion) is introduced to the net. This means that, if the rat is still, the neural configuration will accordingly remain intact. Overall, attractor networks used in models of grid formation are continuous, in the sense that between two stable state configurations there is always a third. The scale at which real space is coded in the cells is controlled by external input and by the relation between the rat speed and the speed of the activity bump moving on the neural layer. Attractor models are generally robust to noise and can store several attractor states (McNaughton et al. 2006).

Classical model for path integration – one dimension

Five years after the report of head direction tuned cells, a one dimensional attractor map model for encoding head angular velocity signals was proposed (McNaughton et al. 1991). In this model, cells tuned for different head direction angles are disposed conceptually in a circular arrangement, ordered by their preferred angles[6] (see Figure 2.1 a). The weight of the excitatory connection between two units is a decreasing function of the difference between their preferred angles. At each point of the trajectory, the activity profile in the disposed cells is concentrated in a region of the ring, centered on the cell tuned to the current direction of the rats' head (see Figure 2.1 b). Because of the connectivity scheme and inputs from the vestibular system, as the rat moves its head, this bump of activity slides on the ring units in a continuous fashion (or quasi, because head-direction units are discrete). The direction of the slide is determined by a two dimensional array of angular rotation cells (in a hidden layer) receiving angular velocity signals and head-directional cells inputs. Units in this layer project asymmetrically to the left/right cells in the outer ring according to clockwise/anticlockwise motion signals, respectively (see Figure 2.1 b). Then, if the head rotates from 2 to 3 o'clock, the hidden layer receives excitation from the 2 o'clock head-direction cell and excites the 3 o'clock cell, inciting

[6] Head-direction cells code the direction of the animal's head. Nevertheless, models that take into account this type of spatial cells input to code direction of motion, assume head direction is highly correlated with direction of movement itself.

the neural activity to accompany the head angular motion. In the absence of head movement (e.g., no input besides random noise) those projections are assumed to be below the activation threshold of angular cells. In addition, and due to the connectivity design, the activity bump remains unchanged as it corresponds to a stable state of the network (see Figure 2.1 c).

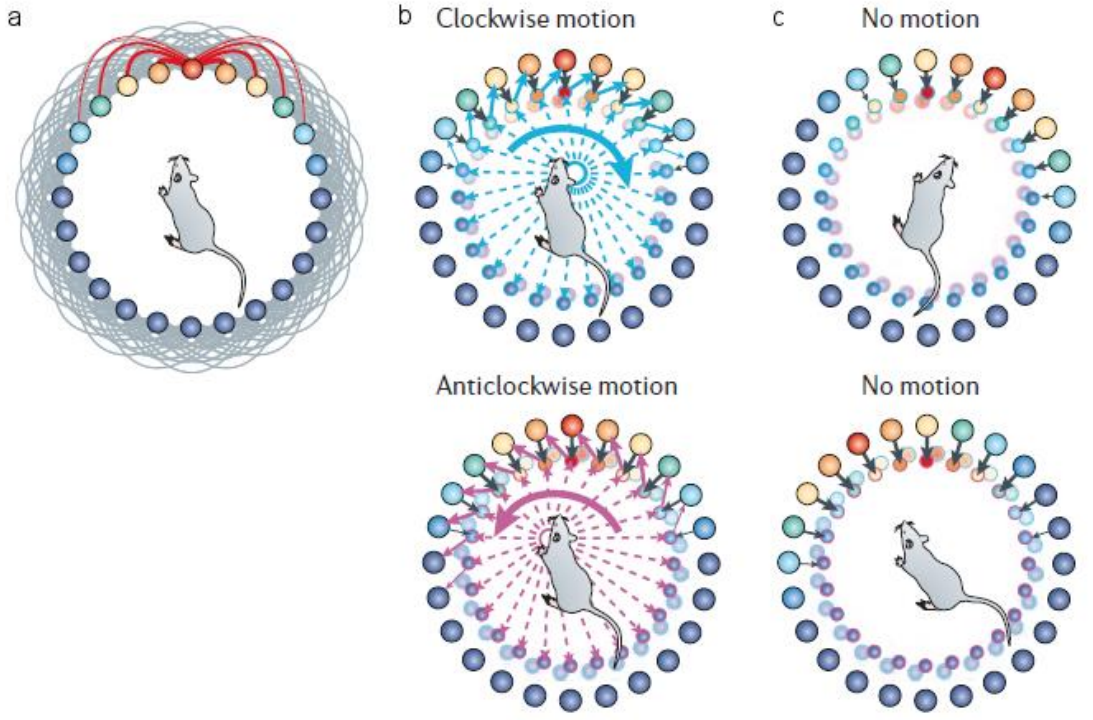

Figure 2.1 Ring attractor model for the head direction system. a – Diagram of head-direction cells organized in a circle, with connections reflecting their preferred head directions. b – In a motion scenario, head-direction cells project to the cells in the hidden layer (cells providing angular input about rat's motion) which project back in an asymmetrical fashion to left or right of the most active head-direction cell depending on the direction of movement of the animals head. c – In the absence of motion input, the activity of the head-direction cells layer is not sufficient to activate the hidden layer (adapted from (McNaughton et al. 2006)).

The mechanism briefly described – based on a ring attractor network – allows for the activity of the cells in the circle to represent online the directions faced by the head of the animal in an expedition, thus performing angular path integration (McNaughton et al. 2006).

Classical model for path integration – two dimensions

A fundamental model for path integration in a two dimensional trajectory was given in 1997 where head-direction cells and place cells were the essential processors (Samsonovich and McNaughton 1997). For their multichart map based path integrator (MPI model), the authors extended the one dimensional angular path integrator model. Here place units are connected through different schemes, originating several charts

which can be active in distinct environments. Thus, several maps can be stored using the same assemble of place cells. Through an attractor map concept a cognitive map was embedded in the model providing a reference frame endowed with reference location, reference direction, a metric system and a clock system. This frame is necessary for the internal representation of planar coordinates. For each map, a two dimensional set of quasicontinuous attractors exists, such that a small dislocation is enough to drive the state shift from one attractor state to another. Such dislocation will be smaller with the increase of map units' density.

When a representation of space is presumed to exist internally, a mechanism for updating that representation according with the rat's motion is required. For that purpose, the integration of velocity signals (speed and direction) is made over time in that reference frame. The weight of excitatory connections between cells in this layer is a decreasing function of their place field centers relative location. Global inhibition is inserted in order to prevent the activity from spreading out. The input array - providing position V, direction H and motion signals M - excites a certain portion of the cells in layer P. By their turn, place units project to the integrator layer I, tuned to the current head direction, exciting there a small region. Connections from this layer to the attractor network are offset by the same direction of active head-direction cells. This asymmetrical connectivity provides excitation to other place units, ahead of the currently active units, in the direction of motion. Together with the connectivity scheme in the place units' network, this results in a moving activity packet along the map in that direction (see Figure 2.2). The mathematical formulation of this model is as follows.

The P-I system is defined by the following system of equations for each iteration t:

$$\begin{cases} V_i^{P,t+1} = \left(1 - S_i^{P,t}\right) e^{-\frac{\Delta}{\tau}} V_i^{P,t} + \sum_{j=1}^{N} W_{ij}^{PP} S_j^{P,t} + \sum_{j=1}^{N} W_{ij}^{IP} S_j^{I,t} + \mu \sum_{k=1}^{n} e^{-\frac{\left(\mathbf{x}^t - \mathbf{r}_i^k\right)^2}{2\varepsilon^2}} \\ V_i^{I,t+1} = \left(1 - S_i^{I,t}\right) e^{-\frac{\Delta}{\tau}} V_i^{I,t} + \sum_{j=1}^{N} W_{ij}^{PI} S_j^{P,t} + \mathbf{v} \cdot \mathbf{b}_i \\ S_i^{P,t} = \theta\left(V_i^{P,t} - h_P^t\right), h_P^t : \sum S_i^{P,t} = M_P^t \\ S_i^{I,t} = \theta\left(V_i^{I,t} - h_I^t\right), h_I^t : \sum S_i^{I,t} = M_I^t \end{cases},$$

where i represents the i^{th} unit and N is the total number of units. V represents the dynamical activity (voltage), S is a Boolean variable signaling the occurrence of spikes and W is the connectivity matrix. Δ represents the time bin, τ is the potential time constant

and θ denotes the Heaviside function.

The sensory system (V), the head-direction system (H), and the motion system (M) are not explicitly simulated and are assumed to be consistent with the rat motion. μ represents the efficacy of the V to P connections, thus affecting the sensory input. The input from the V system takes into account a Gaussian function of the distance between the rat position $\mathbf{x}^t$ (the same as $\mathbf{x}(t)$) and the coordinate of the i cell on the k chart given by $\mathbf{r}_i^k$ (with some width ε).

The modulation of the I network by the head-direction system H is represented by $\mathbf{v}\cdot\mathbf{b}_i$, where $\mathbf{v}$ is a unit vector pointing in the direction of motion (representing the perceived direction of motion) and $\{\mathbf{b}_i\}$ is a set of random Gaussian vectors.

The activity in the I network is controlled by the motion system M. The total inhibition affecting the network P, h_P, is introduced to control the number of active units M_P at each time step. For the P network and the I network, the number of active units is a function of time given by:

$$M_P^t = A\cdot\theta\left[\cos\left(\frac{2\pi\Delta}{T}t\right)\right]\cdot\cos\left(\frac{2\pi\Delta}{T}t\right)+B \text{ and}$$

$$M_I^t = \theta\left[(C+D)\cdot\cos\left(\frac{2\pi\Delta}{T}t\right)-D\right]\cdot\left[(C+D)\cdot\cos\left(\frac{2\pi\Delta}{T}t\right)-D\right],$$

where T represents the theta cycle period. The parameters A, B, C and D were adjusted in accordance with data of theta cells population in CA1 (for P network) and DG (for I network). C and D also reflect the modulation of the I units by the motion system M.

Connections strengths between units in P network, from P network to I network and from I network to P network are all excitatory and represented by slow variables. These connections depend on the distance between the receptive fields of the units being connected (across all the n charts):

$$W_{ij}^{PP} = \frac{1+\eta_{ij}^{PP}}{2\pi\sigma^2}\sum_{k=1}^{n} e^{-\frac{\left(\mathbf{r}_{ij}^k\right)^2}{2\sigma^2}},\quad W_{ij}^{PI} = \frac{1+\eta_{ij}^{PI}}{2\pi\sigma^2}\sum_{k=1}^{n} e^{-\frac{\left(\mathbf{r}_{ij}^k\right)^2}{2\sigma^2}} \text{ and } W_{ij}^{IP} = \frac{1+\eta_{ij}^{IP}}{2\pi\sigma^2}\sum_{k=1}^{n} e^{-\frac{\left(\mathbf{r}_{ij}^k+\mathbf{b}_j\right)^2}{2\sigma^2}}.$$

In the above defining equations, η represents a static synaptic noise, σ is the width of the Gaussian function for the distances and $\mathbf{r}_{ij}^k$ is a vector connecting the units i and j on chart k (n is the total number of charts). The vector $\mathbf{b}_j$ is defined as a constant random vector

(the same as $\mathbf{b}_i$, for the head direction system) which represents the asymmetry in the connectivity scheme between the I network and the P network.

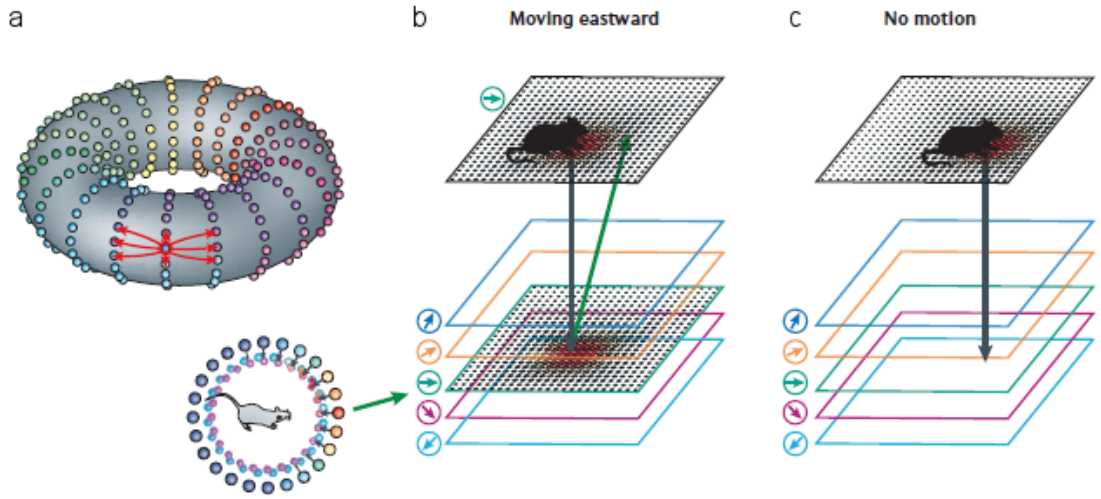

Figure 2.2 Extension of the ring attractor for a model for path integration in a two dimensional space. a - Toroidal topology of the synaptic matrix of place units is assumed. Connection strength decays with distance of receptive fields. b – Sensory stimulation activates the conjunctive layer tuned for the current direction resulting in the bump of activity's displacement. c – In the absence of input, the conjunctive layers are silent and thus the bump is static (adapted from (McNaughton et al. 2006)).

This mechanism just described works almost like a prediction method for the next position of the rat, assuming that the rat's head is not changing its direction in the current time step. The input layer is also responsible for correcting the cumulative drift errors emerging from this mechanism, allowing for the neural activity to reflect the rat's movements in a quasi-online basis. This time advance in neural tissue of the activity bump relatively to the actual movement of the rat, has been suggested as phase precession effect, flowing naturally as a side effect of the model. In particular, the activity bump moves ahead of the rat during each theta cycle and then jumps back to the real rat position in the onset of the next cycle (given that the time step is smaller than theta rhythm period).

To conclude about the place cell activity in this model, the authors state that individual activity has no meaning *per se*, but is acquired in the scenario where other place cells are active with it in a certain location. A constant exchange flow exists between real motion and neural activity, such that self-motion is updated and updates place cell activity (Samsonovich and McNaughton 1997).

Components of the cognitive map concept

In close relation to the above theory of path integration and the cognitive map, if the animal has already a cognitive idea of the environment he is in, then connections between

place units would be already established. If these connections contain information about distance and direction between place fields then physical motion would be sufficient to trigger the accurate sequential activation of position cells. Moreover, there is evidence that before adjusted to signal some external set of cues (for instance, in starting a goal task), place cells are driven by self-motion information solely, i.e. maintain their firing fields in the absence of external signals. Together these findings confirm that place cells are in fact the more suitable neural components (so far) to play the reference place role (Moser et al. 2008) (but see (McNaughton et al. 2006)).

Concerning the usefulness of the grid pattern to retrieve position, some have showed that the difference in phase maps of neighboring grid cells could be used to code for the rat's position in the environment (Fiete et al. 2008). However, the more consensual view is that, since their firing distribution is multimodal throughout the environment, grid cells are considered as part of the navigation distance-measuring device (Jeffery 2013; Moser et al. 2008; Fyhn et al. 2004).

In addition, velocity (direction and speed) inputs necessary to keep an online space representation in the brain are also available since head-direction cells with speed modulation have been reported (Sargolini et al. 2006). As to the recent border cells, they could play a part in the neural representation reset when the animal is placed in a new environment, driving the restructuring of the path integration process (Derdikman et al. 2009).

After the publication of the path integrator model mentioned above (Samsonovich and McNaughton 1997), some realized that if the environment could be sufficiently large, then the toroidal topology would originate the same cell to be active more than once in the same environment, with receptive fields arranged in a square like fashion. If the units disposed on the torus had a rhombic disposition instead of a squared one, then the resultant firing map would exhibit triangular arranged nodes, resembling typical grid cell maps.

2.1.2 Oscillations interference

In 2005, right after grid cells first report, the first model using interference of oscillations was suggested with a dual role: able to produce the effect of phase precession and also the triangular firing pattern of grid cells (originally thought as place fields due to a time

scale issue) (O'Keefe and Burgess 2005). For a one dimensional maze, the base assumption of the oscillation interference approach is the existence of two oscillation signals with distinct frequencies arriving at a cell. If one of the sinusoidal oscillations is at theta rhythm frequency f_θ and the other's frequency is slightly higher f_I, then their interference would predict a repeating series of firing fields, corresponding to the peaks where the cells' firing threshold would be exceeded (see Figure 2.3). The second oscillator f_I, with a higher frequency that theta's, is supposed to be modulated by the speed of the animal (on top of the theta frequency), increasing its frequency with the increase of running speed. The summation of the two oscillations is given by:

$$\cos(2\pi f_I t) + \cos(2\pi f_\theta t) = 2\cos\left[2\pi \frac{f_I + f_\theta}{2} t\right]\cos\left[2\pi \frac{f_I - f_\theta}{2} t\right].$$

The resultant sinusoid has a carrier frequency of $(f_I + f_\theta)/2$ and is modulated by $2\cos\left[2\pi \frac{f_I - f_\theta}{2} t\right]$.

At this point, phase precession is already evident: when firing, the output cell will prefer the upper phases of the oscillation cycles with frequency $(f_I + f_\theta)/2 > f_\theta$. In result, firing threshold will be reached in subsequent earlier phases of f_θ, as can be observed by the phase signaled in Figure 2.3. Whenever the two individual subthreshold oscillations are in phase, the resultant oscillation will be sufficiently depolarized to cause spiking activity. Because $f_I \neq f_\theta$, they will go out of phase again, resulting in silent activity. The envelope of such interference is modulated by $\cos [2\pi(f_I - f_\theta)t/2]$ (see yellow line in Figure 2.3). A complete cycle of the envelope sinusoid lasts for $2/(f_I - f_\theta)$ seconds (time period), and a possible resultant receptive field (if the cell would in fact reach firing threshold) would be crossed during a proportion (<1) of half that cycle time. Then, if s (m/s) denotes the rat constant velocity, the place field size would be proportional to $s/(f_I - f_\theta)$ meters. If the animal is moving at a constant speed and in a linear path, this mechanism is repetitive at constant lengths giving rise to periodic locations where the cell is spiking intercalated with non-spiking periods ($\cos [2\pi(f_I - f_\theta)t]$, note that this frequency is twice the envelope's frequency). Since spiking regions arise with time period $T=1/(f_I - f_\theta)$, then space distance between the grid field nodes (G) will depend on the constant velocity: $G = sT$ (called the spatial wavelength). So basically, different input oscillators' frequencies will produce grids with different spacing. Conveniently, if the second oscillator is modulated at a frequency above theta rhythm by coding velocity then, field size would be independent

of rat's velocity.

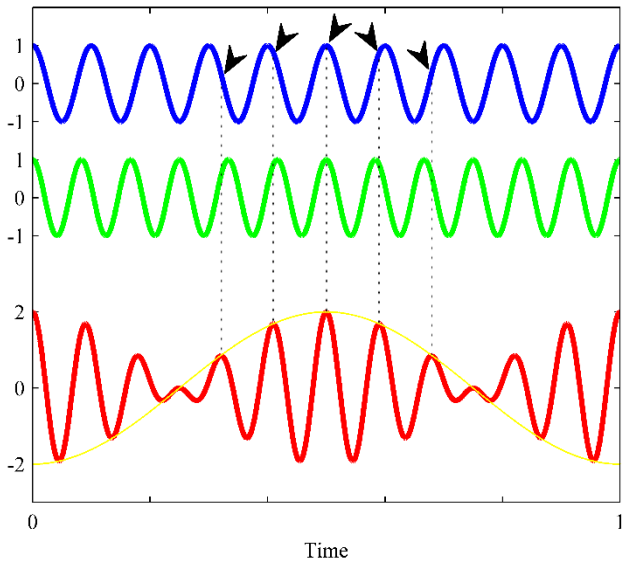

Figure 2.3 Interference of two oscillations with distinct frequencies. Blue signal is a sinusoid with 10 Hz and green sinusoid has 12 Hz of frequency. Their summation (red oscillation) has a sinusoid envelope with frequency 1 Hz, represented by the yellow curve. The red oscillation has a frequency of 11 Hz, which results in precession of phase relative to the theta frequency, indicated by the arrows. Time axis represents one second.

Hence, a direct prediction of oscillations interference (OI) models is that on a longer time scale (as happened in the CANs models history), the cell receiving the two oscillations would evidence not a unique but several receptive firing regions, with equal spacing distance. Before grid cells were found, this was actually a problem of a model which originally intended to mimic place fields and phase precession. However this side effect was a great insight which provided the basis of an oscillation interference model for grid cell formation.

Despite of all the attention this type of models have attracted and the subsequent models build on top of this one, interference of oscillations class of models show intrinsic biological incoherencies. Although the authors state the existence of biological theta signals impinging the same cell at slightly distinct frequencies, this feature is only transient and local, interfering on the results consistency of the model. The unsuccessful search of cells modulated at other frequencies that theta's, in the major hippocampal sources of inputs (EC and medial septum) made the authors suggest that this second oscillator could be received by the cell's dendrites, instead of directly in its soma (as is the case of the theta modulated input). In addition, neural oscillators are rather noisy, which disrupts completely the resultant envelope pattern (O'Keefe and Burgess 2005).

2.2 Previous models for the phase precession effect

One of the most well-known hypothesis/models for phase precession is grounded on the mechanism of interference between two slightly different oscillations, mentioned above (O'Keefe and Burgess 2005). Although widely accepted, this and other oscillation interference models (see also (Lengyel et al. 2003)) are grounded on the assumption that two consistent and distinct θ oscillators, with slightly different frequencies, exist in the hippocampus. However the existence of two independent θ oscillations is not corroborated by many independent experimental results (for review see (Buzsaki 2002)). Other models rely on synaptic properties, such as asymmetric connectivity matrices (Tsodyks et al. 1996) or synaptic plasticity (Baker and Olds 2007), but while elegant these models fail to account for the important experimental result that phase precession can be observed prior to any training of the animal in the maze. There is also the hypothesis that phase coding could be generated by intrinsic cellular properties in the entorhinal cortical neurons, and inherited by downstream structures such as dentate gyrus and CA fields (Hasselmo et al. 2009).

Using a different approach, the model by Bose and coworkers (Bose et al. 2000) relies on the interaction between two coupled neurons, one pyramidal (excitatory) and one interneuron (inhibitory), to show phase precession of place cells in region CA3 of the hippocampus. In this model, general independent oscillators are used to describe the neuronal dynamics which means that if one is turned off the other continues to exist. The interneuron's average firing frequency behaves as a new theta-independent oscillator generating oscillations at a fixed frequency, which is not supported by experimental results as already mentioned. A single input to the principal cell is sufficient to produce a reorganization of the network's dynamics, leading to a transient increase in the principal cell frequency. This increase generates phase precession.

2.3 Previous models for the formation of grid cells

Since the report in 2005 with the first characterization of grid cells, several computational models have been published aiming to provide plausible mechanisms to explain how hexagonal firing patterns could emerge within the activity of medial entorhinal cells (for

a recent review see (Giocomo et al. 2011)). Moreover, given the loop architecture of the circuits involving mEC and the hippocampal formation, interesting models describing how place fields can be generated from grid cells inputs have also been created (for a review see (Moser et al. 2008)). Experimental work required to properly disentangle the right direction (if grid cells are generated by place cells or if it is the other way around) is far from being simple.

In this thesis, the focus is given to the formation of grid cells based on place cells existence. The direction adopted is supported on two main reasons. The first concerns the development order, experimental work on rat pups provide evidence that adult like place cells precede adult like grid cells (Ainge and Langston 2012; Langston et al. 2010). The second reason concerns the firing patterns of cells. In fact, grid firing patterns are more robust to environmental changes while also exhibiting some generalizing ability. Additionally, their multi-peak firing pattern seems to be a more complex behavior than the unimodal distribution of place cells firing.

In the following sections we travel through the most relevant existent models of grid cells formation. This subsection is divided into three parts. The first two are within the classification already mentioned: oscillations interference models and continuous attractor network models. These two approaches are not exclusive and one can find in the literature models combining ingredients of both classes (Blair et al. 2008; Mhatre et al. 2012; Grossberg and Pilly 2012). A third class of models is also presented, whose main difference from OIs class and CANs class is the way weight matrixes are built. In this third class of models, hexagonal pattern emerges in the output cell's firing maps as a result of self-organizing mechanisms during learning.

2.3.1 Continuous attractor networks

This section intends to cover the major available models in the literature which are based on attractor networks dynamics to model the properties that characterize grid cells.

Spin glass model

In the subsequent year of the discovery of grid cells in rodents, one of the first published models focused on generating grid cells using continuous attractor networks (CANs), while also providing a mechanism for path integration. By construction, recurrence

between neurons and their topographic organization were 2 key assumptions for the model to generate perfect hexagonal firing cells. The putative grid cells are localized in a two dimensional neural sheet, disposed in a rectangular lattice (aperiodic connectivity), connected to each other with weights that vary according to the distance between them. This implies that their mutual interaction is symmetric and is constrained to neighboring cells.

In a first step, this spin glass model comprises the emergence of such a connection scheme for weights which is as follows. For a certain period of time there is a packet of 3 waves (equally oriented) that smoothly crosses through all cells within a band with orientation perpendicular to the randomly set wave packet orientation (between 0 and 2π). Out of that band, cells will fire at a tonic level which is set at 1. Cells with centers within the band see their firing rate increase to 2 or fall to 0 depending on the phase position of the 3 wave packet they fall into. So the firing rate of each cell, in this weight matrix generation part, is a function of their packet phase. Each traveling wave has some time to cross the neural tissue and change the firing rates of the cells affected. The weights are updated according to a simple rule: as the wave passes through a cell, its weights onto the coactive cells suffer a glimpse of the sinusoidal characteristic collapsed into them. So after a considerable amount of waves with distinct orientations had passed, the weights are expected to reflect concentric rings of high and low scales. The learning rate increases within each packet wave crossing but is resettled when a new packet wave arrives. According to the authors, this description is that of a spin glass model (for a contrary opinion check (Burak and Fiete 2006)) and represents a system where each initial configuration will in general converge to a global minimum energy state (with the help of noise) where the system meets stability. The cells are subject to a competition with their closest neighbors for neural space to settle. They eventually converge to the optimal packing layout which is known to be the hexagonal geometric shape.

After the symmetric recurrent weight matrix is computed, reflecting concentric rings of connectivity in topographic layout fashion, the second part of the model with a path integration mechanism takes place. The units of the system are integrate-and-fire neurons which activity is the reflection of their synaptic inputs with a noise term and a velocity input. The full weight matrix comprises also an asymmetric component matrix (inhibitory and offset of the symmetric one) which plays a part in path integration by translating the activity pattern across the sheet (in a similar way as the MPI model). So every time this

inhibition is activated, the current local of activity will be slightly inhibited and a set of others cells in the portion of space which was not inhibited is activated. Moreover, rat's position is encoded by ensembles of cells with distinct scales and/or orientations (Fuhs and Touretzky 2006). Regardless of the lack of biophysical support for the mechanism used to compute the weight learning rule in this model, traveling waves have been widely and successfully applied in the context of visual cortex. However, in contrast to what is known about grid cells in mEC, visual cortex cells show a topographic relation between neural and space coordinates.

In a 2006 short publication, is stated that using the spin glass model in a simulated rat trajectory, with reality inspired changes in velocity (meaning speed and direction), the cell's firing map obtained does not exhibited a multi-peaked arrangement as experimental data does. According to their study, when the rat is moving around inside the maze and the velocity information is not being correctly updated in mEC units, then the model fails to work. This happens because rat's movements in space are not accompanied by correspondent translations in the neural pane (Burak and Fiete 2006).

McNaughton's 2006 PI model

In 2006, a review for path integration proposes another attractor model that concerns the early emergence of grids, which can be separated in four steps. In the early pups, there is a "teaching" layer which has Mexican Hat type connectivity (center-surround profile) between its units (Turing layer). There also exists a set of modules similar to a cortical column where connectivity is high within each module but weak between modules. Each synapse weight obeys one of two distinct learning rules. The first is a competitive learning rule and operates in the connections between the teaching layer and the modules. This rule sets the occurrence of LTP or LTD, dependent on the activity of the cell. While each module starts with random connections from the Turing layer, this one is alternatively visiting all possible grid phases. This way cells in the modules would become tuned to the different phases of the grid, without exhibiting any topographic relation between them. The other learning rule operates in the connections within the modules and is a Hebbian like LTP. This rule will strengthen the connections between units that are tuned to similar phases of the Turing layer. Therefore, within each layer, a synaptic matrix with a torus shape would emerge, setting the hexagonal grid cell firing in the adult animal (without requiring topography relations in the neurons of the adult animal). Once this

process is completed, the teaching layer disappears or is allocated to other functions (McNaughton et al. 2006). This idea for a model seems to assume that each module is attached to a different maze or class of mazes memorized by the animal. However, if the teaching layer vanishes at some time in the animal's life, then he will not be able to learn new classes of mazes from that time on.

Artificial Neural Network

In 2007, another model for generating grid cells activity patterns together with a path integration mechanism is published, suggesting for the first time a role for the projections from hippocampus place cells to mEC lower layers. They suggest an artificial neural network with grid cells synapses' weights obtained from a Gaussian function of the distance on a torus, exciting neighbors and inhibiting distal cells (assumes topography in grid cells disposition). The recurrent connectivity structure is that of a twisted torus in order to generate a triangular tessellation. Cells are firing rate units with a linear transfer function of the synaptic input. In contrast to other models where velocity is provided from cells to cells, here strength connections incorporate the simulated animal velocity. This allows for a transformation of the rat's motion into neural activity. The correction of large path integration errors is mediated through Hebbian learned connections between a simulated place cell population and the grid cells population. All the grid cells are connected to an external cell that computes their summed activity and is responsible for the stabilization of the overall neural activity. As the simulated animal moves, a bump of activity slides on the grid cell population's weights such that the same synapse may change between excitatory and inhibitory regimes. The designation of an artificial neural network comes from (at least) the synaptic nature change and also from the velocity affecting directly the synapse weights (Guanella et al. 2007).

Single neuron (SN) response

A different model for PI and grid formation was suggested in 2009, employing spiking units and firing rate recurrently connected neurons. In contrast with previous ones, in this approach, external sensory cues frequent update is not a requirement. This model aims to provide evidence that accurate velocity inputs integration is possible under certain conditions related to: the topology and size of the network, distribution of the weight connections and the noise present in cells firing rates. In this model, the neurons activity is specified by:

$$\tau \frac{ds_i}{dt} = -s_i + f\left(\sum_j W_{ij} s_j + B_i\right),$$

where: f represents the linear threshold function, τ is the time constant of the neural response, W_{ij} is a recurrent weight matrix from neuron j to neuron i and B_i represents a feed-forward input to neuron i.

A patch of neural tissue is filled with neurons disposed in a regular triangular lattice (with $n \times n = N$ cells). The units' geometrical disposition is thought to be driven by a global feed-forward excitation and inhibitory projection toward each neuron, coming from a surrounding ring of neural local neurons. This pattern, formed at the neural level, is coupled with rat´s velocity in the sense that each neuron will have a preferred direction. W_{ij} is given by:

$$W_{ij} = W_0\left(\mathbf{x}_i - \mathbf{x}_j - l\hat{\mathbf{e}}_{\theta_j}\right) \text{ and } W_0(\mathbf{x}) = \mathbf{a}\mathbf{e}^{-\gamma|\mathbf{x}|^2} - \mathbf{e}^{-\beta|\mathbf{x}|^2},$$

where x_i is the location in the sheet of neuron i and θ_i denotes its preferred direction. The weight matrix assumes a topographical organization of units and has a center-surround shape located at a shifted location relative to the position of its units. This shift is related to the preference in direction of the input unit ($\hat{\mathbf{e}}_{\theta_j}$ is the unit vector pointing along θ_j). The parameters γ and β are tuned according to the periodicity of the lattice. Moreover, a is set to 1, resulting in a local surround inhibitory connectivity.

Direction preferences are distributed randomly throughout the population of neurons and may be explained by velocity tuned projections from head direction single cells. Accordingly, each 2×2 block of neurons is defined as to span all possible preference directions, restricted to W, N, S or E. The idea of the model is that each cell synapses form a ring of inhibition upon other cells that are slightly ahead of the cell, in its preferred direction. So the bumps formed are not dependent on the rat's trajectory but on the direction preferences of the activated cells. For the simulation of the model, data was taken from a rat's real trajectory over a circular maze with diameter length of 2 meters. From this data they obtained inputs referent to velocity which were injected in the simulated network neurons. The feed-forward input to neuron I is defined as:

$$B_i = A(x_i)\left(l + \alpha \hat{\mathbf{e}}_{\theta i} \cdot \mathbf{v}\right),$$

where $\mathbf{v}$ is the velocity vector of the rat, parameters l and α determine the speed of the

neural activity flow, for a fixed speed of the rat, and function A determines the spatial modulation in the inputs to the neurons.

In the model with a periodic network – torus topology for connectivity – the results were that path integration was accurately derived. The aperiodic network regime, that has a sheet topology for connectivity, raises the problem of borders already addressed in previous models. Here the authors opted to maintaining the strength of recurrent connections throughout the neural sheet and gradually reducing the external excitatory input (tapering). For periodic boundary conditions, A=1 and for the aperiodic network A is given by:

$$A(\mathbf{x}) = \begin{cases} 1 & if \ \ |\mathbf{x}| < R - \Delta r \\ \exp\left[-a_0 \left(\dfrac{|\mathbf{x}| - R + \Delta r}{\Delta r} \right)^2 \right] & if \ \ R - \Delta r \le |\mathbf{x}| \le R \end{cases},$$

where R is the diameter of the network, a_0 is a constant parameter, Δr defines the range of radii for the tapering in the inputs. This way the firing pattern is not distorted but neurons are less active near the borders, proportionally to the external input.

The spiking units were generated based on the above equation for neuron dynamics such that at each time step $[t, t + \Delta t]$, neuron i will generate a spike with probability:

$$P_{\text{spk}}(i; t, t + \Delta t) = f\left(W_{ij} s_j(t) + B_i(t)\right)\Delta t .$$

Resizing and rescaling of grid maps as a response to physical changes in the experimental maze are commonly seen as evidences against the class of attractor network models. In this paper the authors conclude that if seen at the single-neuron (SN) response level, this might not be a problem. In CAN models, the set of stable activity states in the grid cells population – the attractor manifold - comprise translations of a canonical pattern and also rotations in aperiodic networks. If stretching and rotation occur at the population pattern level, they are unstable states and so cannot be invoked within the continuous attractor models to explain experimental observations. On the other hand, the SN response is a function of the instantaneous connectivity pattern and the velocity response of the pattern. So if the pattern is flowing more slowly in one dimension than in the other then, for equivalent rat speeds, the SN response (accumulated over the trajectory) would be a stretched version of the regular population grid. Here they demonstrate that geometric manipulations can in fact not disrupt the weights stable configuration acting only by

means of head-direction driven inputs modification. In fact, if the amplitude of the tuning curves is reduced in one or more directions when the maze is expanded in the same directions, then the firing map will show fields expansion in those directions. On the other hand, if head-direction cells change their preferred direction in accordance to the angle of rotation of the maze, then the resultant firing map will evidence rotated fields as has been reported. They conclude that accurate path integration in aperiodic networks only happens in larger networks than the ones needed for the periodic case. In each of the connectivity regimes, the accuracy in the rat's position determination is upper bounded by 10-100 times larger than reported studies until this one (Burak and Fiete 2009).

STDP for grid cell emergence

Spike time dependent plasticity appears for the first time (to our knowledge) associated with grid cell emergence in a model proposed in an abstract conference. The authors take the traditional attractor network model and substitute some mechanism by new ones, with no requirement for topographic organization of cells. STDP rules comprise both symmetric and asymmetric components. The symmetric regime is responsible for the development and maintenance of the stable states, through the strengthening of firing correlations. The other component produces asymmetries in the network weights which allow the shift between the stable states caused by velocity inputs received during the rat journey. The network receives velocity inputs providing information about the speed and direction of movement, but also positional ones driven by place cells. Available only in abstract form, the model's information about how the STDP acts not requiring topographic organization is absent (Widloski and Fiete, 2010).

Integrate-and-fire grid cells

Navratilova and colleagues merged in a recent model the generation of grid cells with the effect of phase precession. This model assumes the same network architecture of previous attractor models inheriting consequently the lack of biological support for either the assumption of topography in grid cells or high recurrence in mEC. The network comprises both grid cells, conjunctive grid cells (accumulate direction and spatial specificity) and pure head-direction cells modeled as integrate-and-fire neurons. Between grid cells, synapses drive AMPA and NMDA currents while their connections to and from conjunctive cells only comprise AMPA currents. Grid cells are arranged as in a ring, with connections strength obeying Gaussian functions of the distance between them. When the

rat is in a certain position of the 1D apparatus, the grid cell coding for that position is active and consequently its closest neighbors are active too, forming thus an activity bump. Meanwhile, in another two rings, conjunctive cells are disposed in a way that one ring codes north directions and the other codes for south. These conjunctive cells also receive inputs from head-direction cells and project back to grid cells but with a shift opposite to the direction of the movement of the rat. Conjunctive cells receive a theta frequency input and are activated by inputs from head-direction cells with correspondent orientation preferences and intensity proportional to rat's speed. Asymmetry in the connections to grid cells from conjunctive cells allows them to drive the activity bump through the grid cell network. Although not explicitly modeled, inhibitory cells operate between all excitatory units to regulate the total activity through GABA channels. Feedback inhibition is the strongest and acts in the grid cell network. Feed-forward inhibition is weaker and acts between grid cells and conjunctive cells. Phase precession is generated due to resetting of that bump which is attributed to specific conductances of mEC II stellate cells, responsible for hyperpolarization and depolarization peaks after a spike. The neural units are conjunctive cells which activity is modulated at theta frequency with intensity proportional to the rat's speed which moves an 'activity bump' forward in the connected network. However, in contrast with other models, the shift of the neural activity bump is undertaken by cellular mechanisms (dynamic model currents) with no need for external inputs. In particular, after spike conductances temporal variability is used to obtain the differences of grid spacing found along the dorsal ventral axis of mEC. The maintenance of membrane activity of approximately 100 milliseconds duration, allows neurons that were active some time ago to reactivate causing a shift on the bump and the reset in the alignment with the theta rhythm. This model constitutes an extension of the original Samsonovich model to accurately account for reported features of the phase precession effect (Navratilova et al. 2012).

Final comments

Recurrence in mEC layers had been previously reported for excitatory connections in layers III and V (around 10%) and not for layer II (Dhillon and Jones 2000), but currently there is still some ambiguity related to the extent of recurrence in mEC (Giocomo et al. 2011). Moreover, if the aim is to provide plausible explanations for the emergence of grid cells for the first time, as with rat pups, further study must be embraced. Namely, it might be of interest to verify the functional correlates of the cells (recurrence may exist

anatomically but be used for other tasks rather than navigation related ones) and also if recurrence is present temporally consistent with the first grid cells emergence (Wills et al. 2012).

2.3.2 Oscillations interference

In this section we refer to the main approaches found in the literature with strategies for grid cell firing patterns formation, within the class of oscillations interference.

The first OI model for grid cell formation

Two years after the first OI model for grid formation (see section 2.1.2), Burgess and colleagues developed a more complete and refined version with its expansion to a two dimensional maze. In this setting, the second oscillation (thought of as inputs at dendrites) is tuned to a preferred direction (by speed modulated inputs from head-direction cells), and its frequency is raised above the theta rhythm as it codes the speed, s, of the animal in that direction. More precisely, if ϕ is the direction of the animal movement and ϕ_{HD} is the preferred direction of the cell, then the velocity $\bar{v}$ of the movement of the rat can be given by:

$$\bar{v} = s\cos\left(\phi - \phi_{HD}\right).$$

Adapting the one dimensional formula of the scaling parameter to the open maze, one obtains:

$$G = \bar{v} \cdot T = \frac{s\cos\left(\phi - \phi_{HD}\right)}{f_I - f_\theta}.$$

As mentioned in the original formulation, if the oscillators frequencies difference is related to velocity components by some scale factor B, $f_I - f_\theta = B\, s\, \cos(\phi - \phi_{HD})$, then the grid spacing becomes independent of changes in speed and direction of movement, $G = 1/B$, as planned. Then, for the directional preference ϕ_{HD} of the current head-direction cell, the output cell shows a constant spacing.

When considering a two dimensional maze, the interference oscillating pattern will produce high activity bands with directions perpendicular to their preferred direction. The hexagonal pattern emerges as two or three of this simple interference patterns are multiplied, provided that their orientations differ by multiples of 60º (in the three pattern

case, orientations can be obtained with self-organizing rules, because they differ in the same angle from each other).

The first weakness of the model is that the location of the grid vertices will depend on the precise trajectory of the rat since the last reset phase point. Here they consider that as the grid is being created, each grid node will be connected to the place cell that has its receptive field in the location of the node. As a result, grid nodes become locked to locations in the now familiar environment. Moreover, they assume that in each node of the grid, this connection to the place cell drives the dendritic oscillators to realign their oscillation phase with the somatic theta, thus producing a phase reset. Additionally, the interference of the patterns will produce the desired map if the oscillations involved are in the correct phase with each other, and this is what sets the spatial position of the grid. Different values for this phase difference will generate grid maps with the same spacing but different orientation, resembling the reported feature of real grid cells maps.

In accordance to the known anatomy of this brain regions, the authors suggest that place cells and grid cells could be wired in a loop such that place cells could provide the position input to keep the grid firing fields with a stable position in the environment and, on the other hand, grid cells that overlap with place fields could provide them the path integrative input. Each time a grid cell suffers a phase reset, its phase propagates on the same local group to cells with distinct phases, by delay connections that depend on the speed of the animal (this means that some grid cells have their phase realignment triggered by place cells and others by the grid cells in the same local population). This propagation of phase reset driven by place cells enables the correction of the path integration error in grid cells firing locations, requiring recurrence and probably also a topographic relation of grid cells (Burgess et al. 2007).

Scaling factor for grid nodes' spacing

In the same year of this publication, an experimental work reports the existence of subthreshold membrane potential oscillations differences in the dorsal-to-ventral axis entorhinal neurons which could account for the different spacing between grid fields. Using real data, they determined a scaling factor to be incorporated in the oscillation interference canonical model for obtaining grid spacing of cells from the frequency of the subthreshold oscillation in the same anatomical location (Giocomo et al. 2007). At the same time this scaling factor was appended to the model of Burgess and colleagues and,

by varying the oscillation frequencies, they replicated grids with different spacing from dorsal to ventral mEC.

Regarding the type of currents that could underlie the presence of the subthreshold dendritic oscillations required for such a model, the authors refer a commonly used persistent sodium current (NaP), which is an inward current. By its interaction with a reduced inward current or an increased outward current, the subthreshold oscillations would resemble an oscillation in the net membrane current. The fact that at the soma the recordings made show that oscillations have small amplitude, the authors suggest that at distal dendrites the amplitude of oscillations could be higher (for instance by an increase of the h-currents in more distal dendrites without disruptions caused by somatic oscillations). According to the authors, small oscillations happening in faraway dendrites could be responsible for the maintenance of phase information which would be again used on the onset of the soma's spiking activity (Hasselmo et al. 2007).

Velocity input from theta cells

By 2008, a new envelope for the interference oscillatory model was created, describing the way grid cells could convert the interference patterns into their characteristic spatial firing coding location. With this intent they add, to the oscillatory interference model circuit, the familiar ring attractor which has previously been proposed as a way to perform angular path integration in the head-direction system (described in section 2.1.1). Each ring attractor is formed by theta cells and is supposed to exist in subcortical regions. Theta cells are expected to burst at a frequency proper of each ring and at a phase determined by the position of the theta cell in that same ring. So theta cells in different rings oscillate at different frequencies and theta cells in the same ring oscillate at the same frequency but in different phases. This model provides an alternative for the nature of the velocity modulated theta oscillations relative the previous models, in the sense that each velocity modulated oscillation is supposed to correspond to a theta cell. The correction of path integration errors in the determination of the animals' location may also be here performed by phase-reset derived by place cells assuming that it can back propagate to reset ring attractor's phases (Blair et al. 2008).

Velocity-controlled oscillators (VCOs)

To overcome the constraint related to the lack of noise in oscillations of OIs models, a

new foundation for the oscillations involved has been proposed. In this model, each oscillation is the result of a set of singular noisy and thus more realistic oscillations coupled together. Each network represents a velocity-controlled oscillator (VCO) with a certain preferred direction. In fact, a network of cells coupled all to all, with noisy activity produces a synchronized population of units with low period variance either measured between all the units either within each unit activity. The model consists of a grid cell receiving input from three identical oscillatory networks which differ in their own inputs. One of the three VCO's, termed Vo, is considered the baseline oscillator, as it sets the timing for the other networks activity to affect the grid cell. The combination of three such network oscillations (Vo plus VCO's oriented at angles 0º and 120º) can produce grid cells with positional firing activity relatively stable in realistic timescales. Each one of the VCO units project to the grid cell, but the networks are not coupled with each other in order to prevent synchrony. The spacing of the grid is set by the parameters chosen to perform the change from velocity to frequency at the VCO's and their velocity inputs. Although this model conveys many simplifications, it provides evidence that interference of noisy oscillatory signals may produce regular hexagonal firing patterns under certain conditions. Grid cells sharing the same set of VCO's will have the same spatial scale. On the other hand, this architecture predicts that displacement of the nodes in individual cells may be partially correlated (Zilli and Hasselmo 2010). In fact it has been reported that cells recorded in the same set of different mazes show similar grid phase vectors (Fyhn et al. 2007) translation, in the sense that not only the angle of rotation is similar between pairs of cells tested, but also its length. Interestingly, both of the behaviors described are not present in interference models of single oscillators but are a characteristic of attractor network models.

Final comments

The diversity of models that have been suggested in such short period of time since the first report on grid cells is remarkable. Not less important are the predictions arisen from proposed model about features of those cells and related matters. A recent example is the result that when theta oscillation is reduced (by disruption of the activity of the medial septum), grid patterns lose their hexagonal regularity although place cells and head directional cells do not lose their characteristic firing (Brandon et al. 2011; Koenig et al. 2011).

2.3.3 Self-organizing models

This recent class of models comprehends essentially two distinct models, described shortly.

Self-organizing units with adaptation

By the year of 2008 an alternative class model was published. The most differentiating characteristic of this model is that it uses place cells as the source of spatial information input arriving grid cells. In this model, random initial weights make the output cell fire in random places of the maze and increase (by a Hebbian learning regime) the synapse weight with the place cells that were responsible for that increase. The adaption mechanism makes the overall rate to decrease after some time of high activity, decreasing then connection weights from place cells that code de current location. This process creates dispersed multi-peaks of activity that become hexagonally arranged because fields move around to minimize their distance from each other producing the most compact form of arrangement. The change in connections strength from input cells to grid cells are subjected to a slow learning process and the total input weight arriving each neuron is obligatory constant. The amount of synaptic input coming to each cell is subject to a mechanism of adaptation before being subject to the transfer function. This transfer function produces grid cells activity and includes two parameters of interest: a threshold parameter and a gain parameter. mEC neurons perform competition in such a way that the threshold parameter increases if the average activity is high when compared to a target mean activity. At the same time, the gain parameter is used to control the sparseness of the ensemble's activity relatively to a desirable sparseness value. For the Hebbian learning rule, knowledge about a temporal mean of the presynaptic activity and the postsynaptic activity is required. The model evolves as the simulated rat randomly moves within a square box and it takes about 10^7 time steps for the hexagonal configuration to stabilize. In this model recurrent connections between grid cells are only used between local populations to stabilize cells in a common grid orientation.

The mathematical formulation of this model is as follows. The total synaptic activation of the units is given by:

$$h_i^t = \frac{1}{N_I} \sum_{j=1}^{N_I} J_{ij} r_j^t \ ,$$

where N_I is the number of units in the input layer, J_{ij} is the weight of the synapse from neuron j to neuron i and r_j^t is the firing rate of the input neuron j.

The transfer function is given by:

$$\psi(h) = \psi_{\text{sat}} \frac{2}{\pi} \arctan\left[g\left(h-\theta\right)\right] \Theta\left[h-\theta\right],$$

where ψ_{sat} is the saturation rate and Θ represents the Heaviside step function. Parameters θ and g are the threshold and the gain, respectively, defined equally for all mEC neurons and updated according to:

$$\theta^{t+1} = \theta^t + b_3\left(a - a_0\right) \text{ and } g^{t+1} = g^t + b_4 g^t\left(s - s_0\right).$$

In these rules, b_3 and b_4 parameters control the speed and smoothness of the changes, a is the mean activity and s is the sparseness of the mEC units, defined by:

$$a = \frac{1}{N_{mEC}} \sum \psi_{\text{k}} \text{ and } s = \frac{\left(\sum \psi_k\right)^2}{N_{mEC} \sum \psi_k^2}.$$

Parameters a_0 and s_0 are the target values for the mean and the sparseness of the units, respectively. N_{mEC} is the number of units in the output layer.

Before transformed by ψ, the input activity is subject to fatigue dynamics (adaptation) by means of activation variables defined by:

$$r_{act}^{t+1} = r_{act}^t + b_1\left(h^t - r_{inact}^t - r_{act}^t\right) \text{ and } r_{inact}^{t+1} = r_{inact}^t + b_2\left(h^t - r_{inact}^t\right).$$

Parameters b_1 and b_2 define the speed of rise and fall of the activity of a mEC unit receiving strong input.

Finally, the update rule for the weight matrix is given by:

$$J_{ij}^{t+1} = J_{ij}^t + \varepsilon\left(\psi_i\ r_j - \left\langle \psi_i \right\rangle \left\langle r_j \right\rangle\right),$$

where ε is the learning rate, r_j is the activity of the input neuron and $\langle \cdot \rangle$ denotes the temporal average. Additionally, weights are normalized such that the total input weight to any mEC neuron is constant.

Besides using place cells like input, simulations were made with other type of spatial inputs in order to demonstrate that the model is also valid with other profile spatial cells (Kropff and Treves 2008).

Four years later this model was updated in order to produce not just spatial grid cells, but conjunctive cells, that comprise directional tuning in addition to spatial, and are abundant in several layers of mEC. The architecture of the model contains connection paths from head-direction units, from place units and recurrent connections in the conjunctive population. According to the authors their model focuses on learning happening in layers III to VI, because layer II does not contain head-direction cells nor recurrent collateral connections. The inputs injected in each modeled conjunctive cell are: a population of place cells with self-organizing synapse weights, all conjunctive cells with fixed weights (self-excluding) and one head directional cell. This last one is included to represent the global effect of angular modulation from the local network. As in the original model, place cells inputs are taken to be regularly arranged and their activity rate is modeled with Gaussian curves. The dynamics of conjunctive cell firing rate and adaptation variables, along with the weights update rule is obtained as in the first model. The utility of the collateral connections is to obtain the units (grid cells) with the same orientation and spacing but distinct phases. This allows for units with similar direction preferences to have strong collateral connections. Ellipsoidal grid fields are produced by learning weights if the foraging is undertaken with anisotropic[7] speed of the rat and collateral connections are present. Collateral connections comprise a delay which must be above 130 ms (is the time the rat needs to go in a straight line from one place field to the next) in order to avoid the collapse of subpopulations with similar direction tuning. The network activity is regulated by the gain and threshold parameters which stabilize in an ad hoc fashion. The authors argue that this method is intended to mimic homeostasis[8] in a local portion of mEC. In this model and its previous iteration, grid spacing is originated in the mean speed of the simulated rat during learning and on the time constant for adaptation. Collateral connections weights are dependent on distance between two imaginary fields with no requirements for topographic relations between units. However, a biophysical explanation for how synapses obtain such strength values was not explored (Si et al. 2012).

[7] Variable with respect to direction.

[8] Metabolic equilibrium actively maintained by several complex biological mechanisms that operate via the autonomic nervous system to offset disrupting changes

GRIDSmap model

Self-organizing maps have also been used in a broader model that intends to mimic the emergence of grid cells as well as place cells in a two dimension maze. This GRIDSmap model, uses path integration signals relative to direction and speed and translates them into spatial representation units such as place cells and grid cells through a network of self-organizing maps. While contemporaneous models of oscillations interference are more devoted to the nature of the oscillations than to the mechanism that would dictate an orientation difference of 60° between the interfering oscillators, one of the main concerns of this paper is to explain this latter preference. The first strong assumption of GRIDSmap model is the existence of the so called stripe cells, which have not, to our knowledge, been reported. These particular cells supposedly fire in a stripe like fashion within a maze, with stripes perpendicular to their preferred direction of movement. Each of these cells is defined by their preferred direction θ, and by the period length, l, of the stripes measured in that same direction (that will be the shortest period of all directions). Stripe cells project to future grid cells and the intermediating connections are subject to a learning process of type on-center off-surround involving a self-organizing map. The co-occurrence of two stripe cells in a maze will be most frequent in the case where their orientation differ by angles of $\pm 60°$ and this is the reasoning behind the choice of the stripe cells to co-occur. The idea is based on the detection on the most common co-occurrences, their amplification and learning and, in addition, on the deletion of the less frequent co-occurrences. Stripe cells are thought to be arranged in 1D ring attractors such that each ring contains cells that have the same orientation preference and spatial period but differ in their spatial position. If the animal is still, there is a bump (stable) in each oriented ring on top of the stripe cell that is coding for the position where the rat is. As the animal starts moving, the vector of displacement is decomposed into the distance traveled in each direction. Consequently, the different rings see their activity bump moving around the ring, from stripe cell to stripe cell, according to the distance traveled in their directional preference. Because the ring has finite length, the bump returns to the same cell after the period length has been traversed by the animal in the direction preferred by the cell. The ring structure implies recurrence in stripe cells with the same orientation preference. In conclusion, the first stage of the GRIDmap model converts small space scales stripe cells into grid cells with multiple spatial scales. The second stage (which is beyond the scope of the present work) converts grid cells of multiple spatial

scales into place cells representing even larger spatial scales. Stripe cells are supposed to be located in layer III of the entorhinal cortex which project randomly to layer II cells. The co-activation principle will emphasize projections coming from stripe cells which differ $\pm 60°$ in their directional preferences generating cells with hexagonally arranged fields in layer II. The simulations of such a model show failure of the representation of grid cells with large scaling as are those located more ventrally in the medial entorhinal cortex. The current model shares with the class of oscillatory interference the idea that spatial scale of grid cells in inherited from the spatial scale of the stripe cells (frequency of oscillators). Moreover they also assume the existence of cells that combine codes of speed and direction. As for the requisites of attractor models, this model uses the moving bump ring attractor mechanism (Mhatre et al. 2012).

A GRIDSmap new generation model (known as Spectral Spacing model) intends to correct some less accurate results of the original version, such as reducing the production of stripe like cells instead of grid cells in some scenarios, simulate the known gradual changes in spatial and temporal feature of grid cells along the dorsoventral axis of mEC. As a side effect of this model, grid cells exhibit membrane potential oscillations with decreasing frequency along with rate from dorsal to ventral locations in mEC. Grid cells recurrently interact in an on-center off-surround network (Grossberg and Pilly 2012).

Final comments

The set of models comprising self-organizing maps described here have received inspiration from successful models for visual system. However, an important feature can make the difference in their effective applicability to positional system: the lack of topographic organization within space cells. It is known that grid cells are also present in deeper layers of mEC and thus, if coming from stripe cells and if the projections inside mEC are feed-forward (or even recurrent) stripe cells must be present in deeper mEC layers or even in CA1 or subiculum, but this remains unknown.

Another limitation of the self-organizing models described concern their results dependency on velocity. Furthermore, they require large scale environments and long exposition periods for the process to result in characteristic grids of ventral mEC regions (greater spacing) (Zilli 2012). Recurrence is also a prevailing requisite for the models in this class.

3. Modelling phase precession

The work described in this chapter originated one publication in an international peer-reviewed journal and two conference abstracts, one of which in an international peer-reviewed conference:

- Luisa Castro and Paulo Aguiar, *Phase precession through acceleration of local theta rhythm: a biophysical model for the interaction between place cells and local inhibitory neurons*, Journal of Computational Neuroscience: Vol.33, Issue 1, Pages 141-150, 2012. DOI: 10.1007/s10827-011-0378-0.

- Luisa Castro and Paulo Aguiar, *Possible roles for inhibition in the linear phase advance of complex spike cells undergoing phase-precession*, XII Meeting of the Portuguese Society for Neurosciences, Unidade de Neurociências Instituto de Medicina Molecular, Lisboa (28 May 2011).

- Luisa Castro and Paulo Aguiar, *Phase precession through acceleration of local theta rhythm: a biophysical model for the interaction between complex spike cells and theta cells*, BMC Neuroscience (18 July 2011) 12 (Suppl 1): P2. DOI: 10.1186/1471-2202-12-S1-P2.

3.1 Introduction

Exploratory activities which involve changing the position of the rat in an environment (like walking, running, swimming) are accompanied by an oscillatory activity pattern in the hippocampus' EEG with a frequency range from 6 to 12 Hz – the θ rhythm. This θ oscillation is believed to have important functional roles in information coding (Buzsaki 2002), and is a key component in the phase precession coding mechanism. Coding through phase precession states that the phase in the θ cycle in which the place cell fires, provides information regarding the position of the rat in the environment, more refined than what is available from firing rate coding alone (O'Keefe and Recce 1993; Skaggs et al. 1996). Many researchers believe that, in terms of space representation, phase coding and rate coding are produced by independent mechanisms (Huxter et al. 2003).

The precise mechanisms underlying the generation of phase precession are still unknown and some hypothesis, together with computational models, have been suggested. Naturally, the majority of these models target key experimental results concerning phase precession properties. In two-dimensional mazes, some of these results are (Harris et al. 2002; O'Keefe and Recce 1993; Skaggs et al. 1996): the total advance in phase can be more than 180° for single trials; firing phase correlates better with location inside the receptive field than with time since entrance; gradual broadening of spike clusters; precession is not confined to spatial tasks, emerging also in not spatial ones; phase advance is faster in the center than in the periphery of the receptive field; the place cell has a Gaussian shaped firing response in the crossing of its place field (slightly asymmetric for linear tracks); phase precession is observed since the first crossing of the receptive field, and not only when the animal has been trained on the maze. Moreover, experiments on rat pups, provide evidence that early place cells are theta-modulated and show phase precession (Langston et al. 2010).

Here we present a minimal spiking model for phase precession generation which uses biophysically plausible neuronal dynamics. Our model shares with Bose's model the importance for the interaction with inhibitory interneurons (Bose et al. 2000), but the dynamics, nature and consequences of this interaction are quite different. Our model is capable of producing many key experimental results and has the advantage of doing so using simpler principles and fewer assumptions than other recent models (Geisler et al. 2010).

3.2 Methods

Pyramidal cells found in layers CA1 and CA3 of hippocampus are of two main cellular types: theta cells or interneurons, which are inhibitory and well correlated with EEG patterns, and excitatory complex spike cells which major correlation is with the location on the animal – place cells (Amaral and Lavenex 2006). The model focuses on the feed-forward network established between the entorhinal cortex and CA1. EC neurons provide input for the CA1 field sending signals simultaneously for excitatory and local inhibitory neurons. The latter are responsible for the control of the network activity: if the input received by the complex cells is too high so will be the input for the interneurons. As a result, interneurons provide feed-forward inhibition to principal cells, which is a frequent

architecture motif in the nervous system (Shepherd 1998). In this particular model, inhibitory neurons may represent basket cells (Freund and Buzsaki 1996) or other local inhibitory units which strongly influence pyramidal cell's activity.

With this in mind, the main units of our simple model are a complex spike cell and an interneuron or theta cell, both fed by excitatory synapses coming from cortical areas. The input spike trains, representing the entorhinal cortex activity, both space modulated and theta rhythm modulated, are generated using a non homogeneous Poisson process. In addition, the interneuron is also affected by a modulatory input, at theta rhythm frequency, which represents the population activity. This input maintains the inhibitory cell firing activity synchronized with the population theta rhythm in the absence of entorhinal excitation. Theta cells are thus assumed to be connected in a weakly coupled network. This weak coupling allows, under certain conditions, for a particular cell to desynchronize its activity from the global population activity. In the model, only that interneuron is present and is connected to the complex spike cell by an inhibitory synapse. This functional block - complex spike cell plus theta cell - constitutes a unit of repetition on the CA1 and is the focal point of our model.

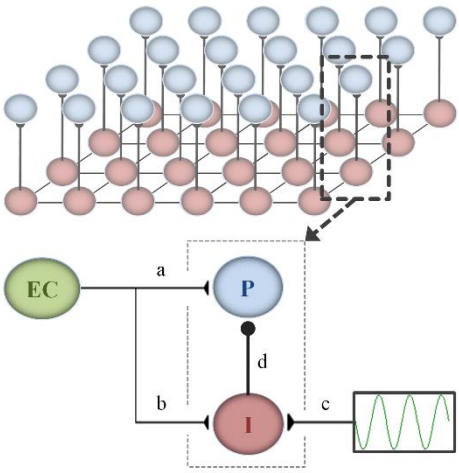

Figure 3.1 The population of inhibitory interneurons is assumed to form a weakly coupled network with synchronized activity at the θ frequency. Each interneuron (I) is connected with a place cell (P) and receives a modulator activity from a common pacemaker. Our model focuses in the functional block consisting of a pair of place cell and local interneuron; the weakly coupled network is not modeled. Both cells in the functional block share an input from the entorhinal cortex (EC) which is, at the same time, space modulated and θ modulated. Connections a, b and c are, therefore, all θ modulated (adapted from (Castro and Aguiar 2012)).

3.2.1 Dynamics for neurons and synapses

The dynamics of the two types of neurons, complex cell and interneuron, are described by the leaky integrate-and-fire model:

$$\begin{cases} \tau_m \dfrac{dV}{dt} = -V + V_{rest} + R_m I(t) \\ V(t) > V_{th} \rightarrow V(t) = V_{rest} \end{cases},$$

where τ_m = 200 ms is the time constant of the neuron; V_{rest} = -70 mV is the membrane resting potential; R_m = 200 MΩ, is the membrane resistance; I is the total current stimuli and V_{th} = -50 mV, is the threshold membrane potential for the neuron to fire. The parameters described are all shared by both the inhibitory neuron and the excitatory neuron, except for the input current components described shortly.

The time varying synaptic currents, I_{syn}, are given by:

$$I_{syn}(t) = g(t)\left[V(t) - E_{syn}\right].$$

The synaptic conductances are modeled with its simplest form, as a single exponential and initialized at zero. Every time a presynaptic spike occurs the conductance value of the synapse is incremented by a fixed amount, Δg. When the presynaptic neurons are silent, the conductance decreases with time constant τ_{syn}. This non linear dynamical behavior is formulated as:

$$\begin{cases} \tau_{syn} \dfrac{dg}{dt} = -g \\ t = t_{sp} \rightarrow g(t) = g(t) + \Delta g \end{cases}$$

, where t_{sp} represents the presynaptic spike time.

The synaptic current for the excitatory neuron is the sum of two distinct currents: one carrying the spatial related information coming from the entorhinal cortex, I_{syn}^{ce}, and the other coming from the inhibitory theta cell, I_{syn}^{ie}. The total current flow impinging on the complex spike cell is then: $I = -I_{syn}^{ce} - I_{syn}^{ie}$.

The current coming into the interneuron (theta cell) is also the sum of two distinct currents: one carrying the spatial related information coming from the entorhinal cortex, I_{syn}^{ci}, and the other with the pacemaker one carrying the spatial related information coming from the entorhinal cortex, I_{Ω}. The total current for the interneuron builds up to:

$I = I_{\Omega} - I_{syn}^{ci}$.

3.2.2 Pacemaker current

The assumed weakly coupled network of inhibitory interneurons is synchronized by a common pacemaker Ω. In the model this weak coupling is not included (for this see (Bendels and Leibold 2007; Loewenstein et al. 2001)), instead, only the global rhythmic theta input to the interneuron is incorporated.

With a sinusoidal shape in accordance with the theta rhythm pattern, the pacemaker current, I_{Ω}, is given by:

$$I_{\Omega}(t) = k\cos(2\pi f\ t + \varphi) + b,$$

where k is the intensity parameter, φ is a free parameter allowing different trials to start at distinct phases of theta, f is set at the theta frequency and b is the baseline constant level for the current. In our simulations, for the sole sake of simplicity we used f=10 Hz, which is in the range of experimental values.

When subject solely to this pacemaker current (with b = 0), the subthreshold membrane potential time course can be computed analytically (check section A.3 for details) from the integrate-and-fire equation described above:

$$V(t) = V_{rest} + \frac{R_m k}{1+(\tau_m 2\pi f)^2} \cdot \left[\tau_m 2\pi f \sin(2\pi f\ t) + \cos(2\pi f\ t) - e^{-t/\tau_m}\right].$$

This function oscillates between two extremes V_{min} and V_{max}, with a dependence on the intensity parameter which is given by (see section A.4):

$$k = \frac{(V_{\max} - V_{\min}) \cdot \sqrt{1+(\tau_m 2\pi f)^2}}{2R_m}.$$

3.2.3 Entorhinal cortex input

The inputs from the entorhinal cortex are considered in the form of spike trains and affect simultaneously the place cell and the interneuron in our model. This stochastic input is assumed to originate from an entorhinal cortex subpopulation composed by 1,000 neurons and is set to be both space modulated and theta modulated. The intensity function defined

for the generation of spike trains subject to this properties includes:

- a sinusoidal component for the theta modulation and
- a Gaussian tuning profile for the space modulation.

Entorhinal cortex spike trains are modeled by the intensity function $\lambda(t)$ given by:

$$\lambda(t) = f_{\min}\left[1 + A_{\mathrm{mod}}\cos\left(2\pi f\, t + \varphi\right)\right]\cdot\left[1 + B_{\mathrm{mod}} e^{-\frac{1}{2}\left(\frac{t-\mu}{\sigma}\right)^2}\right].$$

The parameters A_{mod} and B_{mod} control, respectively, the amount of theta modulation and space modulation; f = 10 Hz represents, as before, the theta rhythm and φ is the same parameter (with the same value) as in the pacemaker current equation. In the Gaussian component, the parameters μ and σ set, respectively, the center and width of the place field. The simulated animal is assumed to move in a straight line at constant velocity, therefore space units are replaced by time units. The spatial input is set as taking off from a minimum level of firing, f_{min}, representing the basal activity level when the animal is outside the receptive field. This spontaneous firing level is set at f_{min} = 0.5 Hz, nevertheless, the stochastic activity is also theta modulated. Once entering the receptive field, a portion of the EC cells is assumed to start firing at a higher rate. In this model, the spatial selectivity shown by the place cell is inherited from the entorhinal cortex: the place field of the modeled place cell results from the combination of spatially tuned activity already present presynaptically. The population average rate of fire was set assuming that around 10% of the 1,000 neurons fires at a high rate, in the order of 40 Hz, while the rest of them remain at the basal level. The percentage chosen is not decisive and the 10% EC neurons are assumed to have co-localized receptive fields. In result, considering the population average, the mean input firing rate at the center of the place is set to f_{max} = 4.5 Hz.

As explained in the following section, the entorhinal spike trains are simulated as realizations of a Poisson process with intensity function $\lambda(t)$. The additive property[9] of the Poisson process allows the construction of a single spike train reflecting the merged activity of the entire EC subpopulation spikes. Therefore, instead of 1,000 intensity functions, only one intensity function $\lambda(t)$ is needed for the generation of the EC spike

[9] The additive property of the Poisson process states that the combination of two independent Poisson processes is another Poisson process which intensity function is the sum of the individual intensity functions (Papoulis and Pillai 2002).

trains. Accordingly, the spatial modulated parameters used are f_{min} = 0.5 kHz and f_{max} = 4.5 kHz. This property in the Poisson process setting the EC spike train also renders the model more general, since less stringent constraints are set for the input population.

In order to assure an f_{max} firing rate from EC units at the center of the place field and a spontaneously firing, f_{min}, outside the place field, the parameter B_{mod} is defined as:

$$B_{\mathrm{mod}} = \frac{f_{\max} - f_{\min}}{f_{\min}}.$$

The Gaussian profile parameters are set to μ = 500 ms and σ = 250 ms. For a simulation lasting 1 s, this means that the center of the place field is reached at t = 500 ms and its crossing lasts less than 10 theta cycles.

Spike train simulation

In vivo recorded cells exhibit stochastic spiking activity with particular statistical properties. When analyzing spike trains it is usual to study not only the characteristics of their time series but also the distribution of their inter spike intervals (ISI's). In fact, samples of ISI's are commonly characterized by an average time interval similar to its standard deviation (Dayan and Abbott 2001). The coefficient of variation, $C_v = s_{\mathrm{ISI}}/\langle \mathrm{ISI} \rangle$, applied to such data produces unitary values, which is the theoretical value for Poisson processes. Moreover, if the spike train is split in subintervals, the number of action potentials (events) happening in two disjoint intervals are independent (independency assumption). The distribution of the number of spikes that occur in a given interval depends only on the length of the interval and not on its location, meaning that equal length intervals should have the same event occurrence probability (this is the stationary assumption).

Supported on the similarity of the described properties, the common way to model spike events is to generate realizations of Poisson processes with the desired spike rate. If the rate has the same intensity throughout the simulation then a homogeneous Poisson process should be used. In the present model however, cells firing rate is variable through time thus, a non homogeneous Poisson process is required for the generation of spike times. In fact, the non homogeneity of the process is a relaxation of the Poisson constraint stating that events are equally distributed in all intervals of identical size.

In this model, entorhinal cortex input, in the form of spike trains, is modeled as events in

a non homogeneous Poisson process using the thinning algorithm "Acceptance-Rejection" method, chosen for its fast computational performance (Ross 2002). The rate function, $\lambda(t)$ for $t \in [0, T]$ defined above, corresponds to the intensity function for the Poisson process realizations to be produced. In the following lines, the algorithm will be presented, but previously the details behind such method are described. The general idea is to generate the time intervals between successive spike events (instead of generating the event times) and then sum them to obtain the event, in this case spike, times.

For a Poisson process of events with intensity λ, the distribution of X_n is the base for the spike train generation, where X_i, with $i \in \{1, 2, \ldots, n\}$ denotes the length of the interval between successive events t_{i-1} and t_i. In order to address the distribution function of the ISI's, the first notion to establish is that if $N(t)$ is defined as the number of events occurred in $[0, t]$, then $N(t)$ is a Poisson random variable with mean[10] λt.

Consider the first ISI event, $\{X_1 > t\}$, which occurs if and only if no Poisson process events have occurred in [0, t[, then $P(X_1 > t) = P\{N(t) = 0\} = e^{-\lambda t}$. In general, the i^{th} inter event interval $\{X_i > t\}$ will occur if and only if no events have occurred since the $(i-1)^{th}$ inter event interval, say $\{X_{i-1} = s\}$, then:

$$P(X_i > t \mid X_{i-1} = s) = P\{0 \text{ events in }]s, s+t] \mid X_{i-1} = s\} = P\{0 \text{ events in }]s, s+t]\} =$$

$$= P\{N(t) = 0\} = e^{-\lambda t}.$$

The reasoning behind the 2nd and 3rd equalities are, respectively, the independency and the stationary principles of Poisson processes mentioned above together with the convention that $N(0) = 0$.

The result[11] is that the inter arrival times X_n are independent and identically distributed exponential random variables with parameter λ (recall that the mean of the exponential distribution is the inverse of its parameter). For the generation of such ISI's, with constant rate λ, the inverse transform method is used (check the section A.1 for details). According to this method, n random (from a uniform]0,1[distribution) numbers are generated,

---

[10] Recall that a Poisson variable with parameter λt has density probability function: $p_i = P(X = i) = \frac{e^{-\lambda t}(\lambda t)^i}{i!}$, with $i = 0,1,\ldots$

[11] Since $P(X_n > t) = e^{-\lambda t}$, then the (cumulative) distribution function for X is $F_X = P(X_n \le t) = 1 - e^{-\lambda t}$, for $t \ge 0$, , which corresponds to the exponential distribution. The corresponding probability density function is $f_X = \lambda e^{-\lambda t}$, for $t > 0$.

$U_1, U_2, \ldots, U_n$, and $X_i = -\ln(U_i)/\lambda$ is defined. with $i \in \{1, 2, \ldots, n\}$. Each X_i corresponds to the length of the interval between the i^{th} event and the $(i\text{-}1)^{th}$ spike, then the array of the n event times builds up to:

$$\{X_1,\ X_1 + X_2, X_1 + X_2 + X_3, \ldots, X_1 + X_2 + \ldots + X_n\},$$

which constitutes a Poisson process with constant rate λ.

The next step is based in the thinning technique (check section A.2 for more details). If each one of these event times is accepted with probability $\lambda(t) / \lambda$ (for $\lambda(t) < \lambda$, for all t), then the process of counted events constitutes a non homogeneous Poisson process with intensity function $\lambda(t)$, $0 \le t \le T$.

The performance of the thinning method is increased when less events are rejected. Then the constant λ must be as close to the intensity function as possible, throughout the simulation time interval. A refinement of the general procedure can be obtained by applying the algorithm in a piecewise fashion, breaking into disjoint intervals the time interval of the simulation. Subintervals must be chosen in order to better comply with the performance hint and their union must be the total time interval, $[0, T]$. Thus, appropriate values k, $0 = t_0 < t_1 < t_2 < \ldots < t_{k-1} < t_k = T$, $\lambda_1, \ldots, \lambda_k$ should be selected in order to have $\lambda(s) \le \lambda_i$, if $t_{i-1} \le s < t_i$, $i = 1, \ldots, k$.

Finally, for each interval (t_{i-1}, t_i) the non homogeneous Poisson process can be generated by the process described above, that is, generating exponential random variables with rate λ_i, and accepting the generated event occurring at time s, $s \in (t_{i-1}, t_i)$, with probability $\lambda(s) / \lambda_i$.

The thinning algorithm for generating the first T time units of a non homogeneous Poisson process with rate $\lambda(t)$ in a piecewise fashion is as follows (Ross 2002).

STEP 1: $t = 0$; $J = 1$; $I = 0$.

STEP 2: Generate a random number U and set $X = -\dfrac{\ln U}{\lambda_J}$.

STEP 3: If $t + X > t_J$, go to STEP 8.

STEP 4: $t = t + X$.

STEP 5: Generate a random number U.

STEP 6: If $U \leq \frac{\lambda(t)}{\lambda_J}$, set $I = I + 1$, $S(I) = t$.

STEP 7: Go to STEP 2.

STEP 8: If $J = k$, stop.

STEP 9: $X = \frac{(X - t_J + t)\lambda_J}{\lambda_{J+1}}$, $t = t_J$, $J = J + 1$.

STEP 10: Go to STEP 3.

In the algorithm above, t represents the present time, J is the present interval (i.e., $J = j$ when $t_{j-1} \leq t < t_j$), I are the number of events generated, and $S(1)$, …, $S(I)$ represent the event times. In step 3, $t + X > t_J$ means that the interval length generated is such that the event time produced, which is $t + X$, falls in the next subinterval. If the next subinterval exists (otherwise the process is finished) then the present generated time event is counted but all the variables must be updated (in step 9). In particular, X is redefined as belonging to the next subinterval and substituted by $(X - t_J + t)\ \lambda_J / \lambda_{J+1}$, t is set as the next interval left value ($t = t_J$) and J is set as the next interval ($J = J + 1$) (Ross 2002).

The piecewise algorithm just described was applied to the intensity function defined above, with 50 equally sized subintervals, $k = 50$. The time events generated together with the respective histogram corresponding to a total of 1,000 neurons is illustrated in Figure 3.2 together with the non homogeneous intensity function (thick green line).

The iterative method used to approximate the model's differential equations was the forward Euler method with a time step of 0.01 ms. The full model was coded and simulated in MATLAB® (R2010a, MathWorks, Natick, Massachusetts, U.S.A.). Source code for the model described in this paper is available from ModelDB [http://modeldb.yale.edu/] (Hines et al. 2004) via accession number 143248.

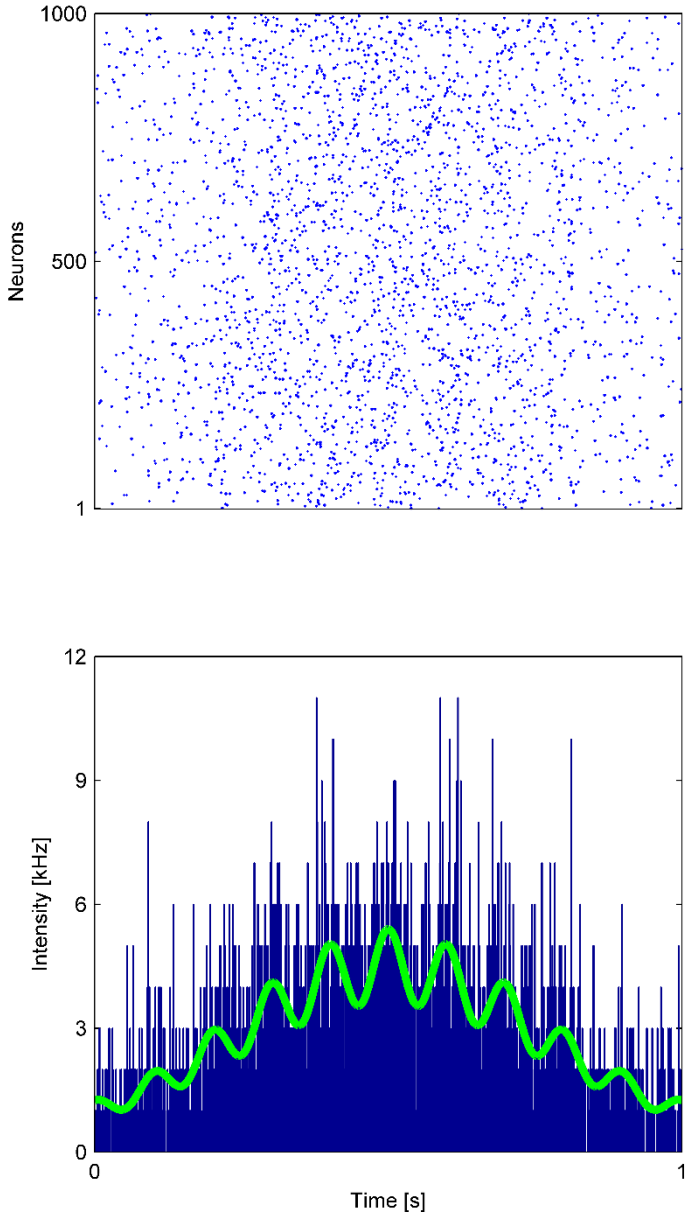

Figure 3.2 Scatter plot (top panel) and histogram with respective intensity function (bottom panel) of a spike train example generated with the piecewise thinning algorithm. The data refers to the spike times of 1000 simulated neurons with mean firing intensities between 0.5 Hz and 4.5 Hz, during one second of real time taken to cross a fictional place cell receptive field.

3.2.4 Parameterizations

The choice of parameters is a critical point in any model. While many clear-cut parameters were already presented along with the description of the model, it is important to segregate the arguments regarding the choice of values for some of the parameters. This dedicated explanation is also used to address the robustness of the model to small changes in the parameters.

Pacemaker

The intensity parameter k is set so that, in the absence of any other stimulation (including $b = 0$), the pacemaker alone is responsible for a membrane subthreshold oscillation in the interneuron of the order of 5 mV of amplitude (between extremes) (Kamondi et al. 1998). Based on this argument the parameter value is set at $k = 0.1$ nA (check calculus details in the Appendix). For the b parameter, the imposed constraint is that, when provided only with the current from the pacemaker, the interneuron (theta cell) should fire at a constant rate of 10 Hz. The value found is $b = 0.25$ nA (check calculus details in section A.5).

Input spike trains

The A_{mod} parameter in the intensity function is set so that, in the absence of spatial modulation ($B_{mod} = 0$), a theta oscillation should be present in the spike times histogram (but not directly visible in the individual raster plots). The used constraint was that the oscillation amplitude (relative to the mean value) in the histogram should be around 20% of the average activity level (Skaggs et al. 1996). The global model dynamics remain the same with changes in this value. By construction, the average level of the oscillating function is defined by f_{min} and A_{mod} sets precisely the amplitude of the deviating from this mean value of the oscillations. Accordingly, the parameter A_{mod} is set to 0.2.

Synaptic connections

In the dynamic activity of the tree synaptic conductances presents in the model, the amounts incremented when a presynaptic spike arrives are represented by (see connections a, b and d in Figure 3.1, respectively):

- Δg_{ce}, for the synapse coming from the cortex to the excitatory neuron;
- Δg_{ci}, for the synapse coming from the cortex to the inhibitory neuron;
- Δg_{ie}, for the synapse coming from the inhibitory neuron into the excitatory neuron.

The parameterization of the synaptic conductances is initiated with the connection between the EC population and the interneuron: constraints about the expected interneuron's activity profile as the animal runs through the place cells receptive field are considered. Out of the place field, EC excitation is residual hence the theta cell is mainly driven by the pacemaker thus firing at the same frequency as the theta rhythm: 10 Hz. Our model is grounded on the assumption that, inside the receptive field, the elements of the functional block, the place cell plus the local interneuron, undergo an increase of their

firing rates. The value for Δg_{ci} is defined accounting for the experimental result that a phase precession close to 360º takes place within about 7 cycles of the theta rhythm (O'Keefe and Recce 1993). If a constant rate is assumed for the input spike train, the inhibitory cell has 7 cycles to perform a total advance of 360º. While constant, the interneuron‘s firing rate is such that in each cycle the advance is around 50º. This means an increase of 20% of the theta oscillation at 10 Hz (driven by the pacemaker) resulting in an average firing rate for the interneuron inside the place field set at 12 Hz. Setting the EC spike train at a constant firing rate of 10 Hz (note that in this case the modulation frequency and the firing rate are the same, which is not always the case), the conductance value was tuned, averaging over 100 simulations, in order to produce a firing rate of 12 Hz for the inhibitory cell.

This means that while the interneurons activity is also space modulated, the magnitude of this modulation is smaller than the modulation in the place cell. Due to the weakly coupling, this firing rate acceleration disrupts only the local interneuron's oscillation frequency while not affecting the global population oscillation frequency.

The parameterization that follows is for the synapse between the interneuron and the place cell. When the EC population is firing at the lower rate, 0.5 Hz, and turning off the connection between from the EC population into the excitatory cell (but maintaining all the others), the complex spike cell should exhibit a subthreshold oscillation of 5 mV approximately (Kamondi et al. 1998). In this case, when the only input to the place cell is the inhibitory one, the complex cell's membrane potential will oscillate between its resting value (set at -70 mV) and a lower one. Through simulation, the parameter value Δg_{ie} is set such that this amplitude matches the 5 mV benchmark (see Table 3.1). The only connection with a non-zero delay, set at 5 ms, is the synapse between the interneuron and the place cell. Changes in the order of milliseconds in this parameter do not affect the global dynamics of the model.

Finally, for the tuning of parameter Δg_{ce}, the excitatory neuron is imposed to be virtually silent outside its receptive field, and firing at its maximum rate, established around 15 Hz, inside the place field. The value chosen is within the range of values reported in experimental findings for firing rates in the center of place fields: 13 Hz in EC layer II, 17 Hz in CA1 and 25 Hz in CA3 (Hafting et al. 2008). In analogy with the Δg_{ci}'s case, the conductance value Δg_{ce} was tuned, averaging over 100 simulations, in order to produce a firing rate of 15 Hz for the place cell (see Table 3.1).

Table 3.1 Parameter values for the synaptic currents between the entorhinal cortex, the local theta cell and the place cell.

Synapse	E_{syn} [mV]	τ_{syn} [ms]	Delay [ms]	Δg [μS]
EC to interneuron	0	5	0	3×10^{-5}
EC to place cell	0	5	0	4×10^{-4}
Interneuron to place cell	-80	20	5	4×10^{-2}

3.3 Results

The core element in our hypothesis/model for phase precession generation lies in the acceleration of the local θ oscillation when the place cell is within its place field. The increased load in excitation, when inside the place field, affects not only the principal cell (place cell) but also the local inhibitory interneurons responsible for activity level control (feed-forward inhibition). This increase in excitation to the interneuron decouples it from the population theta rhythm, and makes it fire at a slightly higher frequency. This above-θ frequency modulates the place cell firings and produces phase precession. This hypothesis implies that, in order to produce a consistent and robust precession, it is necessary that the accelerated interneuron fires consistently at regular times, at a frequency above the population θ rhythm. This key point is shown in Figure 3.3 where the input from EC is not space modulated and where the place cell is discarded: while both inputs to the interneuron are θ-modulated (EC and pacemaker), the output spike times are regularly spaced with a period shorter than the θ-period.

To simulate the crossing of a place field, the input from the EC is subject both to theta modulation and space modulation. The animal's velocity is considered to be constant (reflected in the homogeneous Gaussian profile of the space modulation), and within 1,000 ms the animal enters and exits the place field in a straight path. The intensity function used to generate the EC spike times is illustrated in Figure 3.4 (top panel). For each simulation, the intensity function uses different initial phases of theta (defined randomly). This randomness demonstrates the independence of the results with the theta phase in which the animal enters the place field. The intensity function and the pacemaker

always share the same value for the initial phase. A synchronized θ modulation in both EC and pacemaker inputs (same phase φ) is the worst-case scenario in terms of facilitating the decoupling of the interneuron from the population rhythm.

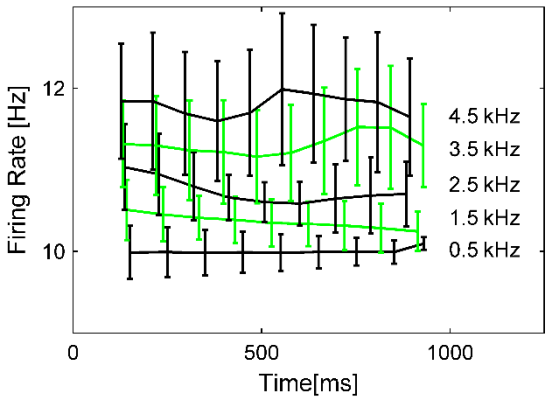

Figure 3.3 Mean and standard deviation of the interneuron's firing rate as a function of EC's input firing activity (50 runs). With space modulation removed, but not θ-modulation, the EC firing activity is kept at different f_{min} levels and the interneuron's ISIs are measured (1,000×[0.5, 1.5, 2.5, 3.5, 4.5] Hz) (adapted from (Castro and Aguiar 2012)).

The spike train generated by this intensity function is delivered to both place cell and interneuron, although with different responses due to differences in synaptic efficacies. The resulting currents, together with the sinusoidal pacemaker current, are shown in Figure 3.4. When inside the place field, the interneuron is accelerated by the additional EC input and fires at a frequency slightly above the population 10 Hz θ-rhythm set by the pacemaker. Whenever the inhibitory cell fires, it sets time bands where the probability for the place cell to fire is lowered. As both neurons are driven by the same excitation, despite the additional delay between the interneuron and place cell, they intend to fire at approximately the same times. The place cell is more probable to fire a few milliseconds before the interneuron does. Representing the place cell's spike times on top of the θ oscillation clearly shows the advance in phase that these times are subject to, while the rat crosses the correspondent place field (see Figure 3.4, lower panel). In the depicted simulation, phase precession takes place within 6 cycles of the theta rhythm, which is coherent with experimental findings, as mentioned in the introduction section. The interneuron activity properties are in accordance with recent experimental data showing that during spatial exploration interneurons also show spatial selectivity and phase precession dynamics (Ego-Stengel and Wilson 2007).

Several simulations, each representing a different run, were combined to compare our model's behavior with the canonical phase precession representation obtained from experimental data. New EC spike trains were generated on each run, each using a different

random initial theta phase φ from the set [0, 2π]. The place cell's spike times for each crossing were plotted in a scatter plot, after shifting every sequence to start at a θ phase of 2π radians.

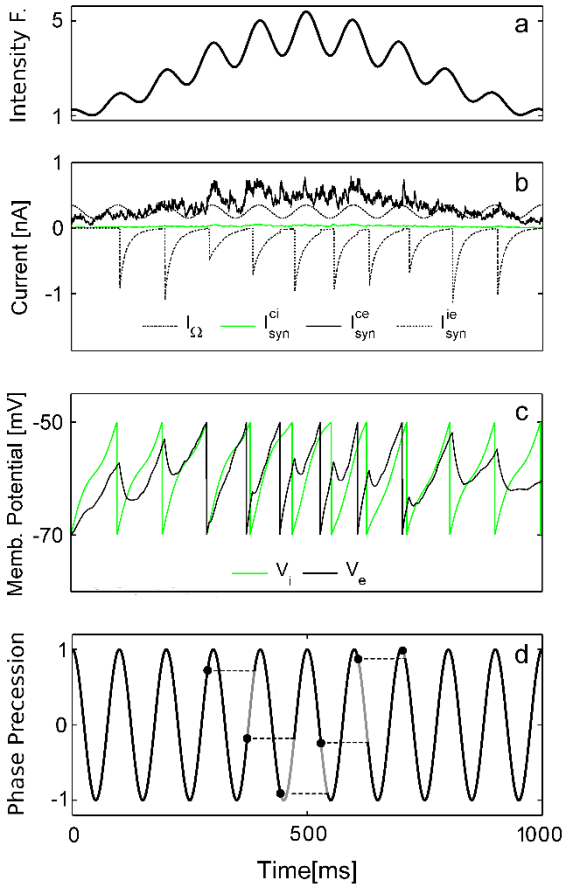

Figure 3.4 Place cell phase precession. a - example of an intensity function representing EC activity during the crossing of the place field (for each value of φ, the model constructs an intensity function with a distinct phase onset); b - currents dynamics affecting the place cell and the interneuron during a simulation of 1 s during which the rat crosses, at constant velocity, the place field; c - membrane potential dynamics of the place cell (V_e) and interneuron (V_i) – the place cell fires systematically a few milliseconds before the interneuron; d - spike times of the place cell advance relatively to the global, population level, θ rhythm during place field crossing (adapted from (Castro and Aguiar 2012)).

While both place cell and interneuron typically produce their first spikes in the upper half of the ascending theta phase, the added noise introduces variability in the precise phase. The shifting of the first spike phase, in every sequence, to 2π radians facilitates the visualization and analysis of the phase precession features.

As can be confirmed in Figure 3.5, phase precession occurs during 5 to 6 cycles of the θ rhythm, with a progression which is approximately sigmoid, and spanning almost 360º. It is important to notice that phase advance is faster in the middle of the place field than in the periphery, reflected in the sigmoid shape of the curve. One can also verify a gradual broadening of spike clusters (vertical bars) representing an ongoing small dispersion of the spike times throughout the consecutive θ windows. In parallel with the phase

precession, the place cell's firing rate is spatially tuned (see Figure 3.5, lower panel). Our spiking model does not support bursting and the firing rate tuning profile comes from lower inter-spike intervals in the center of the place field.

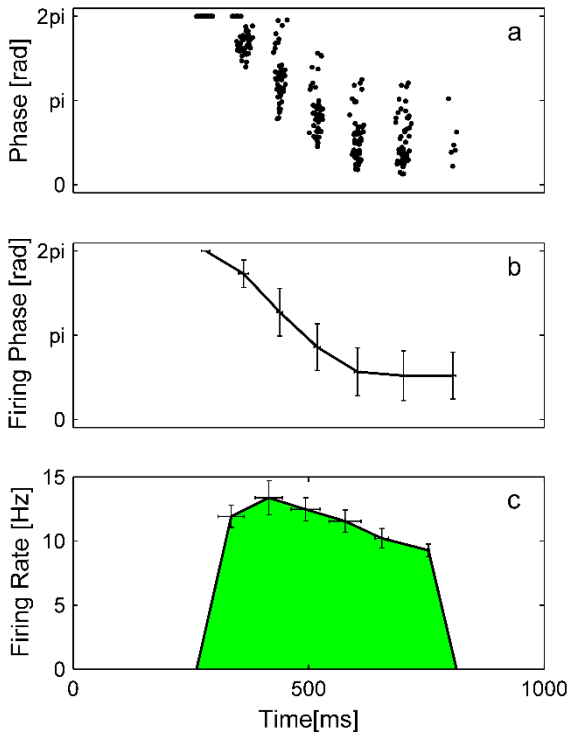

Figure 3.5 Phase precession scatter plots and place cell tuning curve. a - place cell's spike times in 50 combined runs versus the respective phases in the theta rhythm - each run has distinct (random) phase onset and distinct EC spike train; b - mean values for the firing times versus respective phases, with vertical and horizontal error bars (one standard deviation); c - place cell firing rate mean values with respective error bars for the 50 runs - the time for each data point is the mean time of each of the firings for the 50 runs, with respective error bars (adapted from (Castro and Aguiar 2012)).

An alternative way to visualize phase precession in the model is by plotting histograms of the place cell's spike times for a relatively large number of runs. The histogram for 200 place field crossings, using 5 millisecond sized bins, is shown in Figure 3.6. It can be seen that the clusters of spikes precess leftwards with respect to the θ cycles. It is important to notice that spike times dispersion is contained. Removing the randomization of the initial θ phase when animal enters the place field (parameter φ) produces distributions with less dispersion (see Figure 3.6, lower panel).

The crucial role of the interneuron in the generation of phase precession can be appreciated by removing it from the circuit. Without the input from the accelerated interneuron, place cell produces spikes which no longer precess with respect to the θ rhythm (see Figure 3.7, upper panel). However, the firing rate tuning profile is preserved (data not shown).

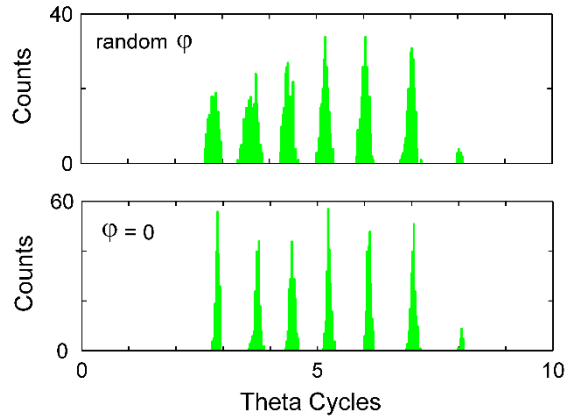

Figure 3.6 Distribution of place cell's spike times for 200 simulations with EC spike trains. Upper panel: each simulation used a different random φ value for the initial θ phase. Lower panel: the same initial phase, $\varphi = 0$, was used in all place field crossing simulations. Bin size is 5 ms (i.e., 0.05 theta cycles) (adapted from (Castro and Aguiar 2012)).

As mentioned earlier, phase precession on the place cell relies on the ability of the accelerated interneuron to fire consistently at regular times, at a frequency above the population theta rhythm. As expected, this means that the local interneuron itself must also exhibit phase precession measured against the global theta rhythm.

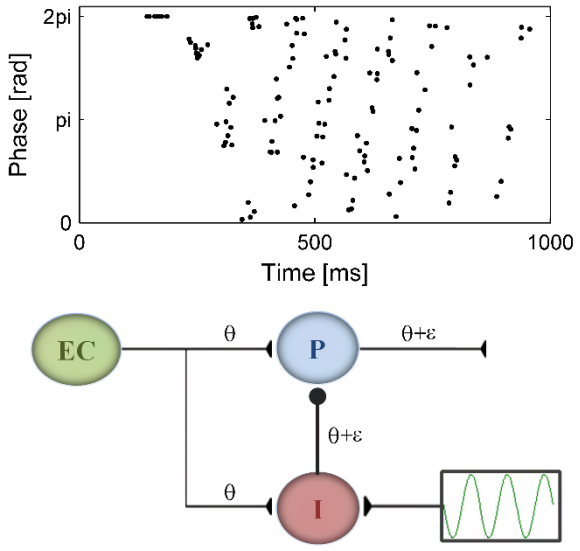

Figure 3.7 Without the interneuron connection (synaptic conductance $\Delta g_{ie} = 0$), phase precession cease to exist (upper panel). While all inputs to the interneuron are θ modulated, this neuron is capable of firing at a frequency above θ, and modulate the place cell responses to this higher frequency (lower panel) (adapted from (Castro and Aguiar 2012)).

This is shown in Figure 3.8: the average firing frequency of the interneuron deviates from the theta frequency as the animal crosses the place field, as a result of the space modulated EC input, and this produces a localized phase precession.

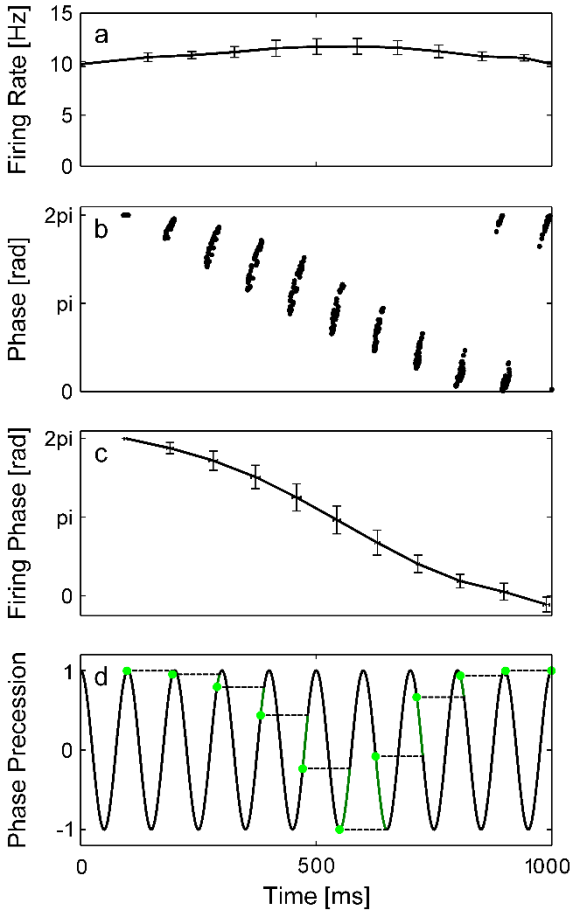

Figure 3.8 Local interneuron phase precession. a - during the crossing of the place field, the mean firing rate of the interneuron accelerates with respect to the θ oscillation, as a result of the increased stimulus drive; b - interneurons' spike times in 50 combined runs versus the respective phases in the θ rhythm – each run has distinct (random) phase onset and distinct EC spike train; c - mean values for the firing times versus respective phases, with vertical and horizontal error bars (one standard deviation); d - spike times of the local interneuron also advance relatively to the global, population level, θ rhythm during place field crossing (adapted from (Castro and Aguiar 2012)).

In order to address the question of which parameters set the slope of phase precession in the scatter plots, some manipulations were introduced in the EC input spike trains. Distinct scenarios were constructed where the rat is considered to be at a fixed position (not moving) inside the place field. Under such constraint, the EC activity is no longer subject to space modulation ($f_{max} = f_{min}$) varying with time. Instead, the EC spike trains have only θ modulation with distinct baseline levels f_{min}. Three baseline levels were considered: 2.5 kHz, 3.5 kHz and 4.5 kHz. Since there are 1,000 synaptic contacts from the EC, this means that, on average, the activation rate on each fiber/synapse was 2.5 Hz, 3.5 Hz and 4.5 Hz respectively. Again this weak constraint provides freedom to consider different scenarios where different fractions of the EC input subpopulation changes from spontaneous/stochastic (low) to evoked (high) spatially modulated activity. As it can be verified in Figure 3.9, the increase in the EC stimulation leads to an increase in the phase precession slope. In other words, the advance in phase is related to the stimuli intensity,

which in turn, in the case of space tuning, is related to the location of the animal. This result is connected with the experimental report that firing phase correlates better with location inside the receptive field than with time since entrance.

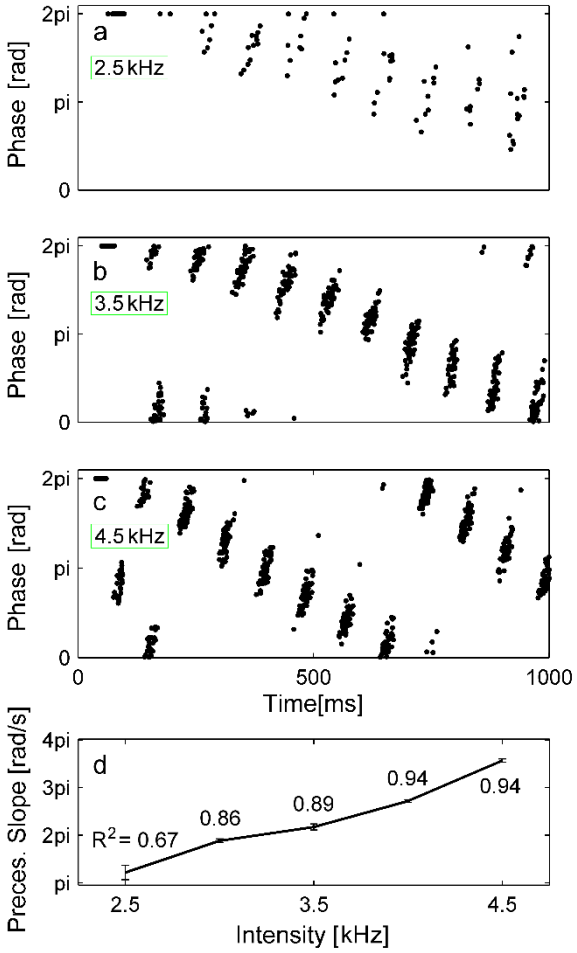

Figure 3.9 Firing times of the place cell in 50 runs with the phase measured relatively to the global θ rhythm (each run used a distinct φ but, as with other phase graphs, all sequences were aligned at 2π). a, b and c – The EC input is subject to different baseline levels f_{min}: 2.5 kHz, 3.5 kHz and 4.5 kHz, respectively. d – Phase precession slopes as a function of the EC stimuli intensity, calculated from linear regression. Error bars represent the 95% confidence bound for the calculated slope coefficients. The values adjacent to each data point correspond to the R^2 statistical measure for the goodness of fit. A stimulus intensity of 2.5 kHz marks the transition below which there is no consistent phase precession (spike times appear scattered). Below a stimulus intensity of 2.0 kHz there are no spikes elicited in the place cell (data not shown) (adapted from (Castro and Aguiar 2012)).

The slope in phase precession is an interesting property, and through the slope this model offers an indirect way of testing and assessing the interaction between place cells and local interneurons. Another interesting piece of information regarding the dependence between phase precession slope and stimuli intensity is the fact that below 2.5 kHz, consistent phase precession is no longer visible, despite activity in the place cell (see Figure 3.9, lower panel). In other words, the place cell firing frequency is still space modulated (even if weakly), while phase precession is less consistent or even absent.

While the simulation results presented so far assumed a standard Gaussian profile for the inputs' space modulation, it is relevant to assess the implications of different EC stimulation profiles on the phase precession properties. This analysis is shown in Figure 3.10 and compares four different input profiles: Gaussian, square, triangular and ramp.

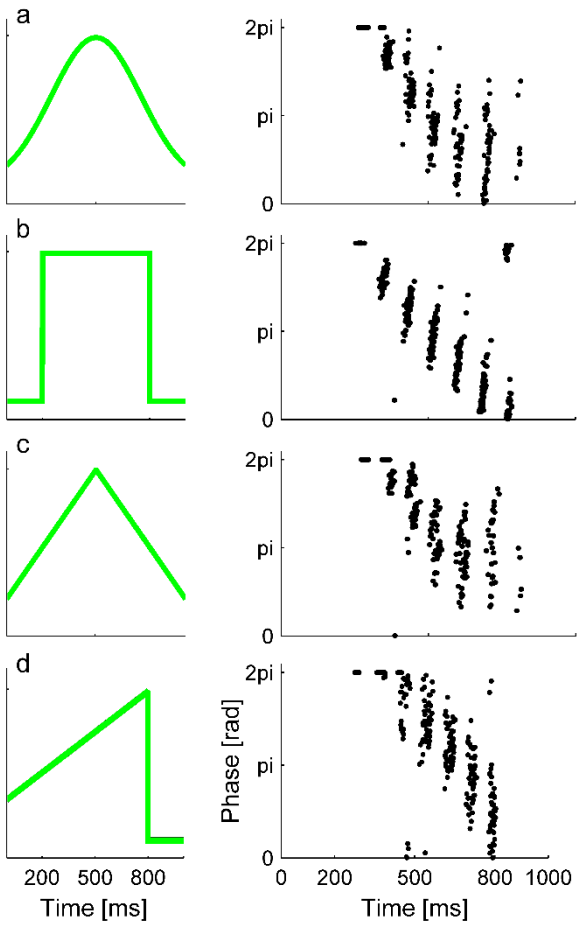

Figure 3.10 Phase precession outline as a function of EC's input stimuli profile. All stimuli profiles share the same baseline, f_{min}= 0.5 kHz, and peak at the same maximum intensity, f_{max} = 4.5 kHz. The beginning and end of each stimuli profile is chosen to match the elicited spikes time interval obtained with the Gaussian profile. Modulation in θ was not added to the input profiles. a - Standard Gaussian profile. b - Square wave. c - Triangular wave. d - Ramp with sudden drop. Different phase precession outlines, from distinct published experiment data, may be explained by differences in the receptive field profiles (adapted from (Castro and Aguiar 2012)).

The ramp profile is in agreement with experimental data suggesting that the depolarization of a place cell during a pass through its place field steadily ramps and suddenly drops off (Harvey et al. 2009). It is interesting to notice that the downward concave shape of the phase precession outline produced by this input profile better resembles some published data (namely (Skaggs et al. 1996)). This model can thus be used to test hypothesis about conditions giving rise to particular features in the phase precession properties.

3.4 Discussion

Understanding how phase precession may arise is an important step in knowing how spatial and non-spatial information is coded in the brain. Here we present an alternative theoretical spiking model, biophysically plausible, which captures key experimental results and shows that phase precession can arise from local θ rhythm acceleration, taking place in local inhibitory interneurons targeting the activated place cell. This is a minimal model in the sense that it shows how phase precession can be generated based on a very limited amount of constraints and principles.

A key advantage of our model is that the functional block - place cell plus local interneuron - is not limited to represent a unit of repetition in hippocampal CA1: it can also represent other regions in the hippocampus formation (DG and CA3) or even in the medial entorhinal cortex where phase precession has also been reported. The absence of particular architectural/connectivity constraints, except for the feed-forward inhibition and the weakly coupled interneuron network exhibiting an oscillation (against which precession can be measured), makes our hypothesis and model relevant to other areas of the brain besides the hippocampus and entorhinal cortex. It should be noticed that the role played by the interneuron in the model can be represented in the neuronal population by a small group of local interneurons. In the hippocampus, basket cells are very good candidates for this role since they are subject to θ oscillations and they have a key influence in the pyramidal cell's activity (Halasy et al. 1996). In the model, both θ modulations in the EC input and into the interneuron are synchronized to the same phase of the global θ rhythm (i.e. the parameter φ is shared). This is not a requirement though, and in fact it is easier to accelerate the interneuron and modulate the place cell at a frequency above θ if all inputs are not synchronized at the same phase. This is stated since different interneuron classes are known to be synchronized to different phases of the population θ rhythm.

The absence of restrictive architectural constraints has even further implications: in our model, the input to the functional block is tuned to spatial information, but a tuning profile with a different nature (non-spatial) would still give rise to phase precession. Our model demonstrates this possibility and, in fact, is in accordance with recent results showing that phase precession is also present in experiments which do not involve spatial tasks. Even in experiments were the rat is running in a wheel, thus in a fixed spatial position, some

cells exhibit phase precession (Harris et al. 2002). It is important to notice that many alternative models for phase precession generation often rely on specific spatial information inputs (head direction cells, velocity tuned cells, among other) to support the phase precession dynamics.

Phase precession observed at all dorsoventral recording levels in CA3 revealed that the slope of the precession decreased as the place field size increased (Kjelstrup et al. 2008). In the model just described, phase precession slope is a function of the input profile. In particular, if the intensity function is set to define a larger receptive field, the model is expected to produce a phase precession effect dispersed by the total field, thus with a decreased slope, according to this experimental result.

A final comment goes to the connection between firing rate coding and phase precession coding. Some authors (Mehta et al. 2002; O'Keefe and Recce 1993; Skaggs et al. 1996) address this two coding schemes as being independent and complementing each other in the sense of providing more spatial information when combined. Our results are coherent with experimental results and do not support this idea: rate coding and the phase precession effect may not be two independent mechanisms.

4. Modeling grid like firing pattern formation

Experimental research has provided several key results which are improving our knowledge about some of the components involved in spatial navigation. Some essential aspects to be considered in grid models are: grids of neighboring cells share a common orientation and spacing, but their vertex location (their phases) differ (Hafting et al. 2005); the representation of space in hippocampal and cortical tissue is non-topographical (Quirk et al. 1992); when rate remapping occurs in place cells, grid vertices remain stable; when global remapping occurs (different set of place cells active), grid fields realign without losing their intrinsic spatial phase structure (Fyhn et al. 2007); gridness scores (measure used to classify grid cells) near adult levels are already present in the early days of rats life (P22) (Wills et al. 2010).

In this chapter, an original model developed for this thesis published in two abstracts in international peer-reviewed conferences are presented (see also section A.7). A paper is currently under review for an international peer-reviewed journal:

- Luisa Castro and Paulo Aguiar, *Inhibitory synaptic plasticity, allied with place fields competition and compactness, can give rise to grid-like firing pattern*, 2nd Champalimaud Neuroscience Symposium, at the Champalimaud, Centre for the Unknown, Lisbon (October 2012). 1st European Neuroscience Conference by Doctoral Students, ENCODS, Bordeaux (April 2013).

- Luísa Castro and Paulo Aguiar, *A model for grid cells where spatially correlated place cells compete for the grid map nodes*, BMC Neuroscience (8 July 2013) 14 (Suppl 1): P2. DOI:10.1186/1471-2202-14-S1-P2.

- Luisa Castro and Paulo Aguiar, *A feed-forward model for grid fields' formation where spatial information is provided solely from place cells*. Submitted to Biological Cybernetics, (BICY-D-13-00060).

4.1 Introduction

Grid cells (GCs), which can be found in the medial entorhinal cortex (mEC), have the

remarkable property of having their firing activity spatially tuned to a regular triangular lattice. Most of theoretical models already proposed for their formation fail to account for important constraints of the GCs system such as lack of high recurrence levels and absence of topographic organization of mEC. As such, models for grid fields' formation are still under active improvement.

In our point of view, another crucial element which is not properly accounted for in existing models concerns the result that grid fields form almost instantaneously when the rat is placed into new environments (Hafting et al. 2005). This is complemented by results from experiments with rat pups (first spatial experiences being formed) providing evidence that head direction cells develop first followed by place cells and finally grid cells (Wills et al. 2010). This development hierarchy suggests that place fields may provide the spatial inputs to the grid cells firing field's formation.

Here we present a novel model for the emergence of grid like firing patterns which stands on two key hypothesis: i) spatial information in GCs is directly linked to place cells (PCs) activity and ii) grid fields result from a complex synaptic plasticity mechanism involving inhibitory and excitatory neurons mediating the connections between PCs and GCs. Depending on spatial location, each PC can contribute with excitatory or inhibitory inputs to the GCs activity. The amount of excitation or inhibition provided by each PC is a function of the distance to the place field center, which is inferred from rate decoding. A complex but biophysically plausible spatially tuned learning rule drives the evolution of the synaptic efficacies mediating the connections from PCs to GCs. The potentiation and depression effects driven by such plasticity rule favor efficient packing of space representation leading to grid like firing patterns, while not requiring a topographic organization. The model described here intends to represent the feed-forward connections from hippocampal fields such as CA1 towards deeper mEC layers.

4.2 Methods

Supported on the low recurrence levels in EC deeper layers and on the existent projections from CA1 onto EC's layers V and VI, the model represents feed-forward projections from place cells in CA1 to grid cells in EC deeper layers.

The output unit, a putative grid cell, is modeled by a firing rate model, where a transfer

function decides the relevant input for inversing the output rate decay tendency while the synaptic dynamics define the way connections strength evolve and settle to a final map. The reason for choosing a firing rate model in the formation of grid patterns is straightforward since the goal is to obtain a firing rate pattern with no dependence on the precise spike timings.

4.2.1 Feed-forward firing rate model

The model proposes a simple feed-forward architecture where one grid cell receives indirect input from *N* place cells associated with different locations (space sampling). The feed-forward connections between each place cell (PC) and the grid cell (GC) are mediated by two pathways of opposite influence: one excitatory and one inhibitory (see Figure 4.1). Each place cell drives one excitatory neuron (E) and one inhibitory neuron (I_1) responsible for these two pathways. The inhibitory pathway is subject to an activity level control by a third class of neurons (I_2). The core assumption of this architecture is that each place cell can have a combined excitatory and inhibitory influence over the grid cell activity. The nature and strength of the influence is determined by the place cell firing activity. This model assumes that the firing rate range in place cells is approximately normalized. In other words, the firing rate coding scheme is shared among the place cell population meaning that the firing rate of a place cell is highly informative about the absolute distance to its place field center.

The dynamics of the grid cell are described using the firing rate model:

$$\tau_r \frac{dv}{dt} = -v + f\left(\sum_{i=1}^{N} w_i u_i\right),$$

where τ_r =20 ms; $f(z) = z$ if $z > 0$ and zero otherwise; u_i and w_i represent respectively the firing rate of the inputs and their associated synaptic efficacies (connection weights). The semi-linear transfer function is used as it represents a good compromise between simple and meaningful way for the neuron to integrate its inputs.

For the purpose of simplification, in most analysis the dynamics of the association neurons[12] E, I_1 and I_2 are not explicitly described by a differential equation and their

[12] An association neuron is nerve cell found entirely within the central nervous system that acts as a link between sensory neurons and motor neurons.

modulatory action on the grid cell is instead represented as a transfer function which is applied to the place cells output activity. This transfer function reflects the combined action of the individual transfer functions of the association neurons and allows the model to be analyzed with only two neuronal classes, one grid cell and *N* place cells, with a simplified direct connection between them.

Exclusively in the detailed analysis of the weight modification rule, and as a proof of concept, the association neurons E, I_1 and I_2 are explicitly described by firing rate models with τ_r =100 ms. Instead of the semi-linear transfer function f of the grid cell, the association neurons use a sigmoid function φ defined by parameters a and b:

$$\varphi(z) = \frac{1}{1+e^{-\frac{z-b}{a}}}.$$

Parameter a defines the width of the sigmoid's slope and was set 0.02 for all neurons. Smaller/higher a values produce sharper/smoother slopes in the transfer function but do not affect the overall behavior of the model. Parameter b assumes distinct values, b_E, b_1 and b_2 corresponding to the three distinct association neurons E, I_1 and I_2 respectively. Note that the same overall effect could be attained if neuron E was not considered and GC played his part (having b_E as an inflexion point in the transfer function). The described architecture was chosen in order to obtain the effect not only on the output grid cell but already in the synapses affecting it. For the simulations presented here the values b_E=0.25, b_1=0.50 and b_2=0.75 were used.

The plasticity of the synapses that project to the GC must reflect the behavior of the presynaptic neurons in order to mimic the desired connections strength modification rule. Therefore, dynamic weights are attributed to both synapses which increase proportionally to their presynaptic rate.

As described, the circuit comprises only canonical tools for neural transmission and processing and could easily fit in the communication projections between CA1 and mEC deeper layers. In our simulations we used a step version of the synapses modification rule derived here just for the sake of simplicity.

The combined excitatory and inhibitory action of each place cell on a grid cell hypothesized in this model allows the formation of different regions of influence, dependent on the distance between the place field center and the animal's position (encoded in the firing rate): a hot spot of excitation in the neighborhood of the place field

center, an adjacent ring of inhibition, a surrounding excitation ring and a neutral peripheral region. This is therefore a center-surround activation profile but modulated by the place cell's firing rate (encoding the distance to place field center) instead of modulated by topographic connections which are known to be absent in the grid field system (Hafting et al. 2005). The borders of the regions are defined by the parameters b_E, b_1, b_2 and σ.

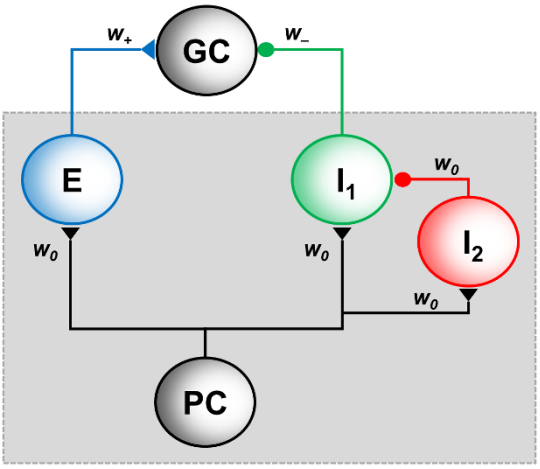

Figure 4.1 Diagram of the model network architecture. The key element in the proposed model is that each place cell PC can both excite (directly or indirectly) and inhibit (indirectly) the grid cell GC. In the presented architecture this modulation is mediated by three types of association neurons: excitatory neuron E, and inhibitory neurons I_1 and I_2. All synapses have a static unit weight w_0 except for the synapses targeting directly the grid cell. The excitatory synaptic weight w_+ and the inhibitory synaptic weight w_- dependent on the firing rates of neurons E and I_1, respectively. A grid cell receives connections from N place cells, each combined with an E, I_1 and I_2 neurons (shaded area).

In this model, place cells compete for grid cell activation. The excitatory and inhibitory pathways of a winning (selected) place cell, ensure that the grid cell is enforced to fire close to the center of the place field. Grid cells continuously recruit new place cells to cover the space. Importantly the recruitment is only possible when the grid cell is freed from inhibitory action from place cells close to the present position. The learning rule supporting these dynamics is described in detail in the synaptic plasticity section.

4.2.2 Spatial input from place cells

In the model, all spatial information reaching the grid cell originates from place cells which encode the position of the hypothetical animal in a maze. Place field centers are positioned, for simplification, in the nodes of a square lattice with 1 cm unit side that covers the entire virtual maze.

Place fields firing intensity is defined as a bi-dimensional Gaussian function. The same

standard deviation σ is used in all place fields and its magnitude can be changed to reflect the hippocampal area that is being modeled (dorsal/ventral). The place cell field's width was set to $\sigma = 0.05$ m. In fact, when modeling dorsal place fields, the radius of the field should be approximately 12 cm. According to (Jung et al. 1994), in dorsal CA1, an average place field occupies an area of 0.0462 m^2 (corresponds to 0.12 meters radius). The same paper attributes 8 Hz for the maximum firing rate for CA1 complex spike cells. Thus, for deriving the place cell width (σ) our normalized firing rate function must satisfy:

$$u(\textit{place field border}) = u_{\max} e^{-\frac{radius^2}{2\sigma^2}} \Leftrightarrow 1 = 8e^{-\frac{0.12^2}{2\sigma^2}} \Rightarrow \sigma = \sqrt{-\frac{0.12^2}{2\ln\left(1/8\right)}} \approx 0.06 .$$

For the parameter values above described, the value for the place cell standard deviation becomes 0.06. However, in our models we have lowered this parameter value to 0.05 meters since recent reports (Hafting et al. 2008) show higher maximum rate values close to 20 Hz.

We use either a path generator function or experimental data to define the position $p(t)$ of the rat in the maze at each time step t. The position $p(t)$ is then used to obtain each place cell's firing rate:

$$u_i\left(p(t)\right) = e^{-\frac{d^2\left(p(t),\mu_i\right)}{2\sigma^2}},$$

where μ_i is the position of the i^{th} place field center, $d()$ is the Euclidean distance and σ sets the scale of the field provided to the grid cell system.

Experimental reports show that place cells fields cover homogeneously the training arena (Hafting et al. 2005). In order to provide such a homogenous positional input to the grid cell, we included place cells which center was outside of the arena but close to its border. This way the average activity level provided from the place cells to the grid cell close to maze periphery is not smaller than the activity in other areas. A border or 40 cm was thus considered around the square maze, increasing the total number of simulated place cells to 180×180 units distributed regularly in a square lattice (100×100 units inside the maze borders). The choice of the cells density in the input layer was made to ensure a close to homogeneous input intensity throughout the virtual maze, avoiding super-sampling. It is relevant to notice that random uniform distribution of the place centers could be used without affecting the qualitative results of the model. In the simulations the grid cell

receives connections from all place cells. This is not a requirement, in fact this condition can be relaxed to a reduced number of place cells inputs producing a reasonable sampling of the maze space. Following the firing rate coding scheme hypothesis, the firing rate of the place cells is considered to be normalized and therefore is constrained to the range [0, 1].

4.2.3 Animal space trajectories

Two types of trajectories were used to set the place cells firing rates: experimentally recorded (real) trajectories and randomly generated (synthetic) trajectories. The real trajectories were obtained from Moser group grid cell raw data database, available for download at *http://www.ntnu.no/cbm/moser/gridcell*, which include the position times for a rat running in a cylinder with a diameter of 180 cm with time step of 20 ms. The simulated animal trajectories were constrained to a square maze with 1 meter side and were used in most analyses.

The rat's simulated path inside the maze for a total time of T milliseconds is defined by $p(t) = (x(t), y(t))$. After choosing an initial position to start the trajectory $p(t_0) = (x_0, y_0)$, with $x_0, y_0 \in [0, 1]$ meters, the position of the rat for the following iterations t_i is obtained accordingly to the recurrent rule:

$$p(t_i) = (x_i, y_i) = \left(x_{i-1} + \frac{\cos(\alpha_i)}{h}, y_{i-1} + \frac{\sin(\alpha_i)}{h} \right),$$

where α_i represents an angle in radians, for $2 \leq i \leq T/dt$. The factor $1/h = dt \times v$ represents the distance traveled in each step, given that dt is the time duration of each step and v is the simulated rat's velocity. A constant velocity is used and, unless otherwise stated, is equal to 0.08 m/s. For step $2 \leq i \leq T/dt$, the direction of the movement of the rat is given recurrently by $\alpha_i = \alpha_{i-1} + k\, dt\, \varepsilon$ radians, where k is the rate of change in direction, and ε is chosen randomly in each step from a Gaussian distribution with mean 0 and standard deviation 1. The initial direction α_0 is set to zero. The rate of change in direction was tuned taking into account the velocity and the time step duration, dt=1 ms, in order to generate qualitatively plausible rat trajectories; a value $k = \pi/120$ radians/ms was used. In artificial animal trajectory just described, the direction of movement of the rat is random at each step, taken from a normal distribution with mean equal to the direction of the last move and a small standard deviation. The reason for such choice was to obtain an overall

effect of reduced changes in the direction of motion throughout the trajectory, as loosely visually observed from real rat trajectories. Examples of a real trajectory and a synthetic trajectory are shown in Figure 4.2.

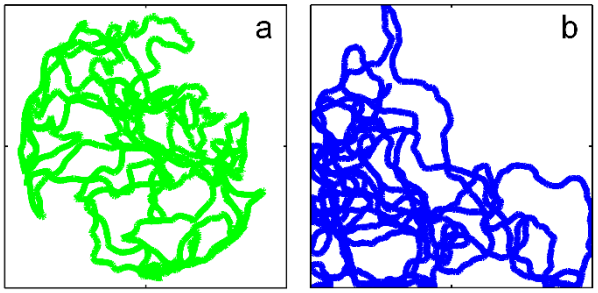

Figure 4.2 Animal trajectories. a - Real trajectory taken from Moser group database (Hafting et al. 2005) and refers to a circular maze of diameter 1.8 m. b - Simulated rat's trajectory on a square maze with 1.8 m side (for comparison with circular maze). Both real and simulated trajectories are for 3 minutes of foraging with velocities of 0.20 m/s (average in real, and constant in simulated). The time steps are 20 ms and 1 ms long respectively.

4.2.4 Synaptic plasticity learning rule

All synaptic connections are static, and take a unit value (w_0=1), with the exception of the synapses E-GC and I_1-GC which are plastic and subject to a fast learning rule (see Figure 4.1).

Learning in these synapses is triggered by a high threshold value r_{th} in the grid cell firing rate; bellow this fixed value no learning takes place. Each time the grid cell's rate rises above r_{th}, the connections with the place cells which are very near their place field center – one or more with their firing rate also above a small threshold value – undergo modifications (association learning rule). The selected cells are recruited from the pool of place cells establishing connections with the grid cell (which provide a space sampling of the arena). These place cells then become responsible for one node of the grid field. In the parameterization of the synaptic plasticity rule proposed here, if the animal crosses the same region again the modified connections keep a high firing rate in the grid cell, but below r_{th}, thus preventing further modifications. As a result, after the complete learning episode, the strengths of the synapses between place cells and the grid cell remain stable as the rat continues foraging/exploring the familiar maze. Nevertheless, if the assemble of place cells involved is changed or suffers remapping, new plasticity episodes can take place.

For the purpose of simplification, plasticity takes place in the collapsed direct connection between PCs and the GC. A synapse between a PC and the GC represents the combined

action of w_+ and w_- (see Figure 4.1). To emphasize this, the terminology connection strength is used instead of synaptic efficacy to address the modifications driven by the learning rule.

A gain modulation mechanism is assumed to take place in the association circuit between PCs and GC during learning episodes. The gain function is implemented by increasing the spatial scale σ of the place fields to $\tilde{\sigma} = 2.5\sigma$, thus broadening the spatial tuning provided by the PCs to the GC. This gain modulation is associated with plasticity (only takes place during learning) and has the purpose of taking into account published studies showing that the place fields in rats foraging in unfamiliar mazes are larger than those reported for familiar arenas (Barry et al. 2012; Karlsson and Frank 2008).

Plasticity occurs in a one-step procedure which is a function of the present weights in addition to the gain modulation of place cells activity. The synaptic strength of the connections is considered to be in one of four distinct levels: baseline w_b, minimum w_{min}, switching w_s, and maximum w_{max}, where $w_{min}<w_b<w_s<w_{max}$. Changes can occur in both directions (potentiation and depression), with consecutive transitions between levels. Note that this does not mean that in our model a synapse can be simultaneously exciting and inhibiting a postsynaptic neuron (contradicting biological evidences (Amaral and Lavenex 2006)). In fact the double modulation effect described is the result of the small network illustrated in Figure 4.1, where each existing synapse has only one of two possible effects: either exciting or inhibiting its goal cell.

In a naïve animal, in an unfamiliar environment, place cells connections are assumed to have similar weights w_b. Also, in the first entry to an unfamiliar environment, the GC is assumed to be in a more depolarized state such that, independently on the animal's position, it easily reaches r_{th} and triggers the first plasticity event. In this initial condition, given the homogeneity of the PCs connection strengths, every place in the maze is a possible place for the emergence of the first grid field node.

Upon the first plasticity event, the strengths of the connections from some place cells are pushed towards one of the three modified levels (w_{min}, w_s or w_{max}) accordingly to each place cell firing rate. The PCs firing rate is considered to be divided into ranges $1>q_1>q_2>q_3>0$, each defining an interval of distances to the place field center. In this first plasticity event, PCs with a rate above q_1 have their connection strength modified to w_{max}. This sets a central disk, region R_1, centered in the position of the animal. Place cells which

place field center is located inside R_1 have their connections set to w_{max}. Surrounding this inner disc, a ring shaped region R_2 is formed with all place cells with rate values in the interval $[q_2, q_1[$. The connections of the place cells within this gain activity range are modified to minimal value (could also be negative) w_{min}. Importantly, place cells firing in the range $[q_3, q_2[$, forming an outer ring R_3, have their connections potentiated to a temporary value $\tilde{w}_s$ slightly above w_s ($\tilde{w}_s$=1.2 w_s, in the simulations). This condition is only required in the formation of the first grid field node, and is necessary for generating a grid cell firing rate above r_{th} (and thus a second learning event) once the animal crosses the center of a place cell which connection has been potentiated to $\tilde{w}_s$. Alternatively to the temporary $\tilde{w}_s$ condition, one can think of the grid cell still having some residual depolarization after entering a novel environment, making it more susceptible to reach r_{th}, in the periphery of region R_1. Finally, place cells with firing rate values below q_3, i.e. fields centers located in the rest of the maze, do not undergo any modification in their connections strengths, these are kept at w_b. The dependence of the synaptic modification with the PC firing rate, triggered only when the GC rate is above r_{th}, is represented in Figure 4.3.

The radius associated with each of the regions R_1, R_2 and R_3 is, respectively, φ_1, φ_2 and φ_3. The initial connections strengths w_{min}, $\tilde{w}_s$ and w_{max} are set in such a way that, after the first learning event, where the grid cell was considered to be more prone to high firing rates, the only region where the grid cell receives enough excitation to reach r_{th} is on the ring R_3. In other words, a range in the firing rate of the PCs encodes a ring of space around the previously created grid field node where a new node can be created.

As the animal explores the environment, each new learning event adds a new grid field node by recruiting some place cells with the field's center (approximately) at the node's location. The connections of the PCs in the inner disc R_1 and inhibitory ring R_2 are set, respectively, to w_{max} and w_{min}, as previously. For PCs in the R_3 region, i.e. gain rates in the interval $[q_3, q_2[$, two types of potentiation may occur: connections that were at level w_s now become w_{max} and connections that were at level w_b now become w_s. Connections that were previously w_{min} or w_{max} do not suffer modifications. Figure 4.3 and Table 4.1 summarize the proposed synaptic plasticity learning rule.

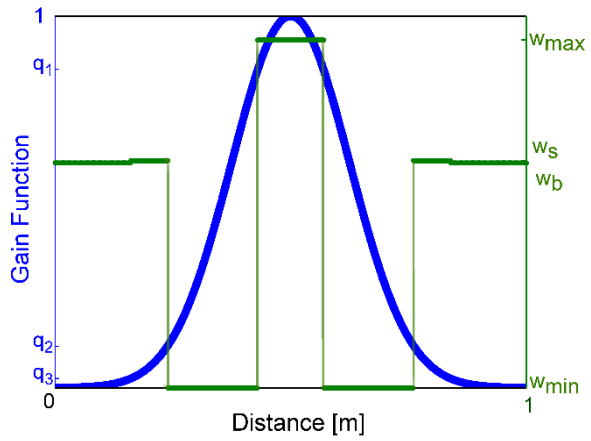

Figure 4.3 Relation between PC rate gain function and connection strength modifications. Output of a PC with place field center at 0.5 m and σ = 0.05 m for a one meter length linear path (blue/dark gray), and associated connection strength modifications (green/light gray).

This mechanism is repeated as the animal explores the environment, with the GC reaching r_{th} (and thus triggering plasticity) only in the intersecting areas of the outer potentiation rings. The grid map is assembled as the rat explores the environment by recruiting new place cells to activate the nodes of the grid field. By construction, the nodes of the grid field form a regular triangular lattice, as a rate range in PCs encodes a specific distance interval.

Different parameterizations of w_{min}, w_b, w_s and w_{max}, for a given σ, can satisfy the constraints of the learning rule to support grid field formation from the recruitment/competition of place cells. The parameterization used to produce the results presented here is the following.

In the inhibitory/depression rings (regions R_2) the grid cell must be silent, leading to the choice of $w_{\min} = 0$ for the connections from place cells which place field center is located in the R_2 rings. Notice that $w_{\min} < 0$ could also be used, reflecting a strong potentiation of the inhibitory pahtway. These R_2 rings are bounded by the PCs' gain firing rates q_1 (inside) and q_2 (outside). Values for q_1 and the connection strength w_{max} of the R_1 discs were chosen so that the total input to GC would produce an elevated firing rate but without crossing the plasticity threshold. Additionally, these two parameters (q_1 and w_{max} combined) should produce a grid field node with a diameter in accordance to experimentally reported values.

Table 4.1 Summary of the discrete learning rule. Synaptic modifications only take place when GC firing rate is above r_{th}. The notation w_* means 'any connection strength level'.

First Learning Event		Subsequent Learning Events	
PC Gain	Modification	PC Gain	Modification
$[q_1,1]$	$w_b \rightarrow w_{max}$	$[q_1,1]$	$w_* \rightarrow w_{max}$
$[q_2, q_1[$	$w_b \rightarrow w_{min}$	$[q_2, q_1[$	$w_* \rightarrow w_{min}$
$[q_3, q_2[$	$w_b \rightarrow \widetilde{w}_s$	$[q_3, q_2[$	$w_s \rightarrow w_{max}$
			$w_b \rightarrow w_s$
			w_{max}, w_{min} static
$[0, q_3[$	w_b static	$[0, q_3[$	w_* static

In the dorsal mEC, grid field nodes should have approximately 10 cm of radius (Sargolini et al. 2006). The size of individual grid field nodes was estimated as the area covered by the central peak of the autocorrelogram, using a threshold correlation of 0.2. Satisfying both constraints, we choose for the R_1 region:

$$q_1 = e^{-\frac{\varphi_1^2}{2\tilde{\sigma}^2}} \text{ and } w_{max} = 1.5\ \rho\ r_{th}.$$

The parameter ρ is a normalization factor: if GC input connections strengths were all ρ then the firing rate would be 1 (check section A.6 for details). The scale 1.5 is used to ensure a GC high firing rate if the inputs were coming only from R_1 (assuming a null contribution from the outer regions). Finally, the distance of $\varphi_1 = 0.07$ was tuned to generate grid field nodes with approximately 10 cm of radius, assuming that the PCs in R_1 are at w_{max} and in R_2 are at w_{min}. The other parameters are dependent on the spacing G between nodes (defining the triangular lattice length), which in the dorsal regions of mEC, is roughly 35 cm (Sargolini et al. 2006).

Quantities $q_2 = e^{-\frac{\varphi_2^2}{2\tilde{\sigma}^2}}$ and $q_3 = e^{-\frac{\varphi_3^2}{2\tilde{\sigma}^2}}$ define the limits of the R_3 region. Distances φ_2 and φ_3 must be such that the intersection of excitatory rings, the diamond zones, fall preferably inside the R_1 disc to be later formed in that intersection. With this in mind, the parameters

adjusted according to simulations results were set to $\varphi_2 = 0.26$ $\varphi_3 = 0.34$ (although these values are below the spacing desired, null weights in R_2 will push the maximum input intensity towards the outside of the region R_3 which results in the threshold for plasticity occurring outside the R_3 region). As a result, firing rate boundaries relevant for plasticity become: $q_1 = 0.85$; $q_2 = 0.11$; $q_3 = 0.025$. Please remember these are normalized rates. Assuming a maximum rate of 40 Hz, these boundaries would become, respectively, 34.0, 4.4 and 1.0 Hz.

Finally, the connections strengths to attribute to regions R_3 and rest of the maze must obey two soft conditions. First, in these regions, the output firing rate must not trigger plasticity, thus both w_s and w_b must be less than $\rho\ r_{th}$. Second, since connections from cells in R_3 have been potentiated once, contrary to the surrounding region, then for coherence $w_s \gtrsim w_b$. The analysis of simulation results supported the following choices for the weight parameter values: $w_s = 0.98\ \rho\ r_{th}$ and $w_b = 0.97\ \rho\ r_{th}$. It is important to emphasize that other combinations of values for connections strengths and distances/rates delimiting the various regions , while keeping the models qualitative results, are possible.

The model was developed, simulated and analyzed in MATLAB® (R2010a, MathWorks, Natick, Massachusetts, U.S.A.). For numerical integration the Euler forward method was used with time step $dt = 1$ ms.

4.3 Results

The learning rule for connections strength update used in this model, plays an important role in the resultant grid fields. Given its non-standard form, this section starts with an analysis supporting the biological plausibility of such rule. Simulation results showing grid map formation, both for synthetic trajectories and real trajectories are then presented, demonstrating also the robustness of the model to variable velocities. Autocorrelograms and gridness scores are presented for the model's generated grid fields.

Biological plausibility of the learning rule

The connections strength between place cells and grid cells in our model are obtained using a non-standard rule. In this subsection we provide biological support to the plasticity rule and show that this rule can be produced by a combination of canonical

synaptic plasticity rules applied in a small excitatory/inhibitory neuronal circuit. In this section, instead of using the simplification of a direct connection between each PC and the GC, we consider the architecture presented in Figure 4.1. Given the parameterization b_E=0.25, b_1=0.50 and b_2=0.75, the excitatory and inhibitory influences of the PC over the GC are segregated into firing rate domains (see Figure 4.4).

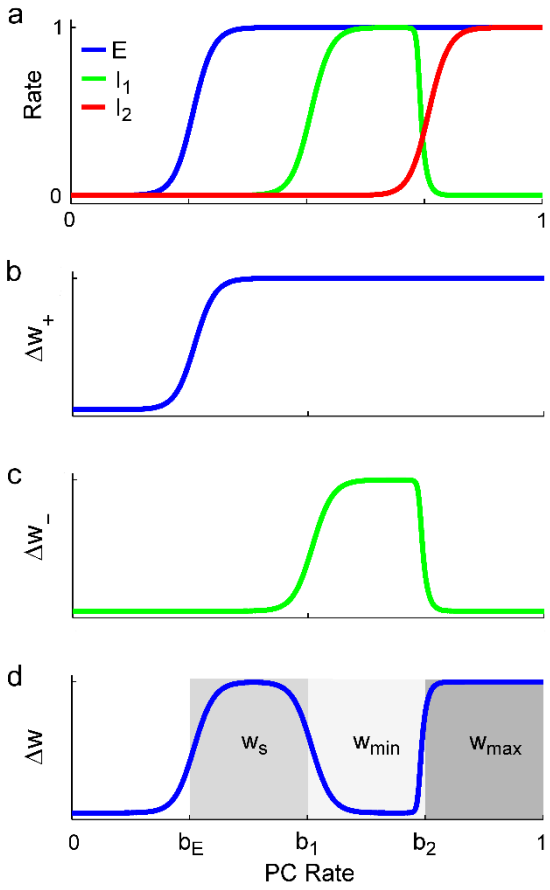

Figure 4.4 Rate profiles and correspondent weight changes illustrating the weight modification rule. a - Associated neurons firing rates as functions of input PC's normalized rate. b - Weight modification for the excitatory synapse from E to GC as a function of PC's rate. c - Weight modification for the inhibitory synapse from I_1 to GC as a function of PC's rate. For the figure, the constant of proportionality between modification amplitude and presynaptic firing rate was 0.01 ms^{-1}. d - Weight modification of a global synapse (comprising both inhibitory effect and excitatory effect) onto the GC, as a function of input rate from the PC.

The excitatory modulation is limited to rates above b_E and the inhibitory modulation is limited to the interval $[b_1, b_2]$. Plasticity takes place in the w_+ and w_- synapses; is triggered by a high activity level in the GC and has a modification amplitude, Δw_+ or Δw_-, proportional to the presynaptic firing rate (canonical Hebbian type learning rule in firing rate models). The distinct frequency domains, and the combination of w_+ and w_- modifications generate the three levels of connections strengths w_{max}, w_s and w_{min}. The connection strength modification to w_{max} results from a strong potentiation in the excitatory (w_+) pathway. The modification to w_{min} results from a shunting or competing

potentiation in the inhibitory (w_-) pathway. The combined connection strength modification to w_s results also from potentiation in the excitatory (w_+) pathway alone (see Figure 4.4 b-d).

Grid field formation

As the rat is placed in the center of a new/unfamiliar maze, the first grid node is quickly formed generating the connection strength map shown in Figure 4.5 a. The connection strength map is used to represent the connection strength between each PC and the GC as a function of the place field center location in space This should not be confused with a topographic map – morphological neighboring PCs are not required to have neighboring place field centers. As the rat crosses for the first time the excitatory ring (R_3), a second field node is formed and now there are only two possible regions for the third field to be raised (diamond zones in Figure 4.5 b). As the animal explores the new environment place cells compete for grid cell activation and become progressively recruited to give rise to the grid field nodes (see Figure 4.5 c and d).

In this simulation, the GC receives inputs from all the PCs, densely covering the maze area. This allows improved visualization of the connection strength maps by avoiding a patchy representation. But a very large number of PCs inputs is not a requisite for the model to work: a reduced number of place cells inputs to the grid cell still produces the same qualitative results as long as the place cells provide a reasonable sampling of the space. The sampling resolution is related to the R_1 disc area – for the parameters of the simulations, a few hundred PCs inputs (with place field centers uniformly distributed in the maze are) are sufficient to support the grid field formation. It is important to notice that in this model the grid map does not extend automatically to infinity; instead, it is progressively extended to the regions being explored. It is reasonable to speculate that the real trajectory of an animal is chosen/conditioned in order to more rapidly and effectively build the grid field through the recruitment process. Using this learning rule, and a constant velocity of 0.08 m/s in a maze with 1 meter side, after approximately 20 minutes of animal exploration the available area is fully tiled and no more learning takes place (GC is no longer able to reach r_{th}).

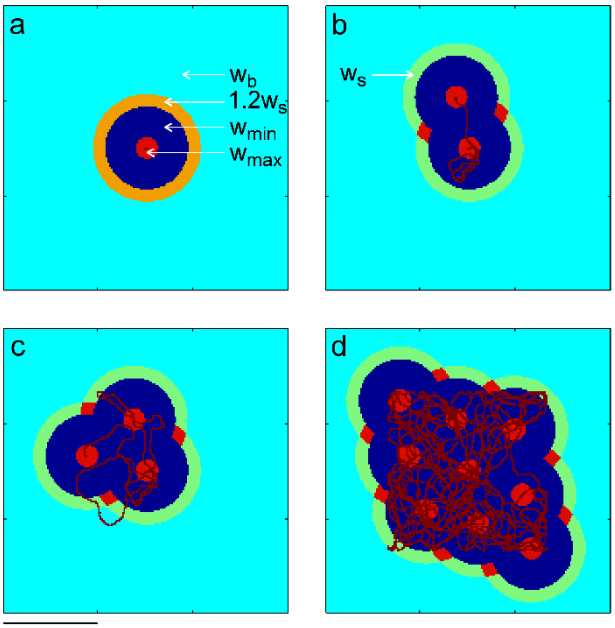

Figure 4.5 Scheme representing place fields centers (cell per pixel) colored according to respective synapse weight (see arrows), together with rat trajectory during learning episode (dark red path). Scale bar is 60 cm. a - Result of the first plasticity episode. b, c and d - Results of the second, third and final learning events, respectively, as the animal explores the environment following a specific trajectory.

During learning, connections strengths are modified resulting in the configuration of Figure 4.5 d. After learning, when the rat is placed back in the same maze, a firing rate map for the grid cell is obtained (see Figure 4.6) and used to compute the gridness score according to Sargolini's method (Sargolini et al. 2006), described previously.

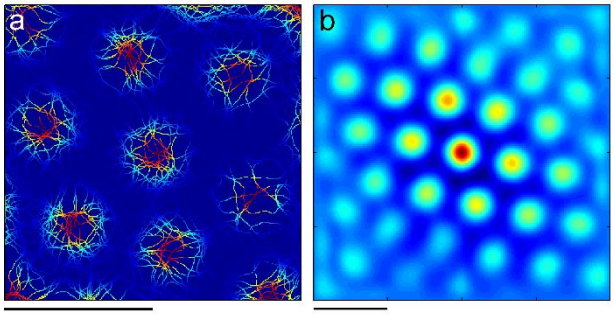

Figure 4.6 Grid cell firing rate map after learning process, for the strength connections shown in Figure 4.5 d. a - Firing rate map of simulated grid cell after learning. Red zones represent higher rates, (~0.90) and dark blue zones are zero rate and unvisited locations. b – Normalized autocorrelogram of field shown in a. Scale bars are 0.5 m.

Before computing the gridness score for the firing rate map, the autocorrelogram is obtained. Grid maps measures for this simulation/parameterization, 36 cm for spacing and 20 cm for field diameter, are in line with the ones reported for dorsal mEC grid cells (Sargolini et al. 2006). The correlation values obtained from the several rotations of the inner ring and the original are depicted in Figure 4.7. The resultant value for the gridness score, implemented for this purpose as described in the Background, is 1.36.

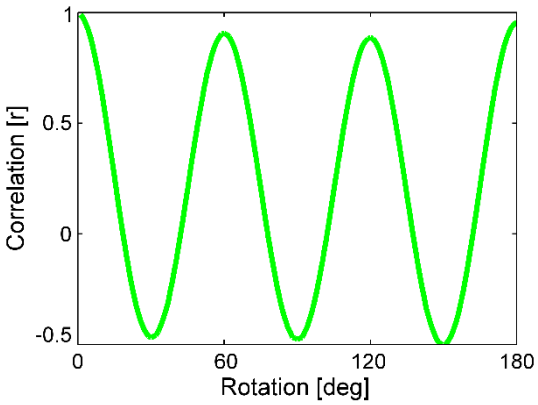

Figure 4.7 Periodicity of the rate map's autocorrelogram. The autocorrelogram shown in Figure 4.6 b was rotated in steps of 1º and the correlation between each rotated map and the original was computed. The gridness score obtained was 1.36.

Running the model with real rat trajectory data, available for download at http://www.ntnu.no/cbm/moser/gridcell) also leads to gridness scores above 1 (see Figure 4.8). As previously stated, it is reasonable to think, that in a real trajectory, the animal favors areas that are less explored, thus actively improving the grid field tessellation/PC recruitment procedure. For a circular maze with 1.80 meters of diameter our model was able to generate a perfect grid mapping covering almost the total extent of the maze, using a real rat trajectory and only 30 minutes of foraging (see Figure 4.8).

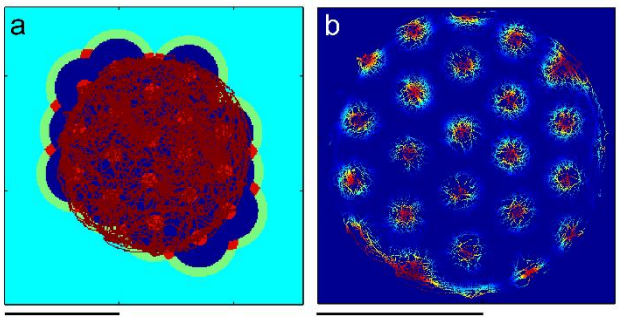

Figure 4.8 Connection strengths and firing map for a real animal trajectory. a - Scheme representing place cells learned weights, as in Figure 4.5 d but using real trajectory data taken from (Hafting et al. 2005), 30 minutes with dt =20ms. b - Normalized average firing rate map of simulated grid cell with the same real trajectory data used in learning epoch a (3:1). Scale bars are 1 meter. Although the path was not enough to generate all possible grid fields, the gridness score obtained was 1.34.

In this model, only the input rates are limited to values in [0, 1]. The weights (apart for the scaling factor $\rho\ r_{th}$) are set initially at unitary value, and throughout the learning process evolve in a step manner. The upper value was chosen by guaranteeing (analyzing simulations results) that grid learned fields do not generate output firing rates above the learning threshold r_{th}. Consequently, the output putative grid cell's activity is not upper constrained explicitly, but by construction, it is also restricted to [0, 1].

4.4 Discussion

Different theoretical models for grid cell patterns formation have been suggested, stimulated by experimental results obtained from a great variety of protocols. As previously mentioned, the majority of attractor network models assume recurrence and a topographic relation between grid cells. Recurrence in mEC layers has been reported for excitatory connections in layers III and V, only around 10%, and not for layer II (Dhillon and Jones 2000) (theoretical models usually do not model grid cells for layer II). Topography for mEC units has not been reported and effective ways to relax this system constraint have not been addressed. Some existent approaches imply path integration ability (Fuhs and Touretzky 2006; McNaughton et al. 2006). The model proposed here has the advantage of not relying on oscillations to generate grid fields. Another important feature of our model, but also present in (Kropff and Treves 2008), is that path integration is not required to produce grid like firing maps.

An interesting result obtained in 1992 was that modifying the shape of the arena had more consequences in positional firing of place cells than on patterns of mEC (Quirk et al. 1992). This particular outcome made the authors suspect that the major information flow could be from hippocampus to mEC, which is in line with the circuitry of this model. The shaped synapses described here could thus refer to the circuit involving hippocampus subfield CA1 place cells feeding the deepest layers of mEC. In accordance with most of grid cells experimental results, the described model is capable of generating a hexagonal grid like firing pattern unit, receiving solely feed-forward inputs from place cells and their associated neurons. The grid cells recently found in pre and parasubiculum (Boccara et al. 2010) can also be derived with the model described here as it only requires place cells input, present in CA1, which has direct projections to subiculum which projects to pre and parasubiculum.

In our model, after 20 minutes of having the rat foraging in the simulated maze, the square maze is totally covered by the grid cell firing map. This behavior is consistent with the finding that the transition from rudimentary to adult-like grid firing structure occurs in a very short time course, of approximately 24 hours in real time (Wills et al. 2012). Moreover, grid structure is expressed instantly in a novel environment maintaining the receptive fields in future visits even if they occur in complete darkness (Hafting et al. 2005). According to our point of view, the “novel environment” (or a maze which the

cells find equivalent to it) could in fact have been already "memorized" by an ensemble of grid cells connections from place cells which were "chosen" as the ones representing that particular class of equivalent mazes. Taking into account that different sets of place cells are active in different environments (Quirk et al. 1992), we can also argue that the same happens with grid cells as a consequence of their connections (place to grids) profile. This idea is also in accordance with the fact that when the rat is placed back in the familiar maze the grid field positions are preserved (Hafting et al. 2005; Derdikman et al. 2009).

Environment shape effects

Rate remapping of place cells is normally observed after performing small changes in the environment such as changing the color of the walls, while global remapping is a consequence of, for example, placing the same box in different rooms or using boxes with different shapes (Fyhn et al. 2007). According to our model, but subject to simulation of the place cells fields in accordance, when the remapping is just in the firing rate of input cells, the hardwire mechanism learned before is not expected to disrupt, and consequently there is a maintenance of the grid field configuration. However, if the maze is now represented by a different set of place cells, then the circuit as described may generate a new grid field structure (with distinct phase and possibly orientation from the previous).

Also, given the model dynamics, if a familiar maze is expanded then one of the two situations described in the previous paragraph might occur. If the rat's space notion recognizes the same type of maze, then the place cells that were active in the small maze will remain active in the large maze and new cells become active to encode the new available portion of the environment. In our model, adding new cells to the familiar place cells set is not expected to disrupt the already generate grid field but will add new ones of the same size and spacing, completing the hexagonal lattice, in agreement with (Hafting et al. 2005). If the expanded maze is categorized by the rat as unfamiliar, then a different set of place cells encodes the space and a new grid field is generated. One way or the other, the path taken by the rat does not need to cover every position of the maze to exhibit the hexagonal structure, in accordance with experimental reports (Hafting et al. 2005).

When Hafting et al performed the cue card displacement experience, they verified that the grid phase and orientation changed in accordance, but the spacing of the grid and its

field size did not suffer any change. In our model, field size and spacing of grid cells is a function of place cells field size. Therefore, if the set of place cells recruited to represent the new maze is within the same neural tissue zone (with respect to the dorsoventral axis) of the previous set of place cells, then the resulting grid fields will share precisely the field size and spacing of the previous ones.

Experimental reports conclude that grid maps and place maps are less likely to reset under food reward displacement than when the local geometry of the arena is changed (Derdikman et al. 2009). Place cells are able to accumulate functions with space representation, related to coding diversified sensory features, such as smell, color, temperature and other experimental cues together with proprioceptive information (O'Keefe 2006). In accordance to our model, grid cells could be devoted to extract only the positional aspects of place cell firing, gathering them in the most compact fashion.

When young rodents are exposed and trained in two different environments, recorded grid cells exhibit nodes displaced by the same offset vector (Wills et al. 2012) (the same behavior is also reported for adult animals (Fyhn et al. 2007)). The same experimental scenario could in principle be used to record CA1 place cells observing their remapping patterns. If fields remapping occurs in a set of place cells displaced by the same offset vector, then it will provide evidence that place cells are feeding positional information to deeper mEC grid cells, supporting the model described here.

A very recent work is devoted to the evolution of grid fields' characteristics while the rat is exploring a novel environment and a familiar one. One important finding is that mEC grid cells have wider fields in the first trials and that they diminish in size during approximately 4/5 days of experiments (the rat gets acquainted with the new maze) while the grid cells in the familiar field do not suffer any change in size. Moreover, in CA1, it is also possible to observe larger fields in the first days while after some days the fields converge to the "familiar" scales. This change for CA1 place cells is not as high as it is for grid cells fields (Barry et al. 2012). In agreement, it has been showed that, during the first visit to a new environment, a significant number of CA1 theta cells turn off their inhibitory action (while DG interneurons are more active). The authors of this study suggest that maybe CA1 interneurons could be part of a broader system that detects new from familiar environments. These cells could be responsible for controlling learning in pyramidal CA1 cells' synapses when the rat is placed in unfamiliar mazes (Nitz and McNaughton 2004). Our model assumes that grid cell detect place cells fields at a higher

scale through the gain function used in plasticity processes, so these reported results provide reliability to our method for grid cell formation.

The feed-forward flow between CA1 and deep mEC

The effect of the inactivation of the hippocampal input to mEC, deserves particular attention when the idea is to learn more about the direction of the information flow in the hippocampus – mEC circuit. Distinct studies (both from Moser's lab thought) state that grid patterns almost disappeared and their firing frequency diminished substantially when hippocampal cells were inactivated. Although referring to layers II and III in mEC, these results suggest that the entorhinal medial cells activity is strongly dependent on excitatory input from hippocampus (Bonnevie T 2006; Hafting et al. 2008). This spatial input is thought to come essentially from CA1 which is the hippocampal region affecting mEC with place correlated inputs. The observation that after hippocampal inactivation several grid cells in layers III were mainly driven by direction is straightforward if we recall that more than half of the grid cells encountered in this layer had conjunctive (directional and spatial) properties (Sargolini et al. 2006). On the other hand, the finding that grid cells in mEC upper layers have less space specificity that lower ones can provide evidence of the spatial flow direction used in this model (hippocampus to mEC deeper layers) (Frank et al. 2000).

Recently visual system experts have reported grid cells in the visual cortex of primates, when those were subject to visual tasks with their head fixed (Killian et al. 2012). Besides its high importance per se, this finding gets highlighted when we notice that the same cells have been found in spatial related activity cells of rats (and bats). This remarkable finding creates a natural partition for the set of grid models. Models that do not need spatial features, such as direction, could be thought in a different scope beyond the spatial one. Such broad class of models may be applied to the visual system, to provide a plausible explanation for the emergence of grid fields in the monkey's entorhinal cortex.

While trying to cope with the great majority of reported features of grid cells firing patterns, this model emerged to provide a possible mechanism underling the almost instantaneous hexagonal grid pattern formation. Our model is able to generate a hexagonal grid cell firing map, while the rat follows a plausible trajectory, using the following principles: 1) the spatial specificity of grid cells is inherited from place cells spatial firing; 2) synapses weights are changed according to a local spatial discriminating

mechanism; 3) a short period of learning time is enough to generate an approximately hexagonal firing pattern.

In this model we used stereotyped circular place fields which does not capture the well-known variability that exists in CA1 (in this region place fields vary in size and shape). But it is important to notice that the circular shape of the nodes in the grid fields do not require homogeneous circular input place fields. In our model each grid field node is produced by recruiting a reasonable amount of neighboring (pseudo co-localized) place fields. Even if each place field is heterogeneous, the node will acquire an approximately circular shape due to the averaging of the input place fields.

As a final remark, our model applies to a single grid cell, but could be extended to multiple grid maps. Assuming competition between grid cells (possibly mediated by inhibitory interneurons), different non-overlapping grid fields can be created. The grid fields would share the same spacing for the same level of mEC, which in turn reflects the scale of the place fields.

5. Final conclusions

Understanding how spatial related mechanisms are generated in the animal brain constitute important steps to understand how animal and thus human neural units cooperate providing a representation of spatial and non spatial information. Theoretical/computational models have proved to be useful in spatial learning study since they anticipated important experimental findings (border cells, grid cells, head-direction cells with speed modulation).

In this thesis we have focused on the study of two distinct spatial processing related brain processes: phase precession effect and grid cell emergence. Recently reported, both processes are still under study in many neuroscience research international institutes, providing every day more relevant data about animal's (mainly rodents) behavior under experimental scenarios. Highly focused on the main features available in the literature about phase precession and grid cells, the strategies employed in this thesis are build up on solid reported data connected by canonical tools, all described to some extent in the first chapter. Accordingly, the models proposed in chapters 3 and 4 of the thesis present evidence that phase precession effect and grid cell firing pattern can be generated without recurring to perfect oscillatory signals interference, high levels of recurrent projections within mEC or topographic assumptions from neural grid cells to physical space.

5.1 Phase precession

Coding information in the hippocampus through phase precession means that the phase in the theta cycle in which a place cell fires provides information regarding the position of the rat inside its place field. There are published models addressing the phase precession effect but commonly they are grounded in stringent assumptions or ignore the fact that signals in the brain are subject to a high degree of variability and noise.

Our theoretical spiking model for the phase precession mechanism is supported on significant experimental results and biophysical plausible tools. In the model proposed, phase advance of place cells spikes is attained from a confined acceleration of the theta rhythm in local inhibitory interneurons affecting the activated spatial cell. Based on a minimal set of constraints, the functional block of the model original representing a unit

of repetition in CA1, can in fact be applied to other regions where phase precession has also been observed (DG, CA3 or mEC). Moreover this model predicts precession in any network with the same architecture and subject to a clocking rhythm, independently of the involvement of the network in spatial tasks (Harris et al. 2002), in contrast with many alternative models that rely on spatial information.

A final important conclusion is that rate coding and phase coding may not be two independent mechanisms, not supporting an existent line of thinking where the two coding schemes are seen as complementary in providing spatial information (Mehta et al. 2002; O'Keefe and Recce 1993; Skaggs et al. 1996).

5.2 Grid cell formation

Grid cells in the medial entorhinal cortex (mEC) encode space in a particular way: their firing rate intensity forms an equilateral triangular lattice as the animal moves in the environment. Models available in the literature addressing the generation of grid fields fall into two major classes, both with important limitations. Most models based on interference of oscillations are not robust to noise and suffer from the prerequisite of two independent and stable network oscillations with similar frequency. Models based on recurrent networks, where the grid pattern emerges as a stable state of the network, suffer from the topographic assumption and the need for dense recurrent connections between mEC cells, which are both not supported by experimental data. Existent self-organizing models are not robust to velocity changes and demand trajectories covering extensively the maze, in order to effectively produce grid cells firing patterns.

Recent reports stating that grid fields' maps form almost instantaneously when rats are placed into new environments motivated experiments on baby animals. One of their remarkable results is that head-direction cells develop first, followed by place cells and finally grid cells. This was a core motivation for our models where, in contrast with the majority of models proposed so far, the spatial information reaches mEC cells through place cells input. The feed-forward firing rate models proposed in this work for single grid cell emergence constitute a main general model where the triangular nodes of the grid map emerge as the result of a novel plasticity scheme. Strength connections from place cells to each grid cell are modeled taking into account the rate coding methodology.

Consequently, potentiation and depression occur as functions of the spatial distance between place fields, resulting in a triangular disposition of the grid nodes. The model proposed does not impose constraints on velocity (suitable for real or simulated paths), high recurrence levels, noiseless neurons, topographic disposition of units, and the animal trajectory is not required to densely cover the maze.

By construction, the general model proposed is expected to comply with experimental features related to grid cells responses to environmental changes as place cells remapping, path equivalence and to spacing scaling differences along the dorsoventral axis of mEC. All these experimental distinct features could be direct consequences of the notion that assembles of place cells, for each location in the dorsoventral axis (Kjelstrup et al. 2008), are needed to represent each class of mazes (Quirk et al. 1992). In our model, place cells in dorsal/ventral regions of CA1 would be in the genesis of grid cells in dorsal/ventral parts of deep mEC, according to results on topographic projections between the two regions (Amaral and Lavenex 2006). The classification of mazes into equivalent classes could be the result of the exploration of many mazes combined with the ability of generalization.

5.3 Final remarks

Experimental studies on hippocampal regions (CA1, subiculum and DG) show evidence that spatial firing fields of interneurons are as spatially tuned as principal neurons (directional and spatially informative). The spatial pattern of activity is distinct from that of the principal cells: they fire continuously at ~20 Hz, show an ON field (where the firing rate reaches ~40 Hz) and an OFF field (~2 Hz) on the trajectory path (Wilent and Nitz 2007). In medial entorhinal cortex, similar evidences have been provided, concerning spatial tuning of mEC interneurons (Savelli et al. 2008). Implicit in our plasticity mechanism employed for place cell onto grid cell connections, is inhibitory synaptic modulation. Both models developed here predict that inhibitory neurons are key elements not only for controlling population activity at a global level (as commonly accepted) but also playing crucial roles in specific spatial processes according to the experimental findings described:

- modeling phase precession of principal cells we also obtained a phase advance

compared to theta rhythm in the spiking times of inhibitory neurons (supported by experimental results);

- on the detailed architecture of the connection strengths modification rule it is also assumed that inhibitory neurons have spatial preferences.

We thus show that inhibitory interneurons have functional roles that go beyond activity level control. Instead they have crucial roles in both the dynamics and plasticity of the neuronal circuits.

Finally, the two models presented are complementary in the sense that both mechanisms could be merged in a broader model exhibiting a phase precession effect and grid like firing patterns. This is a significant step forward towards a holistic model of spatial information coding involving the hippocampus.

6. Future Work

The study made and the models developed for this thesis have originated some valuable suggestions. Such hints could be investigated in further work related with spatial encoding in hippocampal and entorhinal cortex regions. Individual predictions from each one of the chapters 3 and 4 are described in the following lines. This chapter ends with some pioneer ideas for a broader model for the formation of grid cells and place cells combined with the phase precession effect.

6.1 Phase precession

A critical aspect of our proposed model for phase precession is the lack of bursting episodes observed in our results and characteristic of phase precession reports (place cells and grid cells are all complex spike cells). In fact, leak integrate-and-fire models are not suitable for reproducing such complex output activity profiles. Therefore, a possible extension of the model presented in chapter 2 could be the addition of currents suitable for complex spike patterns generation.

In our theoretical/computational model for phase precession, different input profiles (spike trains modulation) revealed phase precession curves with different slopes. This interesting result may predict that particular features present in experimentally reported phase precession can be a result of the type of situation under test. While ramp like input curves are suitable to represent inputs in spatial tasks, other tasks (e.g. sensorial) may be better symbolized by other inputs profile, thus illustrating other phase precession properties. This model can thus be used to test hypothesis about conditions giving rise to particular features in the phase precession mechanism.

6.2 Grid cell formation

The second model proposed for grid cell formation has clearly some limitations, already described in the respective section (see A.7). Overall, some strategies can be imported from the first model: the extension of the space representation by the inclusion of more

place cells (or border cells) to account for homogeneous input in the maze borders and the gain modulation on the plasticity rule to generate plausible spacing values between nodes. The following paragraphs refer to predictions extracted from the more complete model for grid cell formation described in chapter 4.

Path equivalence concept, introduced in 2000 by Frank and colleagues, refers to a pattern that some cells exhibit by firing in the same position relative to start and end points of a maze, on two or more distinct trajectories. Most cells recorded in CA1 area do not show this feature but EC cells, especially from deep layers, do. These results suggest that most deep EC cells have the ability to fire in somehow similar locations across distinct environments. EC deep layers are only fed by inputs from CA1 and subiculum not receiving any direct visual projections (Frank et al. 2000). Then some generalization process may be taking place in EC units to allow for their reported ability of path equivalence. Alternately, another report suggests that subiculum place cells have also shown path equivalence (Sharp 2006). Since no grid cells have been found in subiculum (to our knowledge) the feature of path equivalence in EC may be inherited by upstream path equivalent skilled subiculum place cells. If grid cells are, as thought, responsible for setting the metrics in rodents' spatial navigation, then path equivalence generalization ability seems to be a useful skill for that purpose. Analogous experiments on grid cells from other regions, such as pre and parasubiculum (Boccara et al. 2010) can allow for important data to disentangle the real emergence of characteristic grid cells firing.

Head-direction cells have their tuning set at adult levels even before leaving the nest by the first time (Langston et al. 2010). On the other hand, it has been observed that conjunctive cells are present in young rodents mEC (layers III to VI) since the stage of grid cells emergence (Wills et al. 2012). Together with the hypothesis that head-directional ability could be innate (Langston et al. 2010), the finding of early conjunctive cells could be explained by a competitive Hebbian plasticity mechanism taking place within mEC itself (except layer II) between the two "pure" cell types: grid cells and head-direction cells.

The model proposed here for grid cell formation shows that head-direction cells input is not required for the emergence of triangular patterns on a single cell. However, experimental reports show that head-direction cells, grid cells and border cells all rotate their firing preferences when a cue card is rotated (Hafting et al. 2005; Solstad et al. 2008). Head-direction cells, although not required for their firing pattern shapes, could be the

orientation drive of the cognitive map providing the angular information in mEC for the synchronous rotation of grid cells maps and border cells maps.

A recent experimental report has provided evidence that the organization of the grid cells scale throughout mEC is modular (Stensola et al. 2012) instead of continuous as commonly thought. According to the general model proposed in this thesis, where grid spacing and size are functions of the CA1 place cells field size, then CA1 units' receptive field must also scale in size in a discretized fashion along the dorsoventral axis of that hippocampal region.

An interesting observation is that most of the published reports (to our knowledge) are made in rats which are always placed in constrained mazes (probably due to recording constraints associated with larger environments). These animals (when adults) are able to create the grid tessellation in quite short periods of training time. Would this ability be present in a really larger maze, 10 times larger than the traditional ones?

Experiments in hairpin mazes show that grid cells maps are reset each time the rat moves into a new arm after reaching the end of the previous arm. Arms which were crossed in the same direction revealed path equivalence in grid cells firing. When the same maze had its walls replaced by transparent walls, the different cells behaved in the same way which made the authors conclude that visual access to distal environment did not prevent realignment between the compartments of the hairpin (Derdikman et al. 2009). A possible interpretation for this behavior might be that the animals' responsiveness is towards the portions of the maze he can actually have access to, at each moment. This way, the existence of a wall transparent or opaque, is enough for the animal to understand that he cannot transpose them and have access to the total extend of the maze or even to two arms simultaneously. A possible experience to disentangle this issue would be replacing the interior walls in the hairpin maze with curtains such that the rat could not see other arms/environments but could access them directly by crossing the curtain. Would grid cells keep the discontinuous representation of the maze or will them act as in the case of a two dimensional maze? Would place cells behave in the same manner?

The emergent evidence that place cells signal different shapes by firing or not on similar but different shaped environments motivated the recording of place cells activity while the square maze become octagonal and finally turned circular (Wills et al. 2005). As a result, place cells abruptly remapped, some losing/gaining a receptive field in the maze and others changing their place field to a different position. The same experience protocol

could be applied to grid cells, shedding some light into the way these cells might be wired to each other.

Although designed to model single grid cell formation, the general model of chapter 4 can be extended as to provide multiple grid cells/maps by introducing competition between grid cells (for example intermediated by inhibitory interneurons present in mEC). Such append should accomplish reported results regarding grid cell population properties as grid fields alignment between cells in the same recording location, such as same phase and spacing of maps with random orientation.

6.3 Final remarks

As previously addressed in the review of existent models for grid cell formation, the majority of continuous network models for the reproduction of grid firing patterns assume a topographic relation between neural regions and environment locations. The ones relaxing the importance of this constraint, claim that topography is not required if the connections between grid cells have already in their strength the information regarding phase difference (i.e., fields displacement from one cell relatively to the other) of units. However, the majority of this models do not explore the mechanisms behind the emergence of such connectivity scheme. One exception uses traveling waves, much like in the visual system where topography between units does exist (Fuhs and Touretzky 2006). Another paper suggests a teaching layer, possibly innate, which disappears after some time, disabling the animal from learning more environments (McNaughton et al. 2006).

In a broader view, an improved model for grid cell formation and also place cell emergence could be divided in three distinct parts.

1. In the newly rat, single grid cell formation (not necessarily perfect) could be the result of some self-organizing method, in the absence of topography or recurrence constraints. The model proposed in chapter 4 of this thesis is a plausible one.
2. In a second stage, a class of local inhibitory neurons would interfere, allowing for a more efficient coverage of the environment by population grid nodes. They could be receiving input from one grid cell and locally inhibit the cells with distinct nodes locations (through rate coding). As a side effect, the hexagonallity

of each grid map would be improved. This process could refer to upper mEC layers (such as layer III and II).

3. Grid cells in mEC layer II could provide positional information for the place cell formation in hippocampus regions, such as DG, CA1 and CA3. Place cell fields spatial specificity could be obtained from the intersection of nodes from grid cells. The grid cells used for each place cell should ideally come from different neural locations, since at the same recording locations their nodes are disjoint. Such strategy has been proposed by some models for place cells generation (for a review see (Moser et al. 2008)).

This scheme is not dependent on path integration ability nor needs to account for oscillations interference. The idea shortly suggested is in accordance with several experimental reports referred previously. For example, gridness scores are known to be higher in layers III and II than in layers V or VI (Sargolini et al. 2006)[13]. In step 2, the introduction of interneurons capable of organizing grid cells nodes in a more efficient packing could contribute for such higher scores in gridness measures.

Moreover, it is known that spatial information content decays from deeper to upper mEC layers units (Frank et al. 2000). In fact, if the mEC is receiving refined positional data from hippocampal regions projections, and within mEC the projections are from grid cells to grid cells, then part of the original positional information will be lost in this feed-forward flow. Some models for place cell formation suggest that upper hippocampal layers unimodal cells could result from intersection of EC inputs (also from upper layers) (see the review (Moser et al. 2008)). Being that the case, then the spatial information driving place cells would be the combined spatial information of a set of grid cells. Hence place cells could carry more place specificity than upper mEC grid cells in accordance with experimental results.

Regarding phase precession, the mechanism as proposed in chapter 3 could easily be incorporated in this broader model. This way place cells and grid cells generated by the hypothetic model would exhibit the phase advance in accordance to experimental studies.

Although many aspects are difficult to test at the present time, many others will certainly

[13] This report also shows that gridness scores in layer II are substantially better than in layer III (deduced from histograms showing the distribution of the gridness scores of all cells in mEC layers). A simple explanation for this could be that since there are no conjunctive cells in layer II, then conjunctive cells could be disrupting the results for the deeper layers.

begin and continue to be investigated, providing new features of spatial units and processes. With this input, models advance in their applicability and we become closer to unravel the real mechanisms behind experimental behaviors and consequently understand more about animal navigation abilities.

Appendix

A.1. The inverse transform method

The inverse transform method (Ross 2002) is used for generating random values from the exponential continuous distribution.

Let F be a distribution function which by definition is monotonically increasing. Consider U a uniform random variable in]0, 1[, and X a random variable defined by $X = F^{-1}(U)$ with distribution function denoted by F_X, as usual. Then:

$$F_X(x) = P(X \le x) = P\left\{F^{-1}(U) \le x\right\} = P\left\{F\left(F^{-1}(U)\right) \le F(x)\right\} = P\left\{U \le F(x)\right\}.$$

Now, since U is uniformly distributed in]0, 1[, then it follows that $P\{U \le F(x)\} = F(x)$.

In summary, the method of generating a realization of an X variable with any continuous distribution function F, is to produce a realization of the uniform random variable U and take $X = F^{-1}(U)$ (Ross 2002).

In the ISI's case, X is an exponential random variable, thus its distribution function is:

$F_X(t) = 1 - e^{-\lambda t}$, for $t \ge 0$. To find the inverse function, set $u = F_X(t)$ and do:

$$u = F_X(t) \Leftrightarrow u = 1 - e^{-\lambda t} \Leftrightarrow e^{-\lambda t} = 1 - u \Leftrightarrow t = -\frac{\ln(1-u)}{\lambda}.$$

Finally, generating numbers using $X = -\ln(1 - U)/\lambda$ with U being an uniform random variable, is equivalent to use $X = -\ln(U)/\lambda$, since $1 - U$ is also a uniform random variable.

A.2. The thinning technique

Formally, $\{N(t),\ t \geq 0\}$ represents a non homogeneous Poisson process with intensity $\lambda(t)$, $t \geq 0$, if the following statements are verified:

a) $N(0) = 0$;

b) The number of events that occur in disjoint time intervals are independent;

c) $\lim_{h\to 0} \dfrac{P\left(\text{exactly 1 event in } [t, t+h]\right)}{h} = \lambda(t)$;

d) $\lim_{h\to 0} \dfrac{P\left(\text{2 or more events in } [t, t+h]\right)}{h} = 0$.

The thinning strategy in the generation of non homogeneous Poisson process realizations is based on the following proposition.

Consider that random variables are generated with constant intensity λ such that $\lambda(t) \leq \lambda$, $\forall t \geq 0$ and they are accepted with probability $\lambda(t) / \lambda$, independently of whatever came before. The sequence of the accepted events constitutes a non homogeneous Poisson process with intensity function $\lambda(t)$, $t \geq 0$.

The proof of this proposition is the verification of the four conditions above. The items a), b) and d) are all consequences of the event sequence being obtained from the sequence which is already a Poisson process (but with constant intensity λ). In order to address point c), denote $p(t) = \lambda(t) / \lambda$, $t \geq 0$, and then:

$$\lim_{h\to 0} \frac{P\left(\text{exactly 1 accepted event in } [t, t+h]\right)}{h} =$$

$$= \lim_{h\to 0} \left[\frac{P\left(\text{there is only 1 event in } [t, t+h] \text{ and it is accepted}\right)}{h} + \right.$$

$$\left. + \frac{P\left(\text{there are 2 or more events in } [t, t+h] \text{ and only 1 is accepted}\right)}{h} \right] =$$

$$= \lim_{h\to 0} \left[\frac{P\left(\text{exactly 1 event in } [t, t+h]\right) \times P\left(\text{the event in } [t, t+h] \text{ is accepted}\right)}{h} + \right.$$

$$\left. + \frac{P\left(\text{2 or more events in } [t, t+h]\right) \times P\left(\text{only 1 of the events in } [t, t+h] \text{ is accepted}\right)}{h} \right].$$

Above, the probability of the conjunctions is the product of individual probabilities because the probability of the event being accepted is independent of former procedures.

Moreover the probability of the acceptance of each event is not dependent on the length of the interval, then those can be extracted from the limit. Finally, if the sum of the limits is computed instead of the limit of the sums, the result follows:

$$\lim_{h\to 0}\frac{P\left(\text{exactly 1 accepted event in } [t,t+h]\right)}{h}=$$

$$=P\left(\text{the event in } [t,t+h] \text{ is accepted}\right)\cdot\lim_{h\to 0}\frac{P\left(\text{exactly 1 event in } [t,t+h]\right)}{h}+$$

$$+P\left(\text{only 1 of the events in } [t,t+h] \text{ is accepted}\right)\cdot\lim_{h\to 0}\frac{P\left(\text{2 or more events in } [t,t+h]\right)}{h}=$$

$$=p(t)\times\lambda+P\left(\text{only 1 of the events in } [t,t+h] \text{ is accepted}\right)\times 0=\frac{\lambda(t)}{\lambda}\times\lambda=\lambda(t).$$

As a final remark, in algorithm terms, accepting an event A with probability p means that a random number Y is generated (from the uniform distribution) and A accepted if $Y \leq p$ (Ross 2002).

A.3. Subthreshold membrane potential driven solely by the pacemaker current

When the only current impinging the complex neuron is the pacemaker current, I_{Ω} (taking $\varphi = 0$), the membrane potential is given by:

$$\begin{cases} \tau_m \dfrac{dV}{dt} = -V + V_{rest} + R_m k \cos\left(2\pi ft\right) + R_m b \\ V\left(t\right) > V_{th} \rightarrow V\left(t\right) = V_{rest} \end{cases}.$$

The dynamics of the membrane potential before the threshold for fire is reached, V_{th}, are described by a linear 1st order differential equation, non separable and non homogeneous[14].

$$\tau_m \frac{dV}{dt} = -V\left(t\right) + V_{rest} + R_m k \cos\left(2\pi ft\right) + R_m b\,.$$

The general process for finding the general solution of such differential equation is as follows:

$$\tau_m \frac{dV}{dt} = -V\left(t\right) + V_{rest} + R_m k \cos\left(2\pi ft\right) + R_m b \Leftrightarrow \frac{dV}{dt} + \frac{V\left(t\right)}{\tau_m} = \frac{V_{rest} + R_m b + R_m k \cos\left(2\pi ft\right)}{\tau_m}$$

Since both the coefficient of the term in V and the right side of the equation are continuous functions, the integrant factor is a suitable methodology to apply. In this case, a suitable integrating factor is:

$$\mu\left(t\right) = e^{\frac{t}{\tau_m}} \Rightarrow \mu'\left(t\right) = \frac{1}{\tau_m} e^{\frac{t}{\tau_m}}$$

Multiplying both sides of the main differential equation by this integrating factor results in:

$$\frac{dV}{dt} e^{\frac{t}{\tau_m}} + \frac{e^{\frac{t}{\tau_m}}}{\tau_m} V\left(t\right) = \frac{\left(V_{rest} + R_m b\right) e^{\frac{t}{\tau_m}}}{\tau_m} + \frac{R_m k e^{\frac{t}{\tau_m}} \cos\left(2\pi ft\right)}{\tau_m}.$$

Integrating both members over t, an equivalent equation is obtained:

---

[14] The differential equation is non separable because it cannot be rewritten in the form $dv / dt = g(t) / f(V)$, where g and f are continuous functions of t and V, respectively. Since the equation also has a term independent of V (the last term) it is called a non homogeneous differential equation.

$$V(t)e^{\frac{t}{\tau_m}} + c_1 = \int \frac{(V_{rest} + R_m b)e^{\frac{t}{\tau_m}}}{\tau_m} + \frac{R_m k e^{\frac{t}{\tau_m}} \cos(2\pi ft)}{\tau_m} dt + c_2 \Leftrightarrow$$

$$\Leftrightarrow V(t)e^{\frac{t}{\tau_m}} = c_2 - c_1 + (V_{rest} + R_m b)e^{\frac{t}{\tau_m}} + \frac{R_m k}{\tau_m} \int e^{\frac{t}{\tau_m}} \cos(2\pi ft) dt$$

To solve the above integral, the integration by parts method can be applied recursively.

$$\int e^{\frac{t}{\tau_m}} \cos(2\pi ft) dt = \frac{e^{\frac{t}{\tau_m}} \sin(2\pi ft)}{2\pi f} - \int \frac{e^{\frac{t}{\tau_m}}}{\tau_m} \cdot \frac{\sin(2\pi ft)}{2\pi f} dt =$$

$$= \frac{e^{\frac{t}{\tau_m}} \sin(2\pi ft)}{2\pi f} - \left[-\frac{\cos(2\pi ft)}{(2\pi f)^2} \cdot \frac{e^{\frac{t}{\tau_m}}}{\tau_m} - \int -\frac{\cos(2\pi ft)}{(2\pi f)^2} \cdot \frac{e^{\frac{t}{\tau_m}}}{\tau_m^2} dt \right] =$$

$$= \frac{e^{\frac{t}{\tau_m}} \sin(2\pi ft)}{2\pi f} + \frac{\cos(2\pi ft)}{(2\pi f)^2} \cdot \frac{e^{\frac{t}{\tau_m}}}{\tau_m} - \frac{1}{(2\pi f \tau_m)^2} \int e^{\frac{t}{\tau_m}} \cos(2\pi ft) dt .$$

Finally the integral is obtained from the first and the last expressions.

$$\int e^{\frac{t}{\tau_m}} \cos(2\pi ft) dt = \frac{e^{\frac{t}{\tau_m}} \sin(2\pi ft)}{2\pi f} + \frac{e^{\frac{t}{\tau_m}} \cos(2\pi ft)}{\tau_m (2\pi f)^2} - \frac{1}{(2\pi f \tau_m)^2} \int e^{\frac{t}{\tau_m}} \cos(2\pi ft) dt \Leftrightarrow$$

$$\Leftrightarrow \frac{(2\pi f \tau_m)^2 + 1}{(2\pi f \tau_m)^2} \int e^{\frac{t}{\tau_m}} \cos(2\pi ft) dt = \frac{\tau_m 2\pi f e^{\frac{t}{\tau_m}} \sin(2\pi ft) + e^{\frac{t}{\tau_m}} \cos(2\pi ft)}{\tau_m (2\pi f)^2} \Leftrightarrow$$

$$\Leftrightarrow \int e^{\frac{t}{\tau_m}} \cos(2\pi ft) dt = \frac{\tau_m \left[\tau_m 2\pi f e^{\frac{t}{\tau_m}} \sin(2\pi ft) + e^{\frac{t}{\tau_m}} \cos(2\pi ft) \right]}{1 + (2\pi f \tau_m)^2}$$

The replacement of the above integral expression in the membrane potential equation and replacing the constants difference by a single constant *C*, results in:

$$V(t)e^{\frac{t}{\tau_m}} = C + (V_{rest} + R_m b)e^{\frac{t}{\tau_m}} + \frac{R_m k}{\tau_m} \cdot \frac{\tau_m \left[\tau_m 2\pi f e^{\frac{t}{\tau_m}} \sin(2\pi ft) + e^{\frac{t}{\tau_m}} \cos(2\pi ft) \right]}{1 + (2\pi f \tau_m)^2} \Leftrightarrow$$

$$\Leftrightarrow V(t) = Ce^{-\frac{t}{\tau_m}} + V_{rest} + R_m b + \frac{R_m k}{1+(2\pi f \tau_m)^2} \cdot \left[\tau_m 2\pi f \sin(2\pi ft) + \cos(2\pi ft)\right]$$

, where the last equation corresponds to the general solution of the original differential equation. Now, to obtain a value for constant C, it should be noted that V_{rest} is often taken as the initial value for the membrane constant: $V(0) = V_{rest}$.

$$V(0) = V_{rest} \Leftrightarrow Ce^{-\frac{0}{\tau_m}} + V_{rest} + R_m b + \frac{R_m k}{1+(2\pi f \tau_m)^2} \cdot \left[\tau_m 2\pi f \sin(0) + \cos(0)\right] = V_{rest} \Leftrightarrow$$

$$\Leftrightarrow C + R_m b + \frac{R_m k}{1+(2\pi f \tau_m)^2} \cdot [0+1] = 0 \Leftrightarrow C = -\frac{R_m k}{1+(2\pi f \tau_m)^2} - R_m b\,.$$

In conclusion, the particular solution for the differential equation above subject to $V(0) = V_{rest}$ is given by (Braun 1983):

$$V(t) = V_{rest} + \frac{R_m k}{1+(2\pi f \tau_m)^2} \cdot \left[\tau_m 2\pi f \sin(2\pi ft) + \cos(2\pi ft) - e^{-\frac{t}{\tau_m}}\right] - R_m b\left(e^{-\frac{t}{\tau_m}} - 1\right)$$

In particular, when the baseline level of the pacemaker current is zero (b = 0), the following equation for the membrane potential is obtained:

$$V(t) = V_{rest} + \frac{R_m k}{1+(2\pi f \tau_m)^2} \cdot \left[\tau_m 2\pi f \sin(2\pi ft) + \cos(2\pi ft) - e^{-\frac{t}{\tau_m}}\right].$$

A.4. Pacemaker *k*'s parameter

For the tuning of parameter *k*, the above expression (see section A.3) for the subthreshold membrane potential of the interneuron (with $b = 0$) is used to find two consecutive extremes and then imposing their voltage difference to be approximately 5 mV. The extremes of $V(t)$ are obtained by:

$$\frac{dV}{dt}=0\Leftrightarrow\frac{R_m k}{1+\left(2\pi f\tau_m\right)^2}\cdot\left[\tau_m\left(2\pi f\right)^2\cos\left(2\pi ft\right)-2\pi f\sin\left(2\pi ft\right)+\frac{e^{-\frac{t}{\tau_m}}}{\tau_m}\right]=0\Leftrightarrow$$

$$\Leftrightarrow\left(2\pi f\tau_m\right)^2\cos\left(2\pi ft\right)-2\pi f\tau_m\sin\left(2\pi ft\right)+e^{-\frac{t}{\tau_m}}=0$$

The function on the right side of the above equation describes a sinusoidal pattern with an exponential component, which eliminates the periodicity of the first milliseconds. As the independent variable *t* grows, that exponential term tends to zero and so, and the function is then periodic. If this calculus objective is to obtain the amplitude between two consecutive extremes, then a reasonable condition is to obtain the amplitude in the periodic season of the function. For that purpose it is assumed that t is taking large values such that the term e^{-t/τ_m} can be neglected. In that scenario, the equation left to solve is:

$$\left(2\pi f\tau_m\right)^2\cos\left(2\pi ft\right)-2\pi f\tau_m\sin\left(2\pi ft\right)=0\Leftrightarrow 2\pi f\tau_m\cos\left(2\pi ft\right)=\sin\left(2\pi ft\right) \quad \text{(A1)}$$

A possible approach to extract the values for t that satisfy this equation is to use the Pitagoric Identity in the following manner:

$$\cos^2\left(2\pi ft\right)+\sin^2\left(2\pi ft\right)=1\Rightarrow\cos^2\left(2\pi ft\right)+\left[2\pi f\tau_m\cos\left(2\pi ft\right)\right]^2=1\Leftrightarrow$$

$$\Leftrightarrow\left[1+\left(2\pi f\tau_m\right)^2\right]\cos^2\left(2\pi ft\right)=1\Leftrightarrow\cos\left(2\pi ft\right)=\pm\sqrt{\frac{1}{1+\left(2\pi f\tau_m\right)^2}}\Leftrightarrow$$

$$\Leftrightarrow 2\pi ft=\arccos\left[\sqrt{\frac{1}{1+\left(2\pi f\tau_m\right)^2}}\right]+j\pi\vee 2\pi ft=\arccos\left[-\sqrt{\frac{1}{1+\left(2\pi f\tau_m\right)^2}}\right]+j\pi,\ j\in\mathbb{Z}$$

.

However, not all of these values for *t* satisfy equation (A4), but only those *t* for which $2\pi ft$ has a positive sine (cosine) and simultaneously a negative cosine (sine). In

accordance, $2\pi ft$ is constrained to belong to the 2nd or 4th quadrants of the trigonometric circle. With the values adopted in the model for the parameters τ_m = 200 ms and f=10/1000 = 0.01 kHz, $\arccos\left[\sqrt{\frac{1}{1+(2\pi f\tau_m)^2}}\right]$ is a 1st quadrant's angle:

$$\arccos\left[\sqrt{\frac{1}{1+(2\pi f\tau_m)^2}}\right]=\arccos\left[\sqrt{\frac{1}{1+(4\pi)^2}}\right]\approx 1.4914<\frac{\pi}{2}\approx 1.5708.$$

Consequently, the only possible values for t are described by:

$$2\pi ft=\arccos\sqrt{\frac{1}{1+(2\pi f\tau_m)^2}}+j\pi \ ,\ j\in\mathbb{Z}.$$

For simplification let's denote $\arccos\sqrt{\frac{1}{1+(2\pi f\tau_m)^2}}$ by β in the following calculus.

The amplitude between two consecutive extremes, $|V(t_2)-V(t_1)|$, can be computed, for example, for $j = 2n+1$ and $j = 2n$, $n \in \mathbb{N}$, using the membrane potential equation (A3) without the exponential term.

$$\left|V(t_2)-V(t_1)\right|=$$

$$=\left|V_{rest}+\frac{R_m k}{1+(2\pi f\tau_m)^2}\cdot\left\{\tau_m 2\pi f\sin\left[\beta+(2n+1)\pi\right]+\cos\left[\beta+(2n+1)\pi\right]\right\}-V_{rest}\right.$$

$$\left.-\frac{R_m k}{1+(2\pi f\tau_m)^2}\cdot\left[\tau_m 2\pi f\sin(\beta+2n\pi)+\cos(\beta+2n\pi)\right]\right|=$$

$$=\left|\frac{R_m k}{1+(2\pi f\tau_m)^2}\cdot\left[\tau_m 2\pi f\sin(\beta+\pi)+\cos(\beta+\pi)-\tau_m 2\pi f\sin\beta-\cos\beta\right]\right|$$

Before continuing, and taking into account that $\beta=\arccos\left[\sqrt{\frac{1}{1+(2\pi f\tau_m)^2}}\right]$ is a 1st quadrant's angle, some additional calculus are needed:

- $\sin\left(\arccos\sqrt{\frac{1}{1+(2\pi f\tau_m)^2}}\right)=\sqrt{1-\left[\cos\left(\arccos\sqrt{\frac{1}{1+(2\pi f\tau_m)^2}}\right)\right]^2}=$

$$= \sqrt{1-\left(\sqrt{\frac{1}{1+\left(2\pi f \tau_m\right)^2}}\right)^2} = \sqrt{1-\frac{1}{1+\left(2\pi f \tau_m\right)^2}} = \sqrt{\frac{\left(2\pi f \tau_m\right)^2}{1+\left(2\pi f \tau_m\right)^2}} = \frac{2\pi f \tau_m}{\sqrt{1+\left(2\pi f \tau_m\right)^2}}.$$

- $\sin\left(\beta+\pi\right) = -\sin\left(\arccos\sqrt{\frac{1}{1+\left(2\pi f \tau_m\right)^2}}\right) = -\frac{2\pi f \tau_m}{\sqrt{1+\left(2\pi f \tau_m\right)^2}}.$
- $\cos\left(\arccos\sqrt{\frac{1}{1+\left(2\pi f \tau_m\right)^2}}\right) = \frac{1}{\sqrt{1+\left(2\pi f \tau_m\right)^2}}.$
- $\cos\left(\beta+\pi\right) = -\cos\left(\arccos\sqrt{\frac{1}{1+\left(2\pi f \tau_m\right)^2}}\right) = -\frac{1}{\sqrt{1+\left(2\pi f \tau_m\right)^2}}.$

Substituting these definitions into the above expression for the membrane potential amplitude between extremes, the result is obtained:

$$\left|V\left(t_2\right)-V\left(t_1\right)\right| = \left|\frac{R_m k}{1+\left(2\pi f \tau_m\right)^2}\cdot\left[\tau_m 2\pi f\left(-\frac{2\pi f \tau_m}{\sqrt{1+\left(2\pi f \tau_m\right)^2}}\right)-\frac{1}{\sqrt{1+\left(2\pi f \tau_m\right)^2}}\right.\right.$$

$$\left.\left.-\tau_m 2\pi f\frac{2\pi f \tau_m}{\sqrt{1+\left(2\pi f \tau_m\right)^2}}-\frac{1}{\sqrt{1+\left(2\pi f \tau_m\right)^2}}\right]\right| = \left|\frac{R_m k}{1+\left(2\pi f \tau_m\right)^2}\cdot\left\{-\frac{2\cdot\left[\left(2\pi f \tau_m\right)^2+1\right]}{\sqrt{1+\left(2\pi f \tau_m\right)^2}}\right\}\right| =$$

$$= \frac{2R_m k}{\sqrt{1+\left(2\pi f \tau_m\right)^2}}.$$

Finally, k is chosen such that the amplitude between two consecutive extremes is approximately equal to 5 mV and the remaining parameters are as defined for the model (R_m = 200 MΩ):

$$5 = \frac{2R_m k}{\sqrt{1+\left(2\pi f \tau_m\right)^2}} \Leftrightarrow k = \frac{5\sqrt{1+\left(2\pi f \tau_m\right)^2}}{2R_m} \Rightarrow k = \frac{5\sqrt{1+\left(4\pi\right)^2}}{2\times 200} = 0.1576 \Rightarrow k \text{ is set to } 0.1.$$

A.5. Pacemaker *b*'s parameter

The calculus of the value for the *b* parameter, is based on the following assumption: when provided only with the current from the pacemaker, the interneuron (theta cell) fires at a constant rate of 10 Hz (that is, 10 events for second). This means that the threshold membrane potential value for the cell is reached after T_0 =100 ms of the beginning of the simulation. In summary, the value for the *b* parameter should satisfy the condition: $V(T_0) = V_{th}$, where $V(t)$ is defined by equation (A3).

$$V(T_0) = V_{th} \Leftrightarrow$$

$$\Leftrightarrow V_{rest} + \frac{R_m k}{1+(2\pi f \tau_m)^2}\left[\tau_m 2\pi f \sin(2\pi f\, T_0) + \cos(2\pi f\, T_0) - e^{-\frac{T_0}{\tau_m}}\right] - R_m b\left(e^{-\frac{T_0}{\tau_m}} - 1\right) = V_{th} \Leftrightarrow$$

$$\Leftrightarrow b = \frac{V_{rest} - V_{th} + \frac{R_m k}{1+(2\pi f \tau_m)^2}\left[\tau_m 2\pi f \sin(2\pi f\, T_0) + \cos(2\pi f\, T_0) - e^{-\frac{T_0}{\tau_m}}\right]}{R_m\left(e^{-\frac{T_0}{\tau_m}} - 1\right)}.$$

For the parameter values defined in the model, τ_m = 200 ms; V_{rest} = -70 mV; R_m = 200 MΩ; V_{th} = -50 mV; f = 0.01 kHz and k = 0.1 nA, the value obtained is b = 0.25 nA.

A.6. Scaling factor ρ for connection strengths

In the strength connections parameterization, a scale parameter ρ is used in all the connection strengths, in chapter 4. This is a normalization factor which is computed as to produce a unitary input onto the grid cell if all place fields are homogeneously distributed throughout the maze and their synapses are equally strengthened. To obtain the value for this scale parameter ρ, we start by noting that the mean spatial input our grid cell is receiving in each position inside the maze is given by:

$$\langle I \rangle = \left\langle \sum_{i=1}^{N} w_i u_i \right\rangle = N \cdot \langle w \rangle \cdot \langle u \rangle .$$

It is assumed that all synaptic weights are set to the same value (in average), which can be denoted by the scaling parameter ρ, then the above relation becomes:

$$\langle I \rangle = \left\langle \sum_{i=1}^{N} \rho u_i \right\rangle = N \ \rho \cdot \langle u \rangle .$$

To obtain the mean activity for the place cell units, the average of the Gaussian function u is computed over the region of the maze, A:

$$\langle u \rangle = \frac{1}{side^2} \iint_{maze} u(x,y)\, dxdy = \frac{1}{side^2} \int_0^{side} \int_0^{side} e^{-\frac{(x-\mu_x)^2+(y-\mu_y)^2}{2\sigma^2}} dxdy =$$

$$= \frac{1}{side^2} \int_0^{side} e^{-\frac{(y-\mu_y)^2}{2\sigma^2}} \int_0^{side} e^{-\frac{(x-\mu_x)^2}{2\sigma^2}} dxdy .$$

The function of the above integral in x resembles that of the theoretical Gaussian distribution with a difference that this integral is not defined between -∞ and +∞. In order to apply this result, with no need to consider the erf error, it is assumed that the place field is totally contained inside the maze, and the following approximation is considered:

$$\int_0^{side} e^{-\frac{(x-\mu_x)^2}{2\sigma^2}} dx \approx \sigma\sqrt{2\pi} \int_{-\infty}^{+\infty} \frac{1}{\sigma\sqrt{2\pi}} e^{-\frac{(x-\mu_x)^2}{2\sigma^2}} dx = \sigma\sqrt{2\pi} .$$

Returning to the calculations and repeating the approximation for y it follows that:

$$\langle u \rangle \approx \frac{\sqrt{2\pi}\sigma}{side^2} \int_{-\infty}^{+\infty} e^{-\frac{(y-\mu_y)^2}{2\sigma^2}} dy = \frac{2\pi\sigma^2}{side^2} .$$

For the mean total synaptic current to be 1, then we must set: $1 = N\ \rho \frac{2\pi\sigma^2}{side^2} \Leftrightarrow \rho = \frac{side^2}{N 2\pi\sigma^2}$.

A.7. An alternative model for grid cell formation

This prototype computational model for the emergence of grid like weight patterns stands on the same key principles of the proposed model in chapter 4 (originated the first conference abstract mentioned in that chapter).

In this alternative approach, self-organization in the synaptic efficacies matrix is driven by a similar learning rule but with a different formulation. Plasticity occurs as a function of the input provided by each unit, I_{sep}, in a way that high and low I_{sep} units become potentiated, while units with mean I_{sep} are depressed. Units with very low I_{sep} are not subject to plasticity. This plasticity profile is able to generate a band of inhibited cells in the middle of a range of potentiated cells. This method for modifying the connection strengths of place cells onto grid cells makes this alternative model simpler than the previous one.

Spatial competition and compactness are results of the learning rule, leading to grid like weight patterns. The resultant gridness scores (applied to weight maps) are in the range of the ones reported for mEC's layer V, which is the field receiving direct input from CA1 region. The model takes into account the features already reported about grid cells and can be thought of as a plausible explanation of the mechanisms underlying the emergence of the first grid cells in the rat's early life. In this section we focus essentially on the novel features introduced by this approach.

Methods

This alternative approach to address grid cells firing patterns emergence shares some methodologies with the model of chapter 4 which are: the feed-forward firing rate model (with τ_m = 10 ms); the spatial input from place cells (results presented shortly were obtained considering cells which place field is centered inside the maze) and the animal space trajectories (in this version we used $direc = \pi/180$, however this is not expected to categorically affect the results). The main difference between the two models relies on the implementation of the weights plasticity rule described in the following lines.

In this model, weights evolve according to a complex rule which encompasses the existence of input and output activity above threshold values together with a potentiation component and a pseudo-depression component. The weights (all scaled by ρ, check the Appendix for details) are set initially at unitary value, and throughout the learning process

are allowed to vary in the range [0, w_{max} = 1.5]. The weight update dynamics is given by (see Figure A 1):

$$\frac{d\mathbf{w}}{dt} = \alpha H\left(\mathbf{I_{sep}} - u_0\right) \cdot H\left(v - r_{th}\right) \cdot \mathbf{LTP} \cdot \mathbf{pLTD},$$

where α = 0.5 1/ms is the learning rate; u_0 = 0.02 and r_{th} = 0.98 (bold is used for denoting vectors). The amount of plasticity at each time step is controlled by parameter α.

This plasticity rule produces some grid fields by a unique passage in addition to grid fields which are naturally formed by the intersection of the first's outer ring, without the need for the rat trajectory to pass through them. The parameter α was set such that the unique passage would bring the weights of the place cells synapses to high and low weight values by a significant magnitude but without reaching their limits (0 and 1.5) after less than 5 repetitive potentiation steps or 4 repetitive depressions (see Figure A 1 for the scale of the above rule, with unitary α).

In the weight modification differential equation, H represents the Heaviside step function such that, for $z \in \mathbb{R}$:

$$H\left(z\right) = \begin{cases} 0, & for\ z < 0 \\ 0.5, & for\ z = 0 \\ 1, & for\ z > 0 \end{cases}.$$

In trajectory positions where the animal does not cross the place field of a certain place cell, the weight of that cell synapse should not suffer any changes. Given that place fields are spatially defined by the intensity of firing rates, the referred constraint is included in the plasticity rule in terms of the overall place cell effect, $\mathbf{I_{sep}}$, on the output cell (that is, firing rate together with synapse weight). Accordingly, the term H ($\mathbf{I_{sep}}$ - u_0) assures that weights modification takes place only for place cells contributing to the activity of the output cell. It is assumed that synapses coming from place cells with normalized firing rates below u_0 = 0.02 are not eligible for weight modification.

The term H (v - r_{th}) means that weights modification only occurs if the output cell is very active, i.e., when $v \geq 0.98$. The threshold values choice is not decisive, similar values are expected to produce similar results.

In terms of the plasticity rule, the individual contribution of place cells is normalized, at real time, according to the following expression:

$$\mathbf{I_{sep}} = \frac{\mathbf{wu}}{\max_{1\le i\le N}(w_i u_i)} = \frac{(w_1u_1, w_2u_2, \ldots, w_Nu_N)}{\max_{1\le i\le N}(w_i u_i)}.$$

Given that weights do not take negative values, this measure takes values in the interval [0, 1]. In a given position of the rat there is a great number of place cells who is firing, at different rates. In particular, the firing rate of a given place cell will be higher for those who have their center closer to the current position of the rat. The relevance of this model's component has to do with the competition between place cells synapses. When the output firing rate threshold for plasticity is achieved ($v \geq 0.98$), the weight rule will attribute different values for increase and decrease of weights. The only synapses eligible for that change correspond to place cells that have some activity, in particular to those whose I_{sep} is above u_0.

The amount of synaptic weight change will not depend solely on the magnitude of the firing rate of the unit, but instead a sorting is done depending on the total contribution of each place cell. In this sense, I_{sep} performs is a normalization of all the contributions relative to the strongest at each iteration. *LTP* and *pLTD* are functions of this variable.

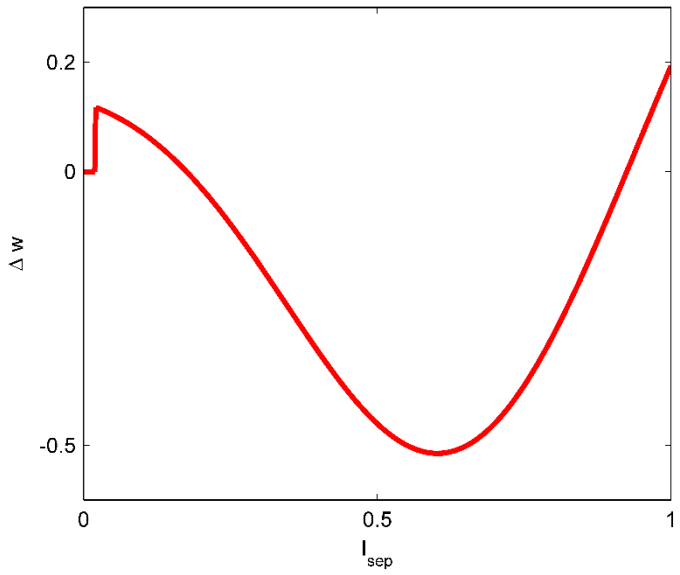

Figure A 1 Profile of the plasticity rule as a function of I_{sep}, for an output rate above the threshold for plasticity. The parameters are set as before except for $\alpha = 1$.

The plasticity components, pseudo depression and potentiation, are as follows:

$$\mathbf{pLTD} = 1 - 2\exp\left[-\frac{(\mathbf{I_{sep}} - \theta_{dep})^2}{\sigma_{dep}^2}\right] \text{ and } \mathbf{LTP} = \frac{1}{1+\exp\left(-\frac{\mathbf{I_{sep}} - \theta_{dep}}{\sigma_{dep}}\right)},$$

where θ_{dep} = 0.55 and σ_{dep} = 0.45. These parameters where tuned in a naïve fashion, and further work to improve the prototype model may involve a rigorous based choice for them. For the model main goal of producing a grid like spatial distribution for the weights, the values chosen were suitable but other similar values are expected to produce appropriate results.

In the range of the normalized input I_{sep}, LTP is a monotonic increasing function that assumes the value 0.236 when I_{sep} = 0.02, goes through 0.5 when $I_{sep} = \theta_{dep}$ and achieves the value 0.73 for I_{sep} = 1. The pseudo depression component has an upside down Gaussian shape. Its lowest value (-1) is at $I_{sep} = \theta_{dep}$, it starts equal 0.5 for I_{sep} = 0.02 and reaches approximately 0.26 in the other extreme. Due to this component, cells with low and high I_{sep} values get potentiated while those with intermediate values are depressed.

In summary, as the virtual rat follows the space trajectory, plasticity occurs whenever the output cell is firing above 0.98 and only for synapses which presynaptic cell has I_{sep} value above 0.02. From those, higher and lower activity neurons synapses will be potentiated and the intermediate ones are depressed, generating concentric rings of low and high input levels around each node of the grid.

This plasticity function, although modeling one synapse for simplification, can in fact be the result of a combined effect between excitatory and inhibitory elements, mediating the connection between the place cell and the putative grid cell. Such biological plausible mechanism has been described in chapter 4.

Results

After a learning episode where the simulated rat runs at constant velocity inside the maze, disjoint clusters of place fields are formed with higher synapse weight values for their cells, surrounded by low weight cells fields (see Figure A 2). However, low weight regions formed are not broad enough when compared to the place cells width. This disables the production of an accurate scaled firing rate map, characterized by silent rates around the grid fields. Even though, we decided to evaluate the gridness of our weight map by performing some manipulations.

Near the walls of the maze there is not sufficient input for the grid cell to achieve r_{th}. Hence, and since the maze was not covered with grid fields, we crop the weight map and used only the centre region. This new map has dimensions 20:80 × 20:80 instead of the

original dimensions of the maze which are 1:100 × 1:100.

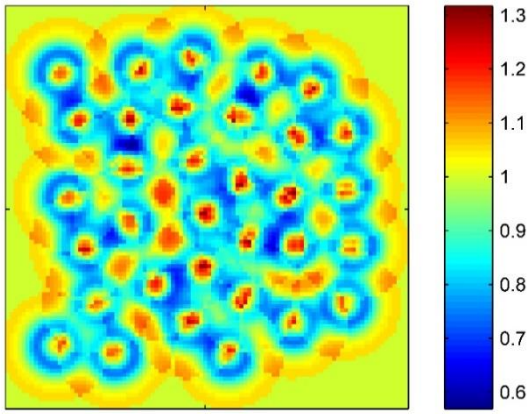

Figure A 2 Representation of the place cells weights placed in the central position of the respective place field after a learning episode (30 minutes). Synapses weight grading values (apart for the scaling factor) are indicated by the colorbar. The square maze is 1 meter wide.

After the resizing, all the weights lower than 1.08 were set to zero (see Figure A 3 a). Finally a smoothing operation was performed over the weights map, which can be regarded as the transformation from weights to rates (two dimensional convolution with a disc pillbox shaped kernel with radius 3 cm/pixels and total side 7 cm/pixels) (see Figure A 3 b).

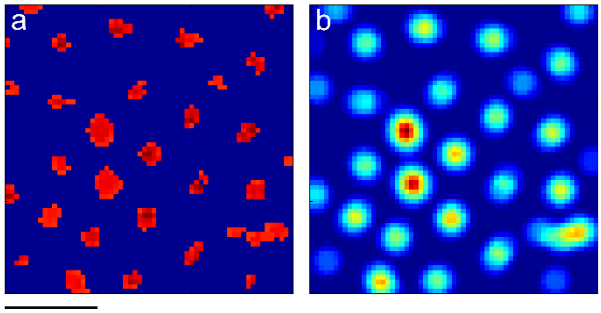

Figure A 3 Pseudo firing rate map of the cell receiving spatial input from place cells in Figure A 2, resized to the central 61 cm (a pixel per cm^2). Scale bar is 20 cm. a – Raw firing rate map. Pixels in blue correspond to zero activity while dark red ones represent maximal firing rate. b – Smoothed firing rate map. Result of a two dimensional convolution applied to the left image, with a circular averaging filter with 3 cm radius.

The gridness score methodology, described previously, was then applied to the resultant map, called pseudo grid map.

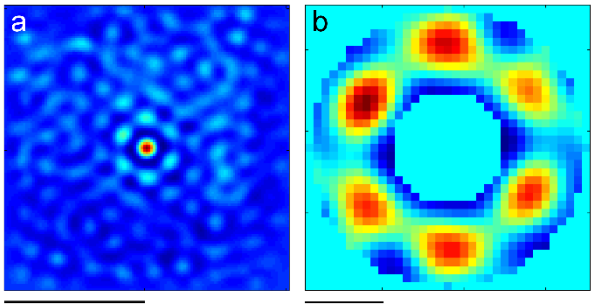

Figure A 4 Artificial grid map normalized autocorrelogram and zoom of its central ring. a - Pseudo grid map normalized autocorrelogram. Scale bar is 60 cm. b - Central ring of the normalized autocorrelogram map containing the six adjacent nodes to the central node. Scale bar is 10 cm.

In this unique trial, the gridness score obtained was of 0.47 for a grid spacing *G* of approximately 12 cm.

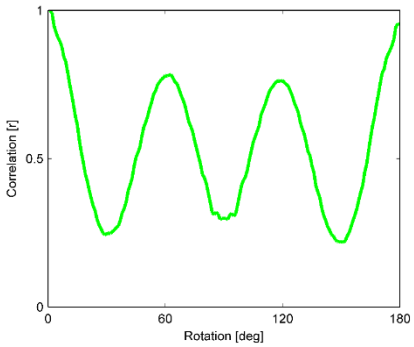

Figure A 5 Correlation values between the ring of the firing rate map autocorrelogram of Figure A 4 and its successive rotations by 1 degree. The gridness score obtained from such correlation values was 0.47.

The plasticity rule in this model implies that the generation of the grid nodes is not constrained to the intersecting regions of the potentiated rings, in contrast to the method in the previous model. In the current version, connections strengths are set to their baseline level which produces a baseline output firing rate above the plasticity firing threshold (r_{th}).

Discussion

The novelty of the approach used in this prototype model for grid formation resides on the plasticity rule which represents a less simplified version (than the previous model) of the biological plausible weight modification rule. In particular, connection strengths evolve smoother and are not collapsed into four levels of amplitudes in the end of the learning episode, but allowed to slide over a continuous range of values.

The gridness score obtained is below the magnitude of the previous model results. In fact,

since learning in this model is driven by a less stringent updating rule and dependent (not only but also) on weight values, this more biological behavior has the expense of lower gridness scores. Nevertheless, the gridness scores to be obtained from the model are expected to fall in the range of the ones reported experimentally, with a distribution similar to the ones obtained for deeper mEC layers. This means that the gridness scores in this model are not expected to be high (close to 1) throughout different trials, but neither are the ones reported in studies made with deeper layers of mEC (Sargolini et al. 2006).

Overall, the main conclusions are similar to the ones obtained with the model described in section 4. The novel plasticity rule formulation produces an approximately hexagonal weight map, while the rat follows a plausible trajectory, using the following principles:

- the spatial correlation of grid cells is inherited from place cells spatial firing;
- synapses weights are changed according to a local spatial modulation mechanism – plasticity in inhibitory cell is important;
- a short period of learning time is enough to generate an approximately hexagonal weights pattern.

Nevertheless less positive aspects are present: the final pattern is obtained with weight maps and not with firing rate maps; the scaling of pseudo grid nodes (from the pseudo grid map) is not in accordance with experimental reports. The implication of the I_{sep} measure on this matter is explored in more detail in the following section.

Another feature of the plasticity mechanism which also decreases the hexagonal disposition of the output cell nodes is related to the weights baseline level allowing the emergence of nodes in every position of the maze (except for near border regions) since the beginning of the trial. However, if the intensity of the maze is homogeneously distributed (e.g. adding an outside band of input cells similarly to the previous model), this situation is less probable to occur. In fact, each path leaving the last node formed will obligatory drive the next node to happen near the potentiated ring around the last node. Moreover, if the baseline level of the weights is lowered to a value not capable to trigger plasticity, by introducing an initial stimuli as in the previous model, the performance of the model will certainly increase.

This model, although not successfully producing firing maps with the scaling observed in recorded grid cells, advances the possibility that the first grid cells to be built in rodents mEC may result solely from place cell's input and a spatial competition mechanism.

The range of the quantitative results obtained together with the objectiveness and originality of the plasticity process provide enough reasons to proceed and correct the punctual imperfections of this prototype model.

Spacing between nodes in firing rate maps

The major drawback present in this preliminary model is that the weight map cannot be transposed correctly to a firing map with the same high bumps and low rings intensity regions. This is mainly because the width of the input place cells is too large relative to the spacing that is being defined by the I_{sep} measure, which is too far from the smallest spacing reported in the available literature for grid cells (approximately 12 cm against 30 cm in dorsal mEC, respectively). In order to address how this problem of the prototype model could be overcome, a hypothetical scenario is designed, for a spacing value of 30 cm between grid cell fields.

To represent this scenario, outer rings are set 30 cm away from the correspondent node center. After the second grid node is created (assuming it is conveniently placed in the outer ring of the first node), the weights map exhibit the intersections of the two rings, which are precisely the two regions where it is convenient to place new grid nodes. Suppose the simulated rat is going away from the second grid vertex approaching one of the outer potentiated rings (check scheme in Figure A 6). Now, for the process to work it should favor triangular arrangement of high weight place fields clusters. If the rat approaches one of the intersection zones (red diamond) by less than a spacing measure (at most) and the threshold for plasticity in the output firing rate is achieved, then the I_{sep} function should elect that diamond region for its maximum value (one).

For a general place cell with place field centered on (μ_x, μ_y), its firing rate is a function of space and in a general position (x, y), its value is given by:

$$u(x,y) = e^{-\frac{(x-\mu_x)^2+(y-\mu_y)^2}{2\sigma^2}}.$$

Now let w_a and (μ_{xa}, μ_{ya}) denote the synapse weight and the field center of the cell located under the arrow (that is, (x_0, y_0) = (μ_{xa}, μ_{ya})). Analogously, w_d and (μ_{xd}, μ_{yd}) denote the same parameters for a generic cell located in the diamond region. By the scenario construction, the weights obey: $w_a \leq w_d$.

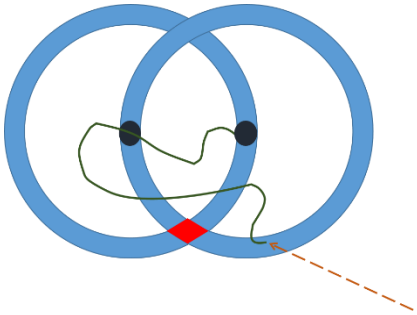

Figure A 6 Cartoon scheme for the exemplification of the problem with the scale dependence between weights and place fields of the I_{sep} strategy. Each point represents a place field center color coded according to the connection strength between the associated place cell and the grid cell, after two grid nodes have been formed. Small dark circles represent place cells centers which are assigned to represent grid nodes. Blue rings correspond to the place cells centers forming the potentiated ring regions. Green line represents the path of the rat and the dashed arrow points to its current position, denoted by (x_0, y_0). The red diamond represents place fields centers which are responsible for the intersection diamond of the two rings closest to (x_0, y_0).

Theoretically, for a specific location (x_0, y_0), if:

$$\left(x_0-\mu_{xd}\right)^2+\left(y_0-\mu_{yd}\right)^2\le G^2,$$

then the cell in the diamond region should be preferred in detriment of the cell in the arrow point (x_0, y_0).

In other words, this relation means that if the current position (where $v \geq r_{th}$ is assumed) is less than a spacing distance from the closest diamond then precisely that diamond region should be the preferred location for the next field, in order to achieve hexagonallity in the grid receptive fields' locations. In I_{sep} terms, this means that the place cell with maximum I_{sep} value (1), should be in the diamond region or, less stringent, that the I_{sep} measure would be much higher for a diamond region cell than for the cell centered in (x_0, y_0). In the prototype model, the cell in the diamond region will be preferred if:

$$I_{sep}(a)\ll I_{sep}(d)\Leftrightarrow w_a\cdot u_a(x_0,y_0)\ll w_d\cdot u_d(x_0,y_0)\Leftrightarrow$$

$$\Leftrightarrow w_a e^{-\frac{0}{2\sigma^2}}\ll w_d e^{-\frac{\left(x_0-\mu_{xd}\right)^2+\left(y_0-\mu_{yd}\right)^2}{2\sigma^2}}\Leftrightarrow \frac{w_a}{w_d}\ll e^{-\frac{\left(x_0-\mu_{xd}\right)^2+\left(y_0-\mu_{yd}\right)^2}{2\sigma^2}}\Rightarrow \frac{w_a}{w_d}\ll e^{-\frac{G^2}{2\sigma^2}}.$$

For the minimum spacing of the range referred above ($0.30 < G < 0.50$ m, approximately) and with the sigma representing typical place fields dimensions, (σ = 0.05 m and σ = 0.10 m, respectively for dorsal and ventral regions), the above relation implies a weight ratio satisfying not plausible magnitude orders:

$$\frac{w_a}{w_d}\ll e^{-\frac{G^2}{2\sigma^2}}\approx 1.5\times10^{-8} \quad \text{or} \quad \frac{w_a}{w_d}\ll 3.7\times10^{-6}.$$

A relaxation of the condition above can be introduced in the sense that the distance from the diamond zone can be defined at half of the spacing (which can bring some non hexagonal nodes), which will relax the above ratios to:

$$\frac{w_a}{w_d} \ll e^{-\frac{\left(G/2\right)^2}{2\sigma^2}} \approx 0.011 \text{ and } \frac{w_a}{w_d} \ll 0.044 .$$

In the present model, the weights ratio can go from 0.67 to near one, but since the spacing is approximately 0.12 cm, the benchmarks for the weights ratio are:

$$e^{-\frac{\left(G/2\right)^2}{2\sigma^2}} \approx 0.49 \text{ or } e^{-\frac{G^2}{2\sigma^2}} \approx 0.056 \text{, for the most stringent case.}$$

The situation described shows that the hexagonallity of the weights map produced by this prototype model is possible to be obtained only through implausible spacing values. Nevertheless, the passage to firing maps is not successful given the large dimensions of the filter constituted by the place cells Gaussian firing profiles which smooth such relative smaller grid spacing's (eliminating any spacing at all). However, the inexistence of smaller grid spacing's in the grid cells ever reported may provide an additional support to our idea that grid fields spacing might be dependent on the place fields size of downstream CA1 fields (in contrast with ideas about its dependence on the frequency of subthreshold oscillations).

References

Ainge JA, Langston RF (2012) Ontogeny of neural circuits underlying spatial memory in the rat. Frontiers in neural circuits 6:8. doi:10.3389/fncir.2012.00008

Amaral D, Lavenex P (2006) Hippocampal Neuroanatomy. In: The Hippocampus Book. Oxford University Press, New York, pp 37-114

Baker JL, Olds JL (2007) Theta phase precession emerges from a hybrid computational model of a CA3 place cell. Cognitive neurodynamics 1 (3):237-248. doi:10.1007/s11571-007-9018-9

Barry C, Ginzberg LL, O'Keefe J, Burgess N (2012) Grid cell firing patterns signal environmental novelty by expansion. Proceedings of the National Academy of Sciences of the United States of America 109 (43):17687-17692. doi:10.1073/pnas.1209918109

Bendels MH, Leibold C (2007) Generation of theta oscillations by weakly coupled neural oscillators in the presence of noise. Journal of computational neuroscience 22 (2):173-189. doi:10.1007/s10827-006-0006-6

Blair HT, Gupta K, Zhang K (2008) Conversion of a phase- to a rate-coded position signal by a three-stage model of theta cells, grid cells, and place cells. Hippocampus 18 (12):1239-1255. doi:10.1002/hipo.20509

Boccara CN, Sargolini F, Thoresen VH, Solstad T, Witter MP, Moser EI, Moser MB (2010) Grid cells in pre- and parasubiculum. Nature neuroscience 13 (8):987-994. doi:10.1038/nn.2602

Bonnevie T FM, Hafting T, Moser E, Moser MB (2006) Misalignment of entorhinal grid fields after hippocampal inactivation. Soc Neurosci abs (68.1/BB9)

Bose A, Booth V, Recce M (2000) A temporal mechanism for generating the phase precession of hippocampal place cells. Journal of computational neuroscience 9 (1):5-30

Brandon MP, Bogaard AR, Libby CP, Connerney MA, Gupta K, Hasselmo ME (2011) Reduction of theta rhythm dissociates grid cell spatial periodicity from directional tuning. Science 332 (6029):595-599. doi:10.1126/science.1201652

Braun M (1983) Differential Equations and Their Applications. 3rd edition edn.,

Burak Y, Fiete I (2006) Do we understand the emergent dynamics of grid cell activity? The Journal of neuroscience : the official journal of the Society for Neuroscience 26 (37):9352-9354; discussion 9354

Burak Y, Fiete IR (2009) Accurate path integration in continuous attractor network models of grid cells. PLoS computational biology 5 (2):e1000291. doi:10.1371/journal.pcbi.1000291

Burgess N, Barry C, O'Keefe J (2007) An oscillatory interference model of grid cell firing. Hippocampus 17 (9):801-812. doi:10.1002/hipo.20327

Burgess N, O'Keefe J (1998) Hippocampus: spatial models. In: The handbook of brain theory and neural networks. Second edn. MIT Press, pp 468-472

Buzsaki G (2002) Theta oscillations in the hippocampus. Neuron 33 (3):325-340

Castro L, Aguiar P (2012) Phase precession through acceleration of local theta rhythm: a biophysical model for the interaction between place cells and local inhibitory neurons. Journal of computational neuroscience 33 (1):141-150. doi:10.1007/s10827-011-0378-0

Cheung TH, Cardinal RN (2005) Hippocampal lesions facilitate instrumental learning with delayed reinforcement but induce impulsive choice in rats. BMC neuroscience 6:36. doi:10.1186/1471-2202-6-36

Dayan P, Abbott LF (2001) Theoretical Neuroscience: Computational and Mathematical Modeling of Neural Systems. 1st edition edn.,

Derdikman D, Whitlock JR, Tsao A, Fyhn M, Hafting T, Moser M-B, Moser EI (2009) Fragmentation of grid cell maps in a multicompartment environment. Nature neuroscience 12 (10):1325-1332. doi:http://www.nature.com/neuro/journal/v12/n10/suppinfo/nn.2396_S1.html

Dhillon A, Jones RS (2000) Laminar differences in recurrent excitatory transmission in the rat entorhinal cortex in vitro. Neuroscience 99 (3):413-422

Ego-Stengel V, Wilson MA (2007) Spatial selectivity and theta phase precession in CA1 interneurons. Hippocampus 17 (2):161-174. doi:10.1002/hipo.20253

Ermentrout GB, Terman DH (2010) Mathematical Foundations of Neuroscience, vol 35. vol Interdisciplinary Applied Mathematics, 1st edition edn.,

Fiete IR, Burak Y, Brookings T (2008) What grid cells convey about rat location. The Journal of neuroscience : the official journal of the Society for Neuroscience 28 (27):6858-6871. doi:10.1523/JNEUROSCI.5684-07.2008

Frank LM, Brown EN, Wilson M (2000) Trajectory encoding in the hippocampus and entorhinal cortex. Neuron 27 (1):169-178

Freund T, Kali S (2008) Interneurons. Scholarpedia. doi:doi::10.4249/scholarpedia.4720

Freund TF, Buzsaki G (1996) Interneurons of the hippocampus. Hippocampus 6 (4):347-470. doi:10.1002/(SICI)1098-1063(1996)6:4<347::AID-HIPO1>3.0.CO;2-I

Fuhs MC, Touretzky DS (2006) A spin glass model of path integration in rat medial entorhinal cortex. The Journal of neuroscience : the official journal of the Society for Neuroscience 26 (16):4266-4276. doi:10.1523/JNEUROSCI.4353-05.2006

Fyhn M, Hafting T, Treves A, Moser MB, Moser EI (2007) Hippocampal remapping and grid realignment in entorhinal cortex. Nature 446 (7132):190-194. doi:10.1038/nature05601

Fyhn M, Molden S, Witter MP, Moser EI, Moser MB (2004) Spatial representation in the entorhinal cortex. Science 305 (5688):1258-1264. doi:10.1126/science.1099901

Geisler C, Diba K, Pastalkova E, Mizuseki K, Royer S, Buzsaki G (2010) Temporal delays among place cells determine the frequency of population theta oscillations in the hippocampus. Proceedings of the National Academy of Sciences of the United States of America 107 (17):7957-7962. doi:10.1073/pnas.0912478107

Giocomo LM, Moser MB, Moser EI (2011) Computational models of grid cells. Neuron 71 (4):589-603. doi:10.1016/j.neuron.2011.07.023

Giocomo LM, Zilli EA, Fransen E, Hasselmo ME (2007) Temporal frequency of

subthreshold oscillations scales with entorhinal grid cell field spacing. Science 315 (5819):1719-1722. doi:10.1126/science.1139207

Grossberg S, Pilly PK (2012) How entorhinal grid cells may learn multiple spatial scales from a dorsoventral gradient of cell response rates in a self-organizing map. PLoS computational biology 8 (10):e1002648. doi:10.1371/journal.pcbi.1002648

Guanella A, Kiper D, Verschure P (2007) A model of grid cells based on a twisted torus topology. International journal of neural systems 17 (4):231-240

Hafting T, Fyhn M, Bonnevie T, Moser MB, Moser EI (2008) Hippocampus-independent phase precession in entorhinal grid cells. Nature 453 (7199):1248-1252. doi:10.1038/nature06957

Hafting T, Fyhn M, Molden S, Moser MB, Moser EI (2005) Microstructure of a spatial map in the entorhinal cortex. Nature 436 (7052):801-806. doi:10.1038/nature03721

Halasy K, Buhl EH, Lorinczi Z, Tamas G, Somogyi P (1996) Synaptic target selectivity and input of GABAergic basket and bistratified interneurons in the CA1 area of the rat hippocampus. Hippocampus 6 (3):306-329. doi:10.1002/(SICI)1098-1063(1996)6:3<306::AID-HIPO8>3.0.CO;2-K

Harris KD, Henze DA, Hirase H, Leinekugel X, Dragoi G, Czurko A, Buzsaki G (2002) Spike train dynamics predicts theta-related phase precession in hippocampal pyramidal cells. Nature 417 (6890):738-741. doi:10.1038/nature00808

Harvey CD, Collman F, Dombeck DA, Tank DW (2009) Intracellular dynamics of hippocampal place cells during virtual navigation. Nature 461 (7266):941-946. doi:10.1038/nature08499

Hasselmo ME, Brandon MP, Yoshida M, Giocomo LM, Heys JG, Fransen E, Newman EL, Zilli EA (2009) A phase code for memory could arise from circuit mechanisms in entorhinal cortex. Neural networks : the official journal of the International Neural Network Society 22 (8):1129-1138. doi:10.1016/j.neunet.2009.07.012

Hasselmo ME, Giocomo LM, Zilli EA (2007) Grid cell firing may arise from interference of theta frequency membrane potential oscillations in single neurons. Hippocampus 17 (12):1252-1271. doi:10.1002/hipo.20374

Hines ML, Morse T, Migliore M, Carnevale NT, Shepherd GM (2004) ModelDB: A Database to Support Computational Neuroscience. Journal of computational neuroscience 17 (1):7-11. doi:10.1023/B:JCNS.0000023869.22017.2e

Huxter J, Burgess N, O'Keefe J (2003) Independent rate and temporal coding in hippocampal pyramidal cells. Nature 425 (6960):828-832. doi:10.1038/nature02058

Jeffery KJ (2013) Neural odometry: the discrete charm of the entorhinal cortex. Current biology : CB 23 (5):R204-206. doi:10.1016/j.cub.2013.01.019

Jung MW, Wiener SI, McNaughton BL (1994) Comparison of spatial firing characteristics of units in dorsal and ventral hippocampus of the rat. The Journal of neuroscience : the official journal of the Society for Neuroscience 14 (12):7347-7356

Kamondi A, Acsady L, Wang XJ, Buzsaki G (1998) Theta oscillations in somata and dendrites of hippocampal pyramidal cells in vivo: activity-dependent phase-precession of action potentials. Hippocampus 8 (3):244-261.

doi:10.1002/(SICI)1098-1063(1998)8:3<244::AID-HIPO7>3.0.CO;2-J

Kandel ER, Squire LR (2002) Memória: da mente às moléculas.

Karlsson MP, Frank LM (2008) Network dynamics underlying the formation of sparse, informative representations in the hippocampus. The Journal of neuroscience : the official journal of the Society for Neuroscience 28 (52):14271-14281. doi:10.1523/JNEUROSCI.4261-08.2008

Killian NJ, Jutras MJ, Buffalo EA (2012) A map of visual space in the primate entorhinal cortex. Nature 491 (7426):761-764. doi:10.1038/nature11587

Kim SM, Ganguli S, Frank LM (2012) Spatial information outflow from the hippocampal circuit: distributed spatial coding and phase precession in the subiculum. The Journal of neuroscience : the official journal of the Society for Neuroscience 32 (34):11539-11558. doi:10.1523/JNEUROSCI.5942-11.2012

Kjelstrup KB, Solstad T, Brun VH, Hafting T, Leutgeb S, Witter MP, Moser EI, Moser M-B (2008) Finite Scale of Spatial Representation in the Hippocampus. Science 321 (5885):140-143. doi:10.1126/science.1157086

Koenig J, Linder AN, Leutgeb JK, Leutgeb S (2011) The spatial periodicity of grid cells is not sustained during reduced theta oscillations. Science 332 (6029):592-595. doi:10.1126/science.1201685

Kropff E, Treves A (2008) The emergence of grid cells: Intelligent design or just adaptation? Hippocampus 18 (12):1256-1269. doi:10.1002/hipo.20520

Langston RF, Ainge JA, Couey JJ, Canto CB, Bjerknes TL, Witter MP, Moser EI, Moser MB (2010) Development of the spatial representation system in the rat. Science 328 (5985):1576-1580. doi:10.1126/science.1188210

Lengyel M, Szatmary Z, Erdi P (2003) Dynamically detuned oscillations account for the coupled rate and temporal code of place cell firing. Hippocampus 13 (6):700-714. doi:10.1002/hipo.10116

Loewenstein Y, Yarom Y, Sompolinsky H (2001) The generation of oscillations in networks of electrically coupled cells. Proceedings of the National Academy of Sciences of the United States of America 98 (14):8095-8100. doi:10.1073/pnas.131116898

Marozzi E, Jeffery KJ (2012) Place, space and memory cells. Current biology : CB 22 (22):R939-942. doi:10.1016/j.cub.2012.10.022

McNaughton BL, Battaglia FP, Jensen O, Moser EI, Moser MB (2006) Path integration and the neural basis of the 'cognitive map'. Nature reviews Neuroscience 7 (8):663-678. doi:10.1038/nrn1932

McNaughton BL, Chen LL, Markus EJ (1991) 'Dead reckoning', landmark learning, and the sense of direction: a neurophysiological and computational hypothesis. Journal of cognitive neuroscience 3:190-201

Mehta MR, Lee AK, Wilson MA (2002) Role of experience and oscillations in transforming a rate code into a temporal code. Nature 417 (6890):741-746. doi:10.1038/nature00807

Mhatre H, Gorchetchnikov A, Grossberg S (2012) Grid cell hexagonal patterns formed by fast self-organized learning within entorhinal cortex. Hippocampus 22 (2):320-334. doi:10.1002/hipo.20901

Moser EI, Kropff E, Moser MB (2008) Place cells, grid cells, and the brain's spatial representation system. Annual review of neuroscience 31:69-89. doi:10.1146/annurev.neuro.31.061307.090723

Moser EI, Moser MB (2008) A metric for space. Hippocampus 18 (12):1142-1156. doi:10.1002/hipo.20483

Navratilova Z, Giocomo LM, Fellous JM, Hasselmo ME, McNaughton BL (2012) Phase precession and variable spatial scaling in a periodic attractor map model of medial entorhinal grid cells with realistic after-spike dynamics. Hippocampus 22 (4):772-789. doi:10.1002/hipo.20939

Nitz D, McNaughton B (2004) Differential modulation of CA1 and dentate gyrus interneurons during exploration of novel environments. Journal of neurophysiology 91 (2):863-872. doi:10.1152/jn.00614.2003

O'Donnell C, Nolan MF, van Rossum MC (2011) Dendritic spine dynamics regulate the long-term stability of synaptic plasticity. The Journal of neuroscience : the official journal of the Society for Neuroscience 31 (45):16142-16156. doi:10.1523/JNEUROSCI.2520-11.2011

O'Keefe J (2006) Hippocampal Neurophysiology in the Behaving Animal. In: The Hippocampus Book. Oxford University Press, New York, pp 475-548

O'Keefe J, Burgess N (2005) Dual phase and rate coding in hippocampal place cells: theoretical significance and relationship to entorhinal grid cells. Hippocampus 15 (7):853-866. doi:10.1002/hipo.20115

O'Keefe J, Dostrovsky J (1971) The hippocampus as a spatial map. Preliminary evidence from unit activity in the freely-moving rat. Brain research 34 (1):171-175

O'Keefe J, Nadel L (1978) Physiology: The model. In: The hippocampus as a cognitive map. Clarendon Press, Oxford, pp 220-230

O'Keefe J, Recce ML (1993) Phase relationship between hippocampal place units and the EEG theta rhythm. Hippocampus 3 (3):317-330. doi:10.1002/hipo.450030307

Papoulis A, Pillai SU (2002) Probability, Random Variables and Stochastic Processes. 4th edition edn.,

Quirk G, Muller R, Kubie J, Ranck J (1992) The positional firing properties of medial entorhinal neurons: description and comparison with hippocampal place cells. The Journal of Neuroscience 12 (5):1945-1963

Ross SM (2002) Simulation. 3rd edition edn. Academic, San Diego

Roth A, van Rossum M (2009) Modeling synapses. In: Schutter ED (ed) Computational Modeling Methods for Neuroscientists

Samsonovich A, McNaughton BL (1997) Path integration and cognitive mapping in a continuous attractor neural network model. The Journal of neuroscience : the official journal of the Society for Neuroscience 17 (15):5900-5920

Sargolini F, Fyhn M, Hafting T, McNaughton BL, Witter MP, Moser MB, Moser EI (2006) Conjunctive representation of position, direction, and velocity in entorhinal cortex. Science 312 (5774):758-762. doi:10.1126/science.1125572

Savelli F, Yoganarasimha D, Knierim JJ (2008) Influence of boundary removal on the spatial representations of the medial entorhinal cortex. Hippocampus 18

(12):1270-1282. doi:10.1002/hipo.20511

Sharp PE (2006) Subicular place cells generate the same "map" for different environments: comparison with hippocampal cells. Behavioural brain research 174 (2):206-214. doi:10.1016/j.bbr.2006.05.034

Shepherd GM (1998) The synaptic organization of the brain. 4th edition edn. Oxford University Press, New York

Si B, Kropff E, Treves A (2012) Grid alignment in entorhinal cortex. Biological cybernetics 106 (8-9):483-506. doi:10.1007/s00422-012-0513-7

Skaggs WE, McNaughton BL, Wilson MA, Barnes CA (1996) Theta phase precession in hippocampal neuronal populations and the compression of temporal sequences. Hippocampus 6 (2):149-172. doi:10.1002/(SICI)1098-1063(1996)6:2<149::AID-HIPO6>3.0.CO;2-K

Solstad T, Boccara CN, Kropff E, Moser MB, Moser EI (2008) Representation of geometric borders in the entorhinal cortex. Science 322 (5909):1865-1868. doi:10.1126/science.1166466

Stensola H, Stensola T, Solstad T, Froland K, Moser MB, Moser EI (2012) The entorhinal grid map is discretized. Nature 492 (7427):72-78. doi:10.1038/nature11649

Taube JS, Muller RU, Ranck JB, Jr. (1990) Head-direction cells recorded from the postsubiculum in freely moving rats. I. Description and quantitative analysis. The Journal of neuroscience : the official journal of the Society for Neuroscience 10 (2):420-435

Tsodyks MV, Skaggs WE, Sejnowski TJ, McNaughton BL (1996) Population dynamics and theta rhythm phase precession of hippocampal place cell firing: a spiking neuron model. Hippocampus 6 (3):271-280. doi:10.1002/(SICI)1098-1063(1996)6:3<271::AID-HIPO5>3.0.CO;2-Q

van Rossum MC, Bi GQ, Turrigiano GG (2000) Stable Hebbian learning from spike timing-dependent plasticity. The Journal of neuroscience : the official journal of the Society for Neuroscience 20 (23):8812-8821

Wade C, Tavris C (2000) Psychology. 6th edition edn.,

Wilent WB, Nitz DA (2007) Discrete place fields of hippocampal formation interneurons. Journal of neurophysiology 97 (6):4152-4161. doi:10.1152/jn.01200.2006

Wills TJ, Barry C, Cacucci F (2012) The abrupt development of adult-like grid cell firing in the medial entorhinal cortex. Frontiers in neural circuits 6:21. doi:10.3389/fncir.2012.00021

Wills TJ, Cacucci F, Burgess N, O'Keefe J (2010) Development of the hippocampal cognitive map in preweanling rats. Science 328 (5985):1573-1576. doi:10.1126/science.1188224

Wills TJ, Lever C, Cacucci F, Burgess N, O'Keefe J (2005) Attractor dynamics in the hippocampal representation of the local environment. Science 308 (5723):873-876. doi:10.1126/science.1108905

Witter M (2011) Entorhinal cortex. Scholarpedia. doi:doi::10.4249/scholarpedia.4380

Yartsev MM, Witter MP, Ulanovsky N (2011) Grid cells without theta oscillations in the entorhinal cortex of bats. Nature 479 (7371):103-107. doi:10.1038/nature10583

Zilli EA (2012) Models of grid cell spatial firing published 2005-2011. Frontiers in neural circuits 6:16. doi:10.3389/fncir.2012.00016

Zilli EA, Hasselmo ME (2010) Coupled noisy spiking neurons as velocity-controlled oscillators in a model of grid cell spatial firing. The Journal of neuroscience : the official journal of the Society for Neuroscience 30 (41):13850-13860. doi:10.1523/JNEUROSCI.0547-10.2010